Large-scale functional connectivity in the human brain reveals fundamental mechanisms of cognitive, sensory and emotion processing in health and psychiatric disorders

Spiro P. Pantazatos

Submitted in partial fulfillment of the
requirements for the degree of
Doctor of Philosophy
under the Executive Committee
of the Graduate School of Arts and Sciences

COLUMBIA UNIVERSITY

2014

ABSTRACT

Large-scale functional connectivity in the human brain reveals fundamental mechanisms of cognitive, sensory and emotion processing in health and psychiatric disorders

Spiro P. Pantazatos

Functional connectivity networks that integrate remote areas of the brain as working functional units are thought to underlie fundamental mechanisms of perception and cognition, and have emerged as an active area of investigation. However, traditional approaches of measuring functional connectivity are limited in that they rely on *a priori* specification of one or a few brain regions. Therefore, the development of data-driven and exploratory approaches that assess functional connectivity on a large-scale are required in order to further understand the functional network organization of these processes in both health and disease. In this thesis project, I investigate the roles of functional connectivity in visual search (Chapter 2, (Pantazatos, Yanagihara et al., 2012)) and bistable perception (Chapter 3, (Karten et al., 2013)) using traditional functional connectivity approaches, and develop and apply new approaches to characterize the large-scale networks underlying the processing of supraliminal (Chapter 4, (Pantazatos et al., 2012a)) and subliminal (Chapter 5, (Pantazatos, Talati et al., 2012b)) emotional threat signals, speech and song processing in autism (Chapter 6, (Lai et al., 2012)), and face processing in social anxiety disorder (Chapter 7, (Pantazatos et al., 2013)). Finally, I complement the latter study with an investigation of structural morphological abnormalities in social anxiety disorder (Chapter 8, (Talati et al., 2013)). Each of these chapters has been or is about to be published in peer reviewed journals and this thesis provides an overview of the entire

body of investigation, based on advances in understanding the role of large-scale neural processes as fundamental organizational units that underlie behavior.

In Chapter 2, Independent Components Analysis (ICA), Psychophysiological Interactions (PPI) and Dynamic Causal Modeling (DCM) analyses were used to investigate the hypothesis that expectation and attention-related interactions between ventral and medial prefrontal cortex and association visual cortex underlie visual search for an object. Results extend previous models of visual search processes to include specific frontal-occipital neuronal interactions during a natural and complex search task. In Chapter 3, PPI analyses revealed percept-dependent changes in connectivity between visual cortex, frontoparietal attention and default mode networks during bistable image perception. These findings advance neural models of bistable perception by implicating the default mode and frontoparietal networks during image segmentation.

In Chapters 4 and 5, an exploratory approach based on multivariate pattern analysis of large-scale, condition-dependent functional connectivity was developed and applied in order to further understand the neural mechanisms of threat-related emotion processing. This approach was successful in extracting sufficient information to "brain-read" both unattended supraliminal (Chapter 4) and subliminal (Chapter 5) fear perception in healthy subjects. Informative features for supraliminal fear perception included functional connections between thalamus and superior temporal gyrus, angular gyrus and hippocampus, and fusiform and amygdala, while informative features for subliminal fear perception included middle temporal gyrus, cerebellum and angular gyrus.

In psychiatric disorders, large-scale functional connectivity is typically assessed during resting-state (i.e. no task or stimulus). However, disorder-dependent alterations in functional

network architecture may be more or less prominent during a stimulus or task that is behaviorally relevant to the disorder, as is exemplified by enhanced long-range, frontal-posterior connectivity during song (vs. speech) perception in autism (Chapter 6). In the case of social anxiety disorder (SAD), pattern analysis of large-scale, functional connectivity during neutral face perception was sensitive enough to discriminate individual subjects with SAD from both healthy controls and panic disorder (Chapter 7). The most informative feature was functional connectivity between left hippocampus and left temporal pole, which was reduced in medication-free SAD subjects, and which increased following 8-weeks SSRI treatment, with greater increases correlating with greater decreases in symptom severity. This finding parallels results from observed neuroanatomical abnormalities in SAD, which include reduced grey matter volume in the temporal pole, in addition to increased grey matter volume in cerebellum and fusiform (Chapter 8). The above findings suggest promise for emerging functional connectivity and structural-based neurobiomarkers for SAD diagnosis and treatment effects.

TABLE OF CONTENTS

LIST OF TABLES iii

LIST OF FIGURES iv

ACKNOWLEDGMENTS vi

DEDICATIONS vii

CHAPTER 1 INTRODUCTION 1

CHAPTER 2 FRONTAL-OCCIPITAL CONNECTIVITY DURING VISUAL SEARCH 13

- Summary 13
- Introduction 14
- Methods 16
- Results 27
- Discussion 39

CHAPTER 3 DYNAMIC COUPLING BETWEEN VISUAL CORTEX, DEFAULT MODE AND FRONTOPARIETAL NETWORKS DURING BISTABLE PERCEPTION 43

- Summary 43
- Introduction 43
- Methods 45
- Results 49
- Discussion 54

CHAPTER 4 DECODING UNATTENDED FEARFUL FACES WITH WHOLE-BRAIN CORRELATIONS: AN APPROACH TO IDENTIFY CONDITION-DEPENDENT LARGE-SCALE FUNCTIONAL CONNECTIVITY 57

- Summary 57
- Introduction 58
- Methods 63
- Results 73
- Discussion 80

CHAPTER 5 CORTICAL FUNCTIONAL CONNECTIVITY DECODES SUBCONSCIOUS, TASK-IRRELEVANT THREAT-RELATED EMOTION PROCESSING 88

- Summary 88
- Introduction 88

Methods 92
Results 96
Discussion 102

CHAPTER 6 LARGE-SCALE FUNCTIONAL CONNECTIVITY DURING SPEECH AND SONG IN AUTISM 108

Summary 108
Introduction 109
Methods 110
Results 116
Discussion 120

CHAPTER 7 REDUCED ANTERIOR TEMPORAL AND HIPPOCAMPAL FUNCTIONAL CONNECTIVITY DURING FACE PROCESSING DISCRIMINATES INDIVIDUALS WITH SOCIAL ANXIETY DISORDER FROM HEALTHY CONTROLS AND PANIC DISORDER, AND INCREASES FOLLOWING TREATMENT 122

Summary 122
Introduction 123
Methods 125
Results 130
Discussion 144

CHAPTER 8 GREY MATTER ABNORMALITIES IN SOCIAL ANXIETY DISORDER: PRIMARY, REPLICATION, AND SPECIFICITY STUDIES 151

Summary 151
Introduction 152
Methods 155
Results 159
Discussion 172

REFERENCES 179

APPENDIX A SCHEMATIC REPRESENTATION OF FUNCTIONAL CONNECTIVITY APPROACHES ALONG TWO DIMENSIONS: ABILITY TO ASSESS CONDITION-DEPENDENCY VS. EXPLORATORY ABILITY 223

LIST OF TABLES

Table 1. Chapter 2: Temporal sorting using regression and group statistics of resulting beta values. 21

Table 2. Chapter 2: Frontal-occipital Independent Component IC20 (t > 2.25, cluster size > 50) 26

Table 3. Chapter 2: Source of ROI definitions for PPI, DCM and DTI analyses..... 27

Table 4. Chapter 4: F vs. N, Top 16 features. Consensus features are shown in bold..... 76

Table 5. Chapter 5: MF vs. MN, Top 9 features..... 99

Table 6. Chapter 7: Demographics table..... 132

Table 7. Chapter 7 Most informative features discriminating SAD. 138

Table 8. Chapter 7: Univariate statistical tests of features identified in the primary sample tested in a second, independent replication sample. 140

Table 10. Chapter 8: Grey Matter Abnormalities Associated with Social Anxiety Disorder..... 162

Table 11. Chapter 8: Relationship between Social Anxiety Severity and Grey Matter volume..... 164

Table 12. Chapter 8: Grey Matter Differences between Panic Disorder and Social Anxiety Disorder..... 170

LIST OF FIGURES

Figure 1. Chapter 2: Visual search task 18

Figure 2. Chapter 2: Search-related spatial independent components. 29

Figure 3. Chapter 2: Functional connectivity between vmPFC and LOC during visual search .. 32

Figure 4. Chapter 2: Effective connectivity between vmPFC and LOC during visual search. 35

Figure 5. Chapter 2: White matter paths between vmPFC and bilateral LOC. 38

Figure 6. Chapter 3: Bistable Schroedinger staircase. 45

Figure 7. Chapter 3: Activation differences between "default" and "alternative" percepts 50

Figure 8. Chapter 3: Functional connectivity of visual cortex during default and alternative percepts. 52

Figure 9. Chapter 4: Experimental paradigm for the interaction of attention and affect (adapted from Etkin, et. al. 2004). 61

Figure 10. Chapter 4: Data analysis scheme. 63

Figure 11. Chapter 4: Node definitions and anatomical locations**.** 68

Figure 12. Chapter 3: Large-scale functional connectivity discriminates between unattended, conscious processing of fearful and neutral faces 75

*Figure 13.*Chapter 4: Classification results using beta estimates as features. 78

Figure 14. Chapter 5: Whole-brain and "sub-cortical alarm" parcellation. 93

Figure 15. Chapter 5: Large-scale functional connectivity discriminates between processing of masked fearful and neutral faces 98

Figure 16. Chapter 6: Song vs. speech large-scale functional connectivity in autism and healthy controls. 119

Figure 17. Chapter 7: Functional connectivity that discriminates SAD in primary sample. 133

Figure 18. Chapter 7: Predicting SAD vs. Controls using beta and contrast estimates as features**.** 137

Figure 19. Chapter 7: Left-Hippocampus-Left Temporal and Left Anterior Middle Temporal gyrus-Left Orbitofrontal Cortex FC predict SAD in the replication sample 140

Figure 20. Chapter 7: Increases in Left Hippocampus-Left Temporal Pole connectivity correlate with greater decreases (ΔLSAS post-pre) in social anxiety symptom severity following 8 weeks paroxetine treatment (or non-treatment for control subjects) in a second, independent replication sample..... 143

Figure 21. Chapter 8: Gray matter differences associated with social anxiety disorder (SAD.. 167

Figure 22. Chapter 8: Gray matter differences between social anxiety disorder (SAD) and panic disorder (PD); 171

Figure 23. APPENDIX A: Current functional connectivity approaches along two dimensions.223

ACKNOWLEDGMENTS

I would like to thank my primary thesis advisor, Joy Hirsch, for her support, mentorship, patience, infectious excitement for cognitive neuroscience research, and for having created a collaborative and team-oriented research environment which inspired creativity and productivity, without which this thesis work would not have been possible. Many fellow lab members and collaborators contributed directly or indirectly to one or more portions of this work: these include Ardesheer Talati, Grace Lai, Michelle Umali, Ted Yanagihara, Xian Zhang, Melissa Sy, Frank Schneier and many others. I would like to also thank my previous rotation mentors and additional thesis advisors at Columbia University: Yves Lussier and Paul Pavlidis, who mentored and encouraged creative neuroinformatics work which then led me to neuroimaging; Reba Goodman and Richard Ambron, whose research project imbued me with excitement to wake up every day for my first rotation in graduate school; Ken Miller, whose lab members helped me efficiently learn MATLAB; and Tor Wager and Martin Lindquist, for advice and guidance in neuroimaging methods and for serving on my thesis committee. Finally, I wish to express my appreciation to my first departmental student advisor, Andrew Marks, who encouraged me to explore the rich research environment and rotation options at Columbia University, and thesis and qualifying exam committee members; Myrna Weissman, Joseph Gogos, Ning Qian, Brian McCabe and Amy MacDermott for their helpful input and feedback along the way.

DEDICATIONS

I would like to dedicate this work to my parents, Angela and Bill Stamoulis, for their support, encouragement, patience and understanding throughout my (prolonged) graduate training career; my brother Dennis, who has been a role model for conducting creative research and achieving authentic academic success; and my spiritual partner Katherine Henry, who has generously imparted wisdom and guidance regarding almost every step of my academic career, and who also inspired the primary research directions for this thesis work.

CHAPTER 1

INTRODUCTION

The study of the brain and its relationship to behavior has historically been approached through the complementary perspectives of functional segregation and functional integration (Friston, 2009). Under the principle of segregation the specialized functional roles of individual brain regions have been described: for example motion sensitivity of lateral occipital cortex (Born and Bradley, 2005) and sensitivity of the fusiform face area in response to face perception (Spiridon et al., 2006). However it is clear that activity of these regions alone is not sufficient to generate the perception of motion or of a facial identity, but rather, interconnectivity among regions within and without visual cortex (i.e. functional integration) is necessary for percept generation. Due to the complexity of connectivity both on the micro- and macro-scale, the continued development of new tools, methods and approaches are required in order to adequately measure and describe functional integration.

Due to its high spatial resolution and minimal invasiveness, functional magnetic resonance imaging (fMRI) has become the most popular technology used to study both functional segregation and integration in the human brain. This technique acquires time-dependent Blood Oxygen Level Dependent (BOLD) signal. The BOLD signal is an indirect measure of neural activity which recruits blood to local regions, and is thought to primarily reflect local field potentials, which consist of local processing of inputs in a given cortical area (Goense and Logothetis, 2008). Typically, whole-brain BOLD signal at a resolution of about 3 mm cubic voxels are acquired every 2 seconds (temporal frequency = 0.5 Hz), though the temporal and spatial resolution of fMRI BOLD imaging are continually improving (Ugurbil et al., 2013).

The primary approach used to measure functional segregation based on fMRI BOLD is Statistical Parametric Mapping (Turner et al., 1998). This approach creates spatial maps of activity, giving probability estimates for activated brain regions in response to particular conditions or stimuli. This approach is considered a 'mass univariate' approach in that many independent statistical tests for activation are conducted across ~100,000 voxels in the brain. The term 'univariate' means that the response of each voxel in relation to a stimulus model or regressor is assessed in isolation of all the other voxels. This approach has been successful in identifying, for example, regions of the brain that are particularly sensitive to the perception of objects (Malach et al., 1995) and faces (Spiridon et al., 2006). However, this approach and related mass univariate approaches are insufficient in modeling and measuring interactions between one or more regions in the brain.

There have been a number of approaches developed to measure functional integration based on fMRI BOLD imaging data, and classically they have been categorized into two main types of approaches: functional (bidirectional) and effective (unidirectional) connectivity (Friston, 2002). Functional (and effective) connectivity can be generically defined as a statistical dependency between two or more brain regions, and many mainstream approaches have been developed to assess condition-dependent (i.e. related to psychological context or stimulus) functional connectivity (Friston et al., 1997; 2003). However, with currently existing approaches there remain some fundamental disadvantages, and there is still a need for whole-brain, exploratory approaches that capture condition-dependent functional connectivity. By "exploratory", I mean the extent to which the approach can assess functional connectivity across the whole-brain as well as with high neuroanatomical resolution of the identified functional connections. By "condition-dependent", I mean the ability of the approach to identify and

estimate connectivity whose strength is modulated by psychological context or stimulus. In general there is a trade-off in that the more exploratory the approach, the less condition-dependent, and vice versa. One contribution of my thesis work is the refinement and application of approaches that are both highly exploratory (i.e. large-scale functional connectivity across the whole-brain), yet also allow for the assessment of *condition-dependent* functional connectivity. Such an approach gives us insight into the large-scale functional network architecture of cognitive, emotional and sensory systems in both health and psychiatric disorders.

In the rest of this introduction, I will give a brief overview of some commonly used functional and effective connectivity approaches, and describe how they were applied in my thesis in order to understand fundamental neural mechanisms of cognitive-sensory processing (Chapters 2 and 3). I will then elucidate the advantages (and relative disadvantages) of these approaches in terms of two previously mentioned desirable dimensions: the extent to which the approach is 1) exploratory and 2) condition-dependent. I will also describe a new approach which was developed and applied as part of my thesis, based on multivariate pattern analysis of condition-dependent, large-scale functional connectivity. This approach is exploratory across the whole-brain while also allowing for the identification and assessment of condition-dependent functional connectivity. I will also briefly introduce how this approach was used in furthering our understanding of emotion and sensory processing (Chapters 4 and 5) as well as in identifying putative functional connectivity-based biomarkers for psychiatric disorder (Chapter 7).

Seed-based functional connectivity approaches

Seed-based analyses are semi-exploratory in that a whole-brain search is conducted to identify regions that exhibit significant functional connectivity with a "seed" region. Seed-based functional connectivity approaches are often applied to resting-state data (i.e. no task) to

characterize intrinsic network interactions of particular regions of interest. These approaches typically calculate functional connectivity using correlation coefficients (Stein et al., 2000) or regression (Di Martino et al., 2008) and identify significant differences in these measures across diagnostic groups (Qi et al., 2013). For example, this approach has been used to assess the resting state functional connectivity of striatum with the rest of the brain and differences in these connections in autism (Di Martino et al., 2011). However a primary disadvantage of resting fMRI it is limited to *intrinsic* connectivity (at best, assuming subjects are not ruminating or thinking about a specific topic which could influence the results).

Psychophysiological Interactions [PPI] analysis is a condition-dependent, seed-based functional connectivity approach that identifies brain regions whose functional connectivity with a "seed" region differs significantly between two or more conditions (Friston et al., 1997). This approach is based on a regression model, similar to a general linear model used for activation analyses, in which the primary regressor-of-interest represents the interaction between one or more psychological contexts (i.e. conditions) and the de-convolved BOLD signal of the "seed" region. This interaction regressor is constructed by convolving (multiplying) the seed region temporal profile with the vector of the psychological variable of interest (i.e. 1*Condition A + -1*Condition B). Regions whose time courses follow this regressor exhibit higher covariation with the seed region during Condition A relative to Condition B. Additional regressors are included to model out variation due to activation and intrinsic functional connectivity. See (O'Reilly et al., 2012) for a tutorial that provides a more comprehensive, conceptual explanation of how PPI works.

For example, PPI analyses have been used to examine functional connectivity during fearful facial emotion processing (Banks et al., 2007; Das et al., 2005), usually using amygdala

as the "seed" region, and anomalies in such condition-dependent functional connectivity in psychiatric disorders have been described (Monk et al., 2008; Ohrmann et al., 2010; Prater et al., 2012). In my thesis work, PPI analysis was used to identify visual association regions that exhibit greater functional connectivity with ventromedial prefrontal cortex, a region implicated in expectation and visual imagery, during visual search for an object (Chapter 2, (Pantazatos, Yanagihara et al., 2012)). Results extend previous models of visual search processes to include specific frontal-occipital neuronal interactions during a natural and complex search task. This approach was also used as part of my thesis to show differential functional coupling between visual cortex and frontoparietal and default mode networks during bistable image perception (Chapter 3, (Karten et al., 2013)). These findings advance neural models of bistable perception by implicating the default mode and frontoparietal networks during image segmentation. Another seed-based approach, Granger Causality Mapping (GCM), allows mapping of *effective* connectivity, or the identification of regions that are sources or targets of directed influence from the seed-region (Roebroeck et al., 2005). Despite the utility and popularity of seed-based approaches, particularly PPI, a primary disadvantage is they do not intrinsically assess functional interactions among three or more regions of the brain. This primarily owes to the fact that they are regression-based approaches and too many predictors (2 for each region) would render the model lacking in degrees of freedom.

Network-modeling approaches

Network-modeling approaches allow for the assessment of intrinsic or condition-dependent functional connectivity among three or more brain regions. These approaches have the additional advantage in that causal effects, particularly unidirectional, causal influences between brain regions that generated the data, can be directly modeled and assessed. The most commonly

used network-modeling approaches are those that measure effective connectivity, such as Dynamic Causal Modeling (DCM) (Friston et al., 2003) and Structural Equation Modeling (SEM) (Horwitz et al., 1999). Both approaches use model comparison frameworks in which inferences can be made about effective connectivity and modulation of this connectivity due to perceptual or cognitive condition, but they differ mainly in their generative models. For a comprehensive comparison of these approaches see (Penny et al., 2004). In my thesis, DCM was used to contribute evidence for bidirectional effective connectivity between object-sensitive visual association cortex and ventromedial prefontal cortex (Chapter 2, (Pantazatos, Yanagihara et al., 2012)). For tutorials and guides on practical application of DCM and SEM respectively see (Stephan et al., 2010) and (https://sites.google.com/site/fmrisem/). Due to the computational complexity entailed in estimating effective connectivity parameters and model comparison, these approaches generally only assess connections among only several (2-8) regions, which must be specified *a priori*. Hence, these are considered hypothesis-driven, as opposed to more exploratory, data-driven approaches. Condition-dependent, network-modeling approaches that use correlation-based measures among many more regions (~40) have also been applied (Dodel et al., 2005), but the ability to assess connectivity across the whole-brain when using univariate statistical inference procedures are hampered by the multiple comparisons problem (described more in the last section).

Matrix decomposition approaches

Matrix decomposition approaches are data-driven and model-free analyses that decompose the fMRI data matrix into a sparse set of linearly orthogonal or uncorrelated spatial components. A commonly used exemplar of this approach is Independent components analysis (ICA), which is used to identify groups of spatially distributed yet synchronized regions (i.e.

spatial independent components, or IC) and their associated temporal profiles (Calhoun et al., 2001). ICA assumes that signal sources (i.e. independent components, or ICs) consist of distributed brain regions that are largely spatially independent (i.e. functional modularity) and add linearly (McKeown and Sejnowski, 1998). Although it is model free, temporal profiles of ICs can be regressed against a temporal model in order to sort ICs according to task-relatedness. In my thesis, this approach was used to identify groups of synchronized regions involved during visual search (Chapter 2, (Pantazatos, Yanagihara et al., 2012)). Related approaches, such as Partial Least Squares (PLS) (Krishnan et al., 2011) and Ordinal Trends analysis (OrT) (Habeck et al., 2005), directly incorporate between-group and within-subject variation in order to identify synchronized regions that exhibit sustained activity across subjects and experimental conditions, respectively. For example, OrT is particularly useful in identifying distributed networks that covary with increasing task difficulty in tasks such as verbal working memory and visuo-motor learning (Habeck et al., 2005). In this sense, these approaches are more "condition-dependent" than ICA. Another approach combines matrix decomposition with network modeling: a first step uses matrix decomposition to identify a set of modules (i.e. groups of synchronized brain regions), and in the second step functional or effective connectivity between these modules as a function of task or group is assessed. An example of this approach is the demonstration of increased correlation between frontoparietal networks and default mode network during internally (vs. externally) oriented attention tasks (Spreng, 2012). Despite the utility of treating the brain as a set of functional modules consisting of spatially distributed regions, a main disadvantage is these approaches are limited in anatomical resolution (i.e. they identify groups of synchronized regions related to a task, as opposed to function connectivity between distinct pairs

of brain regions). Thus they are less sensitive in detecting functional connectivity differences when those differences occur sparsely among pairs of discrete regions.

Large-scale functional connectivity

Large-scale functional connectivity can be considered an extension of the above-mentioned network modeling approaches. Here the goal is typically to characterize the complex network architecture (via graph theory, etc.) or global or local functional connectivity strengths on a whole-brain scale. Such approaches assess bidirectional functional connectivity (i.e. correlation, partial correlation, mutual information, coherence, etc.) among many hundreds of nodes distributed across the whole-brain. These nodes are either defined anatomically according to an atlas or evenly spaced across the brain, and/or defined based on some functional criteria (Craddock et al., 2012). The number of connections increase exponentially with increasing number of nodes (i.e. (n-1)*n/2), thus creating a multiple comparisons problem when using standard univariate statistical inference to identify condition-dependent connections. For example, 200 nodes have 19,900 connections among them, and with a typical alpha level of 0.05 there would be about 1,000 expected false positives. Graph theoretic and related approaches are particularly suited to analyzing these data because they produce local (node-specific) or global measures based on overall properties of the patterns of connectivity. For example, as part of my thesis average global Euclidean distance was used to demonstrate significantly increased long-range functional connectivity during song vs. speech in autism (Chapter 6, (Lai et al., 2012)). This suggests that in autism, long-range, frontal-posterior functional connections are more effectively engaged for song than for speech, which may provide at least a partial neurobiological account for the observed effects of music therapy in autism.

To identify condition dependent functional connectivity and their neuroanatomical

substrates, one proposed solution is a "network-based statistic" which quantifies the probability of observed N linked nodes above a particular threshold used for each edge (Zalesky et al., 2010). This is the equivalent of applying cluster-extent correction for activation mapping (Forman et al., 1995). However, inferences can only be made on groups of interconnected edges, not individual ones, and furthermore the size of each group of interconnected nodes varies as a function of threshold. In addition, there is a substantial loss of information when conducting univariate statistical inference on functional connections averaged over a group of subjects and discounting the multivariate, joint responses among many functional connections.

Information mapping of condition-dependent, large-scale functional connectivity

An alternative approach to univariate statistical mapping is "information mapping" (Kriegeskorte et al., 2006). Rather than identify brain regions (or functional connections) whose average activity changes across experimental conditions or subject group, this approach asks "where in the brain does the activity (or functional connectivity) pattern contain information about the experimental condition or subject group?" This approach has the advantage that it avoids the multiple comparisons problem, and it also take into account the joint multivariate responses among any functional connections. At the same time, this approach is more directly applicable to translational neuroscience in that predictions about individual subjects (i.e. diagnosis, treatment outcome etc.) can readily be made using the same statistical framework.

Due to the above reason, there is great interest in the application of multivariate pattern analysis approaches to large-scale functional connectivity (Turk-Browne, 2013). These measures are typically derived from resting-state data and used to predict disease state (Craddock et al., 2009). However there are several limitations when using this approach with resting-state data: 1)

it cannot be used to understand the large-scale network architecture underlying various cognitive processes and 2) it does not take advantage of task-based paradigms that employ a probe or condition that is relevant to a particular psychiatric disorder. In my thesis work, an approach that combines and leverages the advantages of large-scale functional connectivity, task-based fMRI, and multivariate pattern analysis (i.e. information mapping applied to condition-dependent, large-scale functional connectivity) was developed and applied. This approach is exploratory in that it can identify condition-dependent functional connectivity among many hundred nodes across the whole-brain. A visual comparison of this approach with other functional connectivity approaches is presented in Appendix Figure 1, in which methods are heuristically plotted along two dimensions: 1) exploratory ability of the approach and 2) ability to estimate condition-dependent functional connectivity.

A primary hypothesis of the approach is that pair-wise correlations, from time-series which are segmented and concatenated from different block conditions, could be used to reliably decode the stimulus that was presented during each block. Information mapping (i.e. identification of informative, condition-dependent, large-scale functional connectivity) was applied to reveal novel insights into the neural mechanisms of sensory-emotional processing of supraliminal and subliminal threat-related face perception within healthy individuals (Chapter 4 (Pantazatos et al., 2012a) and Chapter 5 (Pantazatos, Talati et al., 2012b)). Functional connections that discriminated supraliminal fearful from neutral faces included amygdala, fusiform, thalamus, superior temporal sulcus, superior occipital cortex, hippocampus, angular gyrus, and cerebellum, whereas functional connections that discriminated subliminal fear from neutral faces included middle temporal gyrus, angular gyrus, cerebellum, superior frontal gyrus, and amygdala. This approach also identified putative functional connectivity- based biomarkers

for social anxiety disorder, which is known to exhibit anomalies in these processes (Chapter 7, (Pantazatos et al., 2013)). The most informative feature that discriminated social anxiety was reduced left-temporal pole and left-hippocampus functional connectivity. This finding mirrors observed structural abnormalities in the temporal pole (Chapter 8, (Talati et al., 2013)). In summary, these findings indicate that whole-brain patterns of interactivity are a sensitive and informative signature of supraliminal and subliminal fear perceptual states in health and disease.

Summary

In summary of my thesis work, traditional condition-dependent, functional connectivity approaches were used to extend previous models of visual search through the characterization of frontal-occipital interactions related to object-category selectivity, expectation and attention during a natural and complex search task (Chapter 2, (Pantazatos, Yanagihara et al., 2012)). These approaches were also used to reveal percept-dependent changes in connectivity between visual cortex, frontoparietal attention and default mode networks during bistable image perception and advance neural models of image segmentation by implicating the default mode and frontoparietal networks (Chapter 3, (Karten et al., 2013)). New, exploratory approaches based on multivariate analysis of large-scale, condition-dependent functional connectivity were also refined and applied in order to further understand the functional network architecture of supraliminal (Chapter 4, (Pantazatos et al., 2012a)) and subliminal (Chapter 5, (Pantazatos, Talati et al., 2012b)) threat-related emotion processing. Condition-dependent, large-scale functional connectivity was also used to demonstrate enhanced long-range, frontal-posterior connectivity during song (vs. speech) perception in autism, suggesting a putative neurobiological account for the observed effects of music therapy in autism (Chapter 6, (Lai et al., 2012)).

Multivariate pattern analysis of large-scale, condition-dependent functional connectivity was also able to identify putative functional connectivity-based biomarkers for social anxiety disorder, which include reduced left-temporal pole and left-hippocampus functional connectivity (Chapter 7, (Pantazatos et al., 2013)). This finding mirrors structural abnormalities in the temporal pole in social anxiety disorder, identified using voxel-based morphology analysis of structural MRI data (Chapter 8, (Talati et al., 2013)). In summary, the contributions of this thesis comprise advances in computational methods that reveal integrative processes in the human brain that underlie sensory, cognitive and emotion functions in both health and disease.

CHAPTER 2

FRONTAL-OCCIPITAL CONNECTIVITY DURING VISUAL SEARCH[1]

Summary

Although expectation and attention-related interactions between ventral and medial prefrontal cortex and stimulus category-selective visual regions have been identified during visual detection and discrimination, it is not known if similar neural mechanisms apply to other tasks such as visual search. The current work tested the hypothesis that high-level frontal regions, previously implicated in expectation and visual imagery of object categories, interact with visual regions associated with object recognition during visual search. Using fMRI, subjects searched for a specific object that varied in size and location within a complex natural scene. A model-free, spatial-Independent Component Analysis (ICA) isolated multiple task-related components, one of which included visual cortex, as well as a cluster within ventromedial prefrontal cortex (vmPFC), consistent with the engagement of both top-down and bottom-up processes. Analyses of PsychoPhysiological Interactions (PPI) showed increased functional connectivity between vmPFC and object-sensitive lateral occipital cortex (LOC), and results from dynamic causal modeling (DCM) and Bayesian Model Selection suggested bidirectional connections between vmPFC and LOC that were positively modulated by the task. Using image-guided diffusion-tensor imaging (DTI), functionally seeded, probabilistic white matter tracts between vmPFC and LOC, which presumably underlie this effective inter-connectivity, were also observed. These connectivity findings extend previous models of visual search processes to include specific frontal-occipital neuronal interactions during a natural and complex search task.

[1] Pantazatos, Spiro P, Ted K Yanagihara, Xian Zhang, Thomas Meitzler, and Joy Hirsch. 2012. Frontal-occipital connectivity during visual search. *Brain Connect*.

Introduction

Recent studies suggest that in naturalistic situations, when precise visual characteristics of target objects are not known in advance, preparatory activity at higher levels of the visual hierarchy, such as stimulus category-responsive visual regions, selectively mediate visual search (Peelen and Kastner, 2011). Mounting evidence also indicates that prefrontal regions are involved in the anticipation and expectation of abstract visual features such as visual stimulus categories (i.e. face, house, object) (Fenske et al., 2006a; Peelen and Kastner, 2011; Summerfield et al., 2006), and that these regions may constitute a top-down source of preparatory activity observed in visual cortex (Peelen and Kastner, 2011). Indeed, functional interactions between regions in the ventral and medial prefrontal cortex (vPFC and mPFC) and stimulus-category responsive regions (i.e. 'face', 'object' and 'house' areas) in temporo-occipital areas have been described for visual imagery tasks (Mechelli et al., 2004) and during face and object discrimination tasks (Bar, 2003; Summerfield et al., 2006). In contrast to relatively non-content-selective parietal-visual interactions, frontal-visual interactions are thought to reflect stimulus category-specific attentional mechanisms during visual imagery and perception (Gazzaley et al., 2007; Mechelli et al., 2004).

The characterization of frontal-visual interactions during naturally occurring visual tasks i.e. sustained searching for an object embedded within a complex scene, as well as the quantification and characterization of structural connections that underlie these functional interactions, remain an active research goal. Here we hypothesized that during natural visual search, when only the target object category is known in advance, frontal regions interact with

stimulus category-responsive visual areas, and that structural and functional pathways between these regions could be demonstrated.

In the current study, subjects were instructed to indicate the presence and location of a specific object that varied in size and location in a complex natural visual scene. A model-free multivariate analysis (spatial-ICA) was applied to the functional imaging data to identify spatially distributed and synchronized regions engaged during this complex visual search task. We first conducted an ICA (rather than a standard GLM) analysis for three reasons: 1) we aimed to identify groups of synchronized, or "functionally connected" regions, and of particular interest were visual and frontal regions within the ventral and medial prefrontal cortex, (vmPFC); 2) ICA avoids imposing apriori models and assumptions to the data, which was particularly important given that we used a complex and relatively natural and ecologically valid task; and 3) while vmPFC is part of the Default Mode Network (DMN), which is typically deactivated during tasks requiring attention, a component of vmPFC activity that is synchronized with positive visual activity during search should be isolated by ICA.

Independent components (IC) were sorted according to their temporal profiles in order to isolate functionally meaningful brain areas related to the visual search task. The highest task-related spatial component included dorsal and ventral visual areas as well as ventral medial prefrontal cortex (vmPFC). Based on previous findings suggesting a role for vmPFC in stimulus object-category expectation and imagery during object discrimination and detection and concomitant interactions with visual association areas in a stimulus selective manner (Bar, 2003; Mechelli et al., 2004; Summerfield et al., 2006), we hypothesized that vmPFC also interacts with object/feature-sensitive visual regions during visual search. Finally, we employed DTI to test the hypothesized structural connectivity between activated regions in vmPFC and LOC using

probabilistic tractography in a sample of 108 additional subjects that were not participants in the functional study. We focused on LOC, since it is known be highly specialized to visual objects (Amedi et al., 2001; Grill-Spector et al., 2001; Ishai et al., 2000; Spiridon et al., 2006) and also because it has been shown to be responsive to the anticipation of search for an object, even in the absence of visual input, and predicted performance during subsequent detection (Peelen and Kastner, 2011).

Here we show that 1) vmPFC is involved in visual processing during search for an object embedded within a complex scene 2) there is increased functional connectivity and bi-directional, positive effective connectivity between vmPFC and object-sensitive LOC during the task and 3) there exist white matter tracts between these interacting regions. These findings provide evidence of structural and functional paths underlying task-related functional interactions between vmPFC and object-sensitive regions (LOC) during visual search.

Methods

Subjects. 15 (5 female) healthy volunteers (mean age = 31, SD = 10, 13/15 right handed) with normal or corrected-to-normal vision participated in the search study, and 108 subjects (mean age=30.8, SD=11.3) participated in the DTI-only study, in accordance with institutional guidelines for research with human subjects. Recruitment, evaluations and scans were all performed at Columbia University Medical Center in the fMRI Research Center.

Experimental paradigms and procedure. Stimuli were presented in Visual Basic and displayed on a back-projection screen that was viewed by the subjects via a mirror attached to the scanner head-coil. The visual search trials (26 per run) were presented within a slow event-related (non-jittered) design with 20 seconds, or 10 TRs, between the onsets of each trial. Each trial consisted

of a stimulus presentation lasting 10 seconds, with 10 seconds of rest between end of one trial and the beginning of the next. Within each rest epoch, 2 seconds of static noise was presented (to erase iconic memory) followed by 8 seconds of a black, blank field. Total run time was 9 minutes, 12 seconds. Each trial consisted of presentation of 1 of 8 types of pictures: 1 which contained no target, and 7 which contained the target (an object resembling a 2.5 ton truck that was not camouflaged) at one of 7 different sizes, calibrated by distance from the viewer (600, 700, 1100, 1300, 1700 and 2800 meters). Each picture consisted of the same background (i.e. photo of a cluttered landscape). The location of the target also varied so that it appeared pseudo-randomly in one of 9 areas of the picture (left, middle, right and lower, middle, and upper sections of the scene). Each target location was presented 3 times in each run, and the no-target trial was presented 5 times. Stimuli were presented in random order. Subjects were instructed to decide whether a target was present in the image: if "no" they would click on 'next', and if "yes" they would click on the location of the target with a trackball (using the right hand). The task is summarized in Figure 1. The response time and the decision type (correct positive (hits: +C), incorrect positive (false alarm: +F, no target was present or a wrong location was clicked in the image), correct negative (correct reject: -C), and incorrect negative (-F: miss, a false 'no') was recorded. Although eye movements were not measured, subjects were given instructions to scan

the scene while maintaining a stable head position. Figure

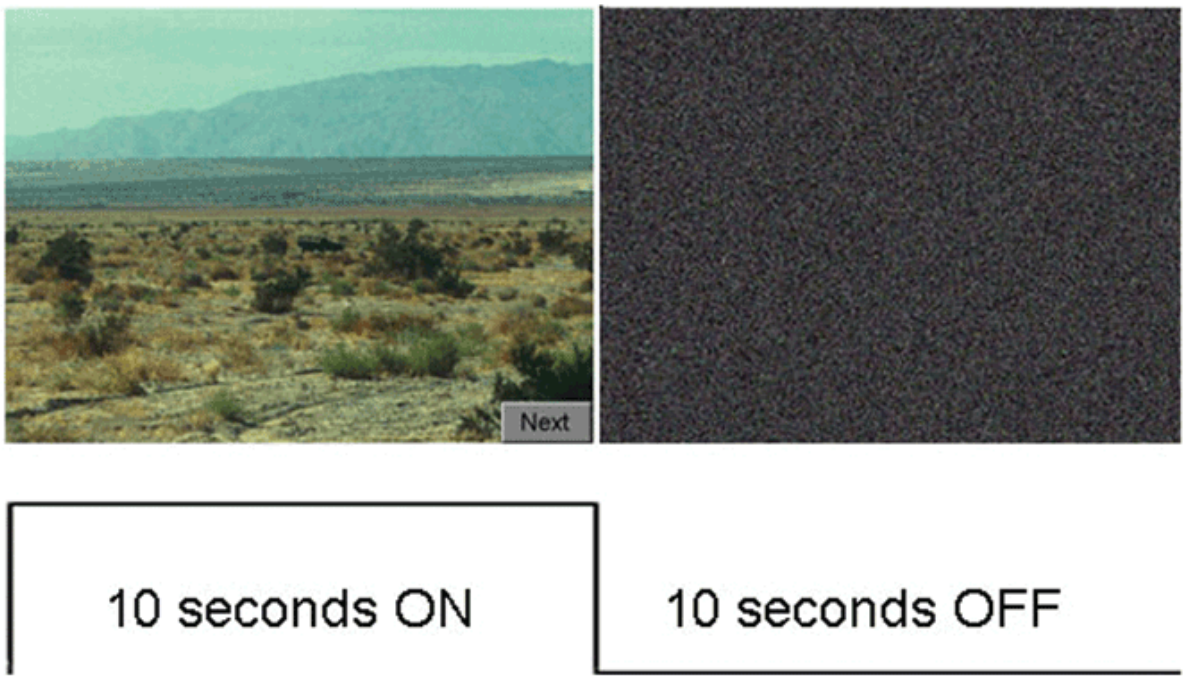

Figure 1. Chapter 2: Visual search task. Subjects were instructed to indicate whether a target was present in the image: if "no" they would click on 'next' in the bottom right corner of the image, and if "yes" they would click on the location of the target with a trackball (using the right hand). Each epoch consisted of the presentation of a picture, which either contained no target, or a target that varied in size and location within the scene (see methods). Each picture consisted of the same background, as shown in the top left panel.

Image acquisition. All functional images were acquired with a GE Twin-Speed 1.5T scanner, with T2*-weighted EPI sequence of 24 contiguous interleaved axial slices [TR=2000, TE=38 ms, field of view (FOV) = 192 mm, array size = 64x64"] of 4.5 mm thickness and 3x3 mm in-plane resolution, providing whole-brain coverage. High-resolution anatomical scans were acquired with a T1-weighted SPGR sequence (TR = 19 ms, TE = 5 ms, flip angle = 20□, FoV = 220x220 mm), recording 124 slices at a slice thickness of 1.5 mm and in-plane resolution of 0.86 x 0.86 mm.

DTI images were acquired on the same scanner using an 8 channel sense head coil with a single-shot sequence of 55 unique diffusion directions at a b-value = 900 with TE=7.8ms and TR=17000ms. A single volume (b-value = 0) was acquired and used as a reference to correct for eddy currents and head motion (Jenkinson and Smith, 2001). Isotropic (2.5 mm3 voxels) diffusion-weighted data were acquired for all subjects except S5, whose voxels had an in-plane resolution of 1.25 x 1.25 mm and slice thickness of 2.5 mm. Array size was 128x128 in a FOV of 32x32mm. A total of 58 slices were acquired and the total scan time was 16 minutes and 32 seconds.

DTI scans from 108 total healthy volunteers which were acquired and archived in our lab were included in the structural connectivity portion of this study that examined pathways between vmPFC and bilateral LOC.

Image analysis: Pre-processing was done in SPM2 (http://www.fil.ion.ucl.ac.uk/spm/software/spm2), while 1st and 2nd-level GLM, functional connectivity (PPI) and effective connectivity analyses were done in SPM8 (http://www.fil.ion.ucl.ac.uk/spm/software/spm8). Prior to preprocessing, the first 12 volumes were discarded. Functional data were slice-time corrected, spatially realigned to the first volume of the first run, and spatially normalized to the MNI template brain (re-sampled voxel size: 2 mm3). These normalized functional images were spatially smoothed with an 8 mm3 kernel.

Spatial-ICA: Group spatial-ICA was implemented with the GIFT toolbox v1.3d (Calhoun et al. 2001). Spatial-ICA assumes that signal sources (i.e. independent components, or ICs) consist of spatially distributed brain regions that are largely spatially independent (i.e. functional

modularity) and add linearly (McKeown and Sejnowski, 1998). Thus, at each voxel in the brain, the BOLD response is decomposed into a sum of sources (time courses of the ICs), each weighted by a different value particular to that voxel. Group ICA is implemented by concatenating the subjects' (spatially normalized) time series together so that the resulting spatial ICs are the same across all subjects (but the temporal profiles may vary from subject to subject). For each IC, statistical inference is then conducted on the loadings across all subjects at voxel. For more details please see (Calhoun et al., 2001). The minimum description length (MDL) criteria (Li et al., 2007) was used to estimate the number of informative ICs (25). Briefly, this approach employs a subsampling scheme to obtain a set of effectively independent and identically distributed samples from the dependent data samples and apply the information-theoretic criteria formulas to the this set to estimate the number of informative components. The Infomax algorithm (default in GIFT) was used to conduct the ICA. ICA is model free and allows for variations in the shape of the HRF (temporal profile) of each spatial IC from subject to subject. We sorted resulting spatial ICs by regressing their temporal profiles with a reference function created by convolving task onsets with the canonical HRF, and ranking the obtained R2 values in descending order (Table 1). The reference function included onsets for all trials, as our main goal was to identify ICs that contained visual activity, which presumably would be high on every trial. This reference function served primarily as a temporal "proxy" for the activation due to the task in order to identify ICs that were search-related. While the rank order of ICs might be affected by the use of a different reference function, the overall set of identified task-related ICs is unlikely to differ. The main goal of sorting was to aid in identifying a task-related IC that contained visual cortex as well as regions in ventral and medial prefrontal cortex. Group statistics were also performed whereby beta values obtained from this regression (done

separately for each subject without concatenation) for each spatial component were averaged over each subject and tested for significance from zero (one-sample t-test).

ICs that were significantly correlated (or anti-correlated) with the reference function and surviving a threshold at $p <= 0.0001$ (for the one-sample t-test of beta weights over all subjects) are listed in Table 1. There were an additional 9 ICs that were correlated or anti-correlated with the task surviving a threshold of $p < 0.05$, three of which were, on average across all subjects, positively correlated. Visual inspection of these ICs, however, revealed they included "non-physiological" spatial patterns indicative of motion artifact coinciding with the task.

Table 1. Chapter 2: Temporal sorting using regression and group statistics of resulting beta values.

Component	R2	Mean beta	Std	T-value	P value
20	0.42	2.27	1.2	7.26	4.2e-06
17	0.34	1.62	1.09	5.74	5.1e-05
6	0.31	1.47	1.30	4.41	0.0006
25	0.28	-0.52	0.41	-4.86	0.0003
23	0.16	-0.88	0.63	-5.34	0.0001

Note: P-values are from one-sample t-tests testing for significance from zero.

General Linear Model (GLM) analysis: Two GLM models were estimated: a single-condition GLM for defining DCM inputs, which consisted of all 26 search trials and a three-condition GLM, where trials were categorized according to response type. For the latter, "negative responses" (Misses and correction rejections; trials in which subjects responded that there was not a target), "positive responses" (Hits and False Alarms (FA); trials in which subjects responded that there was a target, and "no responses" (trials that timed-out before the subject responded) were modeled separately. First-level regressors were created by convolving the onsets of each trial with the canonical hemodynamic response function (HRF), and the duration

of each trial was set equal to the reaction time. The following contrast - "positive response" > "negative response" trials - was then submitted to 2nd-level RFX analyses (one-sample t-test) to identify visual activity associated with perception of the target. For this contrast only subjects that exhibited 3 or more instances of each trial type were included in the group analysis (12 subjects).

PsychoPhysiological Interaction (PPI) analysis: The PPI analysis measures the extent to which regions are differentially correlated during a given task. Ventromedial prefrontal cortex (vmPFC), the primary seed-of-interest, was defined by each subject's maximum loading factor onto IC20 (a highly task correlated IC that contained visual activity). An additional seed included precentral gyrus/dlPFC, which was defined by its peak MNI coordinates in IC20, [62, 0, 40]. Activity was extracted from 6 mm spheres centered at the above coordinate locations. The BOLD signal throughout the whole-brain was then regressed on a voxel-wise basis against the product of this time course and the vector of the psychological variable of interest, (1*Search condition + -1*Non-search condition), with the physiological and the psychological variables serving as regressors of no interest ("non-search condition" was defined as the period encompassing the end of one trial to the beginning of the next). Resulting beta maps were subsequently passed to 2nd level random effects analysis (one sample t-test as well as multiple regression with subjects' accuracy scores). For whole-brain cluster-extent correction, an uncorrected p-value of 0.005 was used and contiguous clusters of size 147 or more were deemed significant at $p<0.05$, corrected. This number was determined by 2000 Monte Carlo simulations of whole-brain fMRI data with respective data parameters of the present study according to the approach as implemented in AFNI 3dClustSim (Cox, 1996).

Effective connectivity: Effective connectivity analyses were carried out using DCM as implemented in SPM8 (http://www.fil.ion.ucl.ac.uk/spm/software/spm8) (Friston et al., 2003). Predictions about the observed data consist of the combination of driving inputs, intrinsic connection activity and bilinear modulation, which reflects the effects of experimental variables. In this case the search task served as both the driving input (on individual regions) and modulatory input (on connections between regions). These effects are modeled by the following equation:

$$dz1/dt=(A+umB)z2+Cui$$

in which dz1/dt is the state vector per unit time for the target region and z2 corresponds to time series data from the source region. ui indicates the direct input to the model while um indicates input from the modulatory variable onto intrinsic pathways specified by the model. Activity in the target region is therefore determined by an additive effect of the intrinsic connectivity with the source region (Az2), the bilinear variable (umBz2, corresponding to the modulatory experimental manipulation), and the effects of direct input into the model (Cui).

A single-condition GLM analysis was conducted (see GLM analysis section) in order to extract time series data from the ROIs. The MNI coordinates of vmPFC activity were the same as those used for PPI analysis (see above). An LOC mask of coordinates containing > 40% probability of the label "lateral occipital cortex, inferior division" was defined using the Harvard-Oxford atlas. Individual subject's MNI coordinates that fell within this mask were specified according to highest T-values from the "positive response" > "negative response" (Hits + FA > Misses + Correct rejects) contrast from the 3-condition GLM analysis described above (see

Table 3). For each ROI, time series data were extracted from a 6 mm diameter sphere around each coordinate and were adjusted for effects of interest.

Model Comparison and Selection: We estimated and compared a set of DCM models that included connections between vmPFC and LOC. Within this set, model parameters were systematically varied with respect to task effects on regions and connections, with the primary goal of determining whether a model that included task-modulated connections between vmPFC and visual cortex was the most likely. Multiple DCM models were evaluated separately for each subject, and random-effects Bayesian model selection (RFX BMS) as implemented in SPM8 was used to identify the optimal model that explained the data. RFX BMS accounts for heterogeneity of model structure across subjects and yields exceedance probabilities, which is the probability that one model is more likely than any other model, given the group data (Stephan et al., 2010). For each connectivity parameter from the optimal model, significance was assessed using a one sample t-test over all subjects. Unless otherwise indicated, there were 14 degrees of freedom for all reported t-values (including those from GLM and ICA analyses).

Tractography analysis: DTI analyses were completed using the FMRIB's software library diffusion toolbox (http://www.fmrib.ox.ac.uk/fsl/) (Smith et al., 2004). As described previously (Behrens et al., 2003), a probability of connectivity map was generated for regions of interest. Briefly, in native diffusion space, the principal diffusion direction (PDD) of non-isotropic water movement was modeled as a tensor for each voxel in the brain (Behrens et al., 2003). Complex fiber structure (i.e. crossing or diverging fibers) increases the uncertainty of the PDD estimate. Bayesian statistics were used to generate probability density functions (pdfs) of PDD uncertainty

allowing for the detection of non-dominant fiber pathways (Behrens et al., 2007). From these pdfs, 5000 tract-following samples were taken with a maximum curvature threshold of +/- 80 degrees and the exclusion of pathways that returned onto themselves.

DTI probabilistic fiber tracking was performed in individual diffusion space, and resulting tracks were then normalized to MNI standard space for visualization purposes. FLIRT (FMRIB's Linear Image Registration Tool) was used to transfer ROIs (and estimated fiber tracks) between subject and standard spaces. Spatially normalized paths were added across all subjects, generating a group representation of individual pathways. A positive (blue) value at each voxel means 50% or more subjects contained at least one streamline (waypoint) passing through that voxel (Fig 5). Note that the group image does not correspond to a map of probabilistic connectivity from the seed to the waypoints mask as presented for individual subjects, but instead represents the importance of each voxel to this pathway with respect to all subjects.

Definition of ROIs: For DTI tractography on 108 subjects (who did not participate in the task), the seed ROI for vmPFC was defined as a 12 mm radius sphere about the peak MNI coordinate for vmPFC [0 62 -4] from the group t-map in IC20 (see Table 2). Bilateral target LOC masks for DTI were defined using 12 mm radius spheres about the peak MNI coordinates from the contrast used to identify object-sensitive LOC in the 15 subjects who had performed the task (left: [--46 -70 -4], right: [46 -68 -10]).

Table 2. Chapter 2: Frontal-occipital Independent Component IC20 (t > 2.25, cluster size > 50)

Region	**L/R**	**BA**	**X**	**Y**	**Z**	**Cluster size (k)**	**t values**
Visual cortex	**L & R**	**7, 17, 18, 19 20, 31, 36, 37, 39, 40**	**-30**	**-90**	**8**	**19,599**	**24.81**
vmPFC	**L & R**	**10, 11**	**0**	**62**	**-4**	**96**	**4.49**
	L		**-4**	**58**	**-14**		**3.82**
LGN	L		-20	-32	-4	115	5.58
Middle temporal gyrus	R	21, 22, 41	54	-24	0	106	3.98
Precentral gyrus	R	6, 8	62	0	40	576	4.34
	L	4, 6	-46	-4	52	650	5.78
Superior parietal lobe	L	7	-22	-68	62	416	4.89

For PPI and effective connectivity (DCM) analyses, vmPFC was defined using individual peak coordinates from each individual's IC20 (μ = [-1.6 56.1 -8.4], stdev = [3.6 5.1 4.1]). For DCM analyses, bilateral LOC was defined for each subject using the coordinate with the maximum T-value from the contrast "positive response" > "negative response" (see GLM analyses section) within the same LOC mask used for DTI analyses above. Table 3 summarizes the ROI definition strategies used for all the analyses.

Table 3. Chapter 2: Source of ROI definitions for PPI, DCM and DTI analyses.

Analysis	ROI	Defined by:	Masked by:	Later-ality	Avg or peak MNI coords (and std)
PPI	vmPFC	IC20 (subject specific)	N/A	N/A	$[\mu_x, \mu_y, \mu_z]$=[-1.6, 56.1, -8.4] $[\sigma_x, \sigma_y, \sigma_z]$=[3.6, 5.1, 4.1]
	LLOC	GLM ROI analysis (subject specific)*	LOC mask - HarvOx 40%	L	$[\mu_x, \mu_y, \mu_z]$=[-51.2, -68, -4.7] & [46.7,-70.5,-6.7] $[\sigma_x, \sigma_y, \sigma_z]$=[6.0, 4.1,5.5] & [5.8,9.6,8.8]
	dlPFC/pre central gyrus	IC20 (group peak)	N/A	R	Peak: [62 0 40], t=4.34
DCM	vmPFC	Same as for PPI			
	LOC	Same as for PPI, but also on right		L & R	
DTI (group)	vmPFC	12 mm radius sphere about peak from IC20	N/A	N/A	Peak: [0 62, -4], t=4.49.
	LOC	12 mm radius sphere about peak from GLM ROI analysis (group average*)	N/A	L & R	Left peak: [-52 -70 -4], t=5.46** Right peak: [46 -68 -10], t=9.02

*Contrast of "positive response" > "negative response" trials (Hits + FA > Misses + Correct Rejects) thresholded at $p < 0.05$ uncorrected, with cluster extent threshold of 30).
N/A = Not applicable.
** To ensure no voxels within ROIs lay outside the brain the center was shifted 3 voxels medially to [-46 -70 -4]

Results

Behavioral results: Overall group mean reaction time (RT) for the task was 6.5 sec (std=2.5) and mean accuracy ((hits+correct rejects)/total trials) was 62.1% (std=20.6). While reaction time increased as target size decreased (reaction time vs. ranked target size, r= -0.77, p=0.02), there was not a significant correlation between accuracy and target size (accuracy vs. target size r=-0.56, p=0.15). Average RT for "positive response" trials was 5.2 s (std=1.98), while average RT for "negative response" trials was 7.87 s (std=1.33).

A cluster within vmPFC is synchronized with primary and association visual areas during visual search: Temporal sorting of ICs derived by spatial-ICA and group statistics of beta values (Table 1) revealed three highly task-related components (Fig2A): 1) IC20, which consisted of primary and association visual areas, LOC, parietal and middle temporal lobe, lateral geniculate nucleus (LGN), superior colliculus, prefrontal cortex and vmPFC, 2) IC17, which consisted of supplementary motor area (SMA), primary motor (M1), thalamus, anterior insula and cerebellum and 3) IC6, which consisted of posterior parietal, prefrontal, and LOC. Two independent components were also significantly anti-correlated to the task: IC25 consisted of the putative 'default network' (posterior cingulate, lateral parietal, and medial prefrontal cortex), and IC23 consisted of lingual and parahippocampal gyrus. In addition to the group T-maps of these five components (Fig2A), their associated time courses averaged over all subjects are shown in Figure 2B.

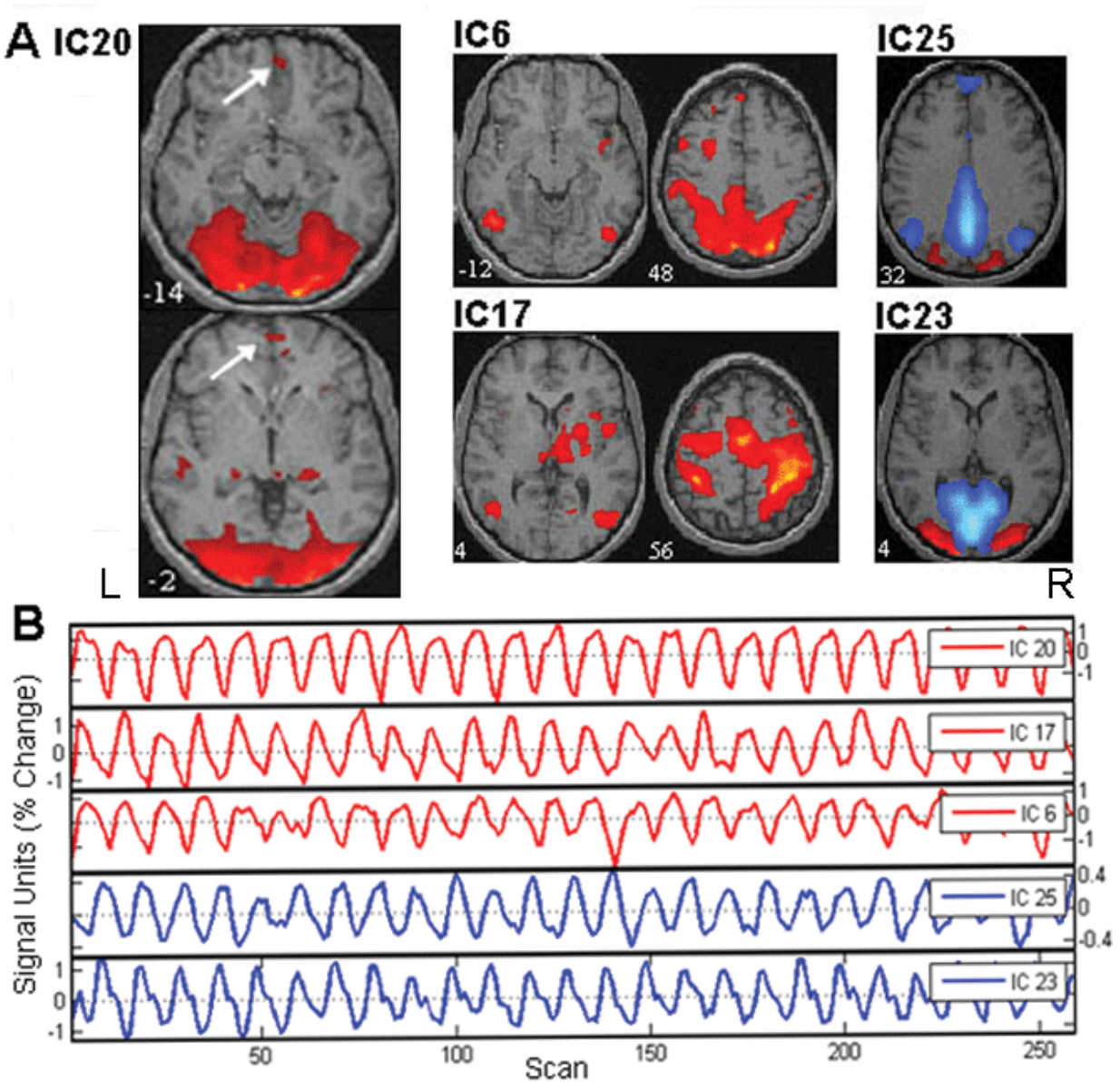

Figure 2. Chapter 2: Search-related spatial independent components. (A) Group t-maps of three ICs most highly correlated to the task (A, red) and the two most anti-correlated to the task (A, blue) and (B) their associated time-courses averaged over all subjects. IC20 consisted of primary and association visual cortex, middle temporal gyrus (MTg) and ventromedial prefrontal cortex (vmPFC, white arrow). IC6 consisted of intra-parietal sulcus and posterior parietal, prefrontal, and lateral occipital cortex. IC17 consisted of SMA, M1, thalamus, cerebellum and lateral occipital cortex. IC23 consisted of the 'default network': posterior cingulate, lateral parietal, dorsal medial frontal cortex and vmPFC. IC25 consisted of lingual and parahippocampal gyrus. All spatial maps were displayed at

t > 2.25, which at 14 d.f. (number of subjects – 1) corresponds to p=0.02 for a one-tailed t-test, and are in Neurological convention (Right=Right).

Given previous reports of ventral and medial prefrontal involvement in expectancy-related visual discrimination tasks (Bar, 2003; Peelen and Kastner, 2011; Summerfield et al., 2006), of particular interest was the appearance and inclusion of a cluster in vmPFC in the most highly task-correlated component (IC20, white arrow in Figure 2 and bold in Table 2), that also included bilateral primary and visual association areas. This observation is consistent with the involvement of vmPFC in visual processing during the visual search task. Based on previous reports that suggest vmPFC is a source of expectancy-related signals (or "predictive codes") and interacts with stimulus-category responsive association visual cortex during the discrimination and perception of face and objects (Bar, 2003; Summerfield et al., 2006), we further tested whether our visual-related vmPFC cluster was functionally connected with object sensitive visual association-cortex during visual search.

vmPFC and LOC are functionally connected during visual search: Based on previous findings that suggest ventral and medial PFC interact with stimulus-category specific visual regions during visual discrimination tasks (Bar, 2003; Summerfield et al., 2006), we hypothesized that vmPFC interacts with object-sensitive LOC during visual search. As there was no independent localizer task for these subjects, we used the contrast positive(Hits + FA) > negative (Misses and Correct Rejections) trials to define object-sensitive LOC for each subject (i.e. visual activity associated the subjective perception of an object). Since vmPFC is not necessarily associated with the perception of objects, but rather the anticipation and expectation of target category features, which should occur on every trial, vmPFC could not be isolated in this same manner.

Instead we relied on ICA to identify the vmPFC cluster whose component was synchronized with visual activity during the task.

We conducted two separate and complementary analyses: 1) we identified which visual areas exhibited increased connectivity with vmPFC during search (described more below) and 2) we located object-sensitive regions in the current design by contrasting "positive response" (i.e. Hits + False Alarms) greater than "negative response" (i.e. Misses and correct rejection) trials to identify regions associated with the perception of the target. We then examined the overlap within visual cortex of the above analyses. For 2) the only significant results in the entirety of visual and visual association cortex, even at a very loose threshold of $p < 0.1$, uncorrected was LOC (left peak at [-52 -70 -4], $t=5.46$, $p < 0.001$, $k=83$; right peak at [46 -68 -10], $t=9.02$, $p < 0.001$, $k=370$). This is consistent with previous evidence that LOC is highly sensitive to object-perception (Grill-Spector et al., 2001; Ishai et al., 2000; Spiridon et al., 2006).

To identify regions that were functionally connected with vmPFC during visual search we performed a PsychoPhysiological (PPI) Interaction analysis, an exploratory approach which identifies regions that are differentially coupled with a particular "seed" region during one conditions vs. another (i.e. searching vs. not-searching). We used each subject's peak w (loading factor from IC20) nearest the vmPFC group peak [2 52 -14] to define the vmPFC coordinates. When the "seed" region was vmPFC, we observed clusters within LOC, but not elsewhere within visual cortex, that were more significantly more coupled with vmPFC during search condition (Figure 3A, circled red). Furthermore, these clusters overlapped regions that were associated with perception of the target in the task (i.e. object-sensitive LOC as defined by the contrast Hits + FA > Misses + Correct Rejections, Figure 3A, circled blue). An ROI analysis (12 mm sphere about peak LOC coordinate in above contrast "Hits + FA > Misses + Correct Rejections")

confirmed that object-sensitive left LOC was significantly more functionally connected with vmPFC during search (t=2.36, p = 0.02), while right LOC failed to reach significance (t=1.18, p=0.13). Event-related averages for the above contrast also reveal that the effect of the perception of the target was stronger in the left LOC (relative to right LOC, Figure 3B). The above results indicate that vmPFC is functionally connected with object-sensitive LOC during visual search.

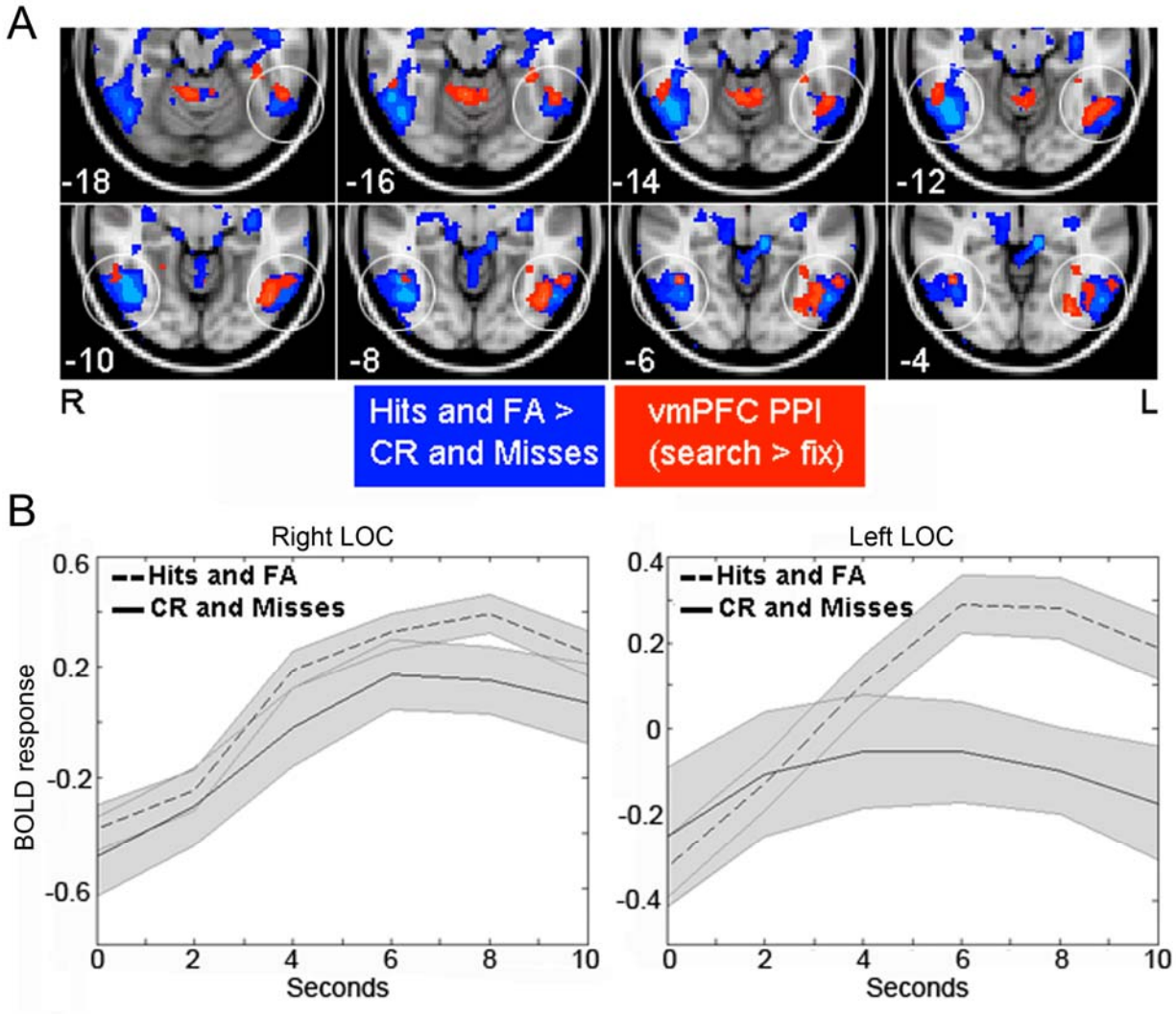

Figure 3. Chapter 2: Functional connectivity between vmPFC and LOC during visual search. (A) Visual regions responsive to the subjective perception of a target (Hits + False Alarms (FA) > Correct Rejections (CR) and Misses) are shown in blue, while visual regions exhibiting greater functional connectivity with vmPFC during visual search

are shown in red (circles indicate overlapping clusters in LOC). For visualization purposes, both statistical maps were threshold at $t > 2.0$. (B) Event-related averages (with 90% CI in shaded grey) for "positive responses" (Hits + FA, dashed lines) and "negative responses" (CR + Misses, solid lines) for left and right LOC.

To further test the relative specificity of the vmPFC-LOC connectivity during visual search, we also conducted the above analyses using another seed region that was also present in IC20 (precentral gyrus/prefrontal cortex, MNI: [62 0 40], Table 2). For this analysis, no cluster within visual cortex survived even a loose threshold ($p < 0.05$ uncorrected, $k=10$), further suggesting that frontal-occipital connectivity during search is relatively specific to the vmPFC. Finally, when LLOC was used as a "seed" region, three clusters survived whole-brain cluster-extent correction at $p < 0.05$ corrected ($p < 0.005$ uncorrected): medial PFC, peak MNI coordinate at [4, 60, 4], $t=4.7$, $k=569$, as well as a cluster in posterior cingulate and anterior middle temporal gyrus (data not shown). Taken together, the above results suggest that connectivity between vmPFC and object-sensitive LOC is preferentially engaged during visual search, and is consistent with the fact that LOC is involved in the anticipation of and search for an object (Peelen and Kastner, 2011). However, this connectivity did not correlate with performance across subjects ($p=0.57$), suggesting this connectivity reflects a neural process that is generally engaged during visual search but is not predictive of overall performance ability in the task.

vmPFC and LOC are effectively connected during visual search: Psychophysiological Interactions (PPI) analyses, a voxel-wise regression approach, were used to test the engagement and relative specificity of vmPFC-LOC frontal-occipital connectivity during visual search.

However, PPI does not measure the directionality of interactions between regions. Therefore we also conducted Dynamic Causal Modeling (DCM) and Bayesian Model Selection (BMS) to infer the directionality of connectivity between vmPFC and LOC and to also provide additional evidence for the existence of effective connectivity between vmPFC (as defined by each subject's IC20) and object-sensitive LOC (as defined above). Given the recently raised technical and theoretical issues regarding DCM and Bayesian Model selection (Lohmann et al., 2012), we present vmPFC-LOC and dlPFC-LOC DCM results primarily as supplementary and as additional confirmation of the above PPI results.

Twenty-one simple DCMs that include vmPFC and bilateral LOC were defined (Fig 4A). The first set of 7 models included the full model (all regions and bidirectional connections modulated by the task) and subsequent variants where task inputs are successively removed from each region. Models 5, 6 and 7 contain no task-modulation of connectivity. The second and third sets of (7) models are structured the same as the first, except that in the first set (8-14) only top-down connections are modeled, and in the second (15-21) only bottom-up connections are modeled. The primary aim of model specification and selection was to determine whether a model that included task-modulated connectivity between vmPFC and LOC was most optimal. Coordinates defining LOC for each subject were informed by the GLM analysis ("positive response" > "negative response" trials) restricted to left and right LOC masks (see methods, Table 3).

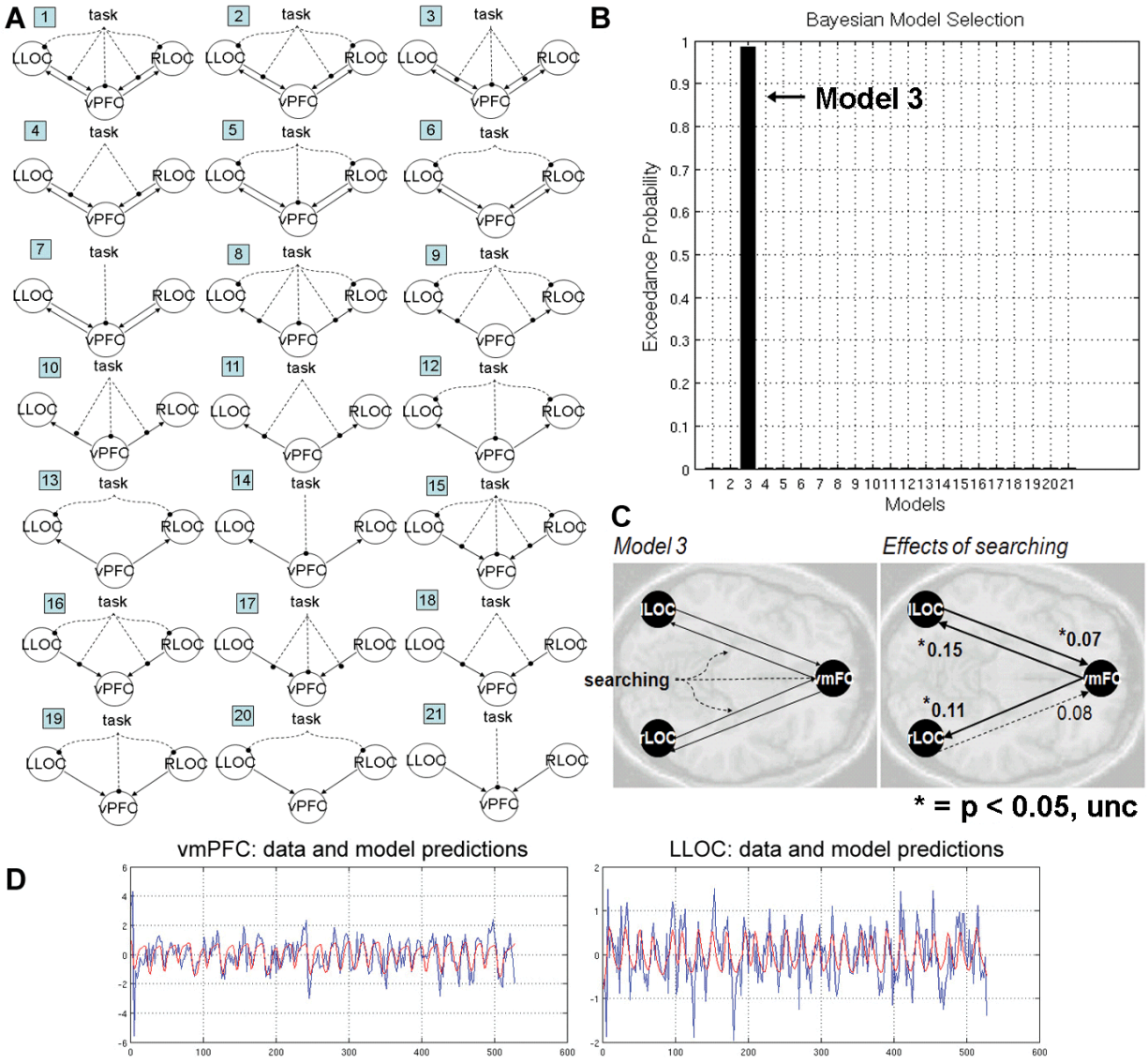

Figure 4. Chapter 2: Effective connectivity between vmPFC and LOC during visual search. (A) Twenty-one Dynamic Causal Models (DCM) that include vmPFC and bilateral LOC and their modulation during the visual search. Models were grouped into sets of 7 in which the 1st set contained bidirectional connections, the 2nd only top-down connections, and the 3rd only bottom up connections. Within each group of 7, models varied with respect to direct inputs and contained task-modulated connectivities (models 1-4), or connectivities that were not modulated by the task (models 5-7). (B) Exceedance probabilities of each model produced by RFX BMS implemented in SPM8. Of these 21 models, model 3 was the most optimal (exceedance probability =0.99). (C) Task-induced connectivity parameters (maximum a posterior estimates, MAP) averaged over subjects are reported for model 3. (Note: correction for multiple comparisons was not applied since there were only four inferences on connection

parameters). (D) Data (blue) and model predictions (red) for Model 3 are shown for vmPFC and RLOC for a representative single subject (S11).

According to Bayesian model selection (BMS, see methods), the most optimal DCM included direct input of the task into vmPFC and bidirectional connections between vmPFC and bilateral LOC that were modulated by the task (exceedance probability = 0.99, Fig 3B and C). The mean exceedance probabilities over all models was 0.05, std=0.21, and the maximum was 0.99. For the optimal model (Model 3), task-induced effective connectivities in both directions between vmPFC and bilateral LOC were positive and significant across all subjects at the $p < 0.05$ level (Fig 3D).

We further tested whether increased frontal effective connectivity with LOC was specific to the vmPFC, in order to help ensure that the estimation of significant connectivity parameters was not a product of relatively few parameters and regions included in our model. For this we reran the above 21 DCMs for 200 iterations, in which vmPFC was replaced with a randomly selected coordinate in the dorsal prefrontal cortex (defined by the AAL masks Frontal_Sup_L, Frontal_Sup_R, Frontal_Sup_Medial_L, Frontal_Sup_Medial_R, Frontal_Mid_L and Frontal_Mid_R in the WFU_Pickatlas). In this "null" distribution, model 3 was still the most optimal model, but the mean exceedance probability was only 0.56 (stdev=0.20, data not shown), while the maximum observed value was 0.96 (as stated above the exceedance probability with vmPFC was 0.99). The mean of the mean exceedance probabilities over all models was 0.05, std=0.13, and the maximum was 0.56. For model 3, and for each of our 200 null iterations, we conducted one-sample t-tests overall all subjects and generated a null distribution of t-scores for each of four connectivity parameters (bidirectional connections between a frontal region and left

and right LOC). The mean t-values of these four connectivity parameters fell between the range of t = -0.48 to t = 0.40. We ascribed nonparametric p-values (npp) to the t-values observed for each connectivity parameter when using vmPFC as a frontal node based on the observed frequency of greater t-values when using a random dorsal prefrontal region: vmPFC->lLOC, t=2.62, npp=0.02, vmPFC->rLOC,t=2.41, npp=0.04, lLOC->vmPFC, t=2.24, npp < 0.005, rLOC->vmPFC, t=1.65, npp=0.065. Taken together, the above results indicate that increase effective connectivity with the LOC was relatively specific to the vmPFC.

Structural connectivity between vmPFC and LOC: Although strong effective and functional interactions may still occur without direct anatomical connectivity, it is assumed that anatomical connectivity data is important in guiding the construction of neurobiologically realistic models of effective connectivity (Stephan et al., 2010). Therefore we also tested the extent of structural connectivity between vmPFC and LOC. It should be noted that DTI does not necessarily assess direct anatomical connectivity, and the observed structural paths may be polysynaptic. For DTI analyses, seed and target masks were created from 12 mm radius spheres about the peak coordinate for vmPFC from IC20 (table 2) and bilateral LOC as defined above (i.e from the contrast Hits+False Alarms > Misses and correct rejections, see table 3). Structural paths between vmPFC and left and right LOC for 108 subjects who did not complete the task are shown in Fig 5. These findings confirm substantial white-matter connectivity between vmPFC and (particularly left) LOC. The DTI results are based on a large sample of subjects, most of which did not perform the task. Since only 6 of the subjects who actually performed the task also acquired DTI scans, association of the integrity of this and other tracts with performance and/or functional connectivity measures is not possible in this study.

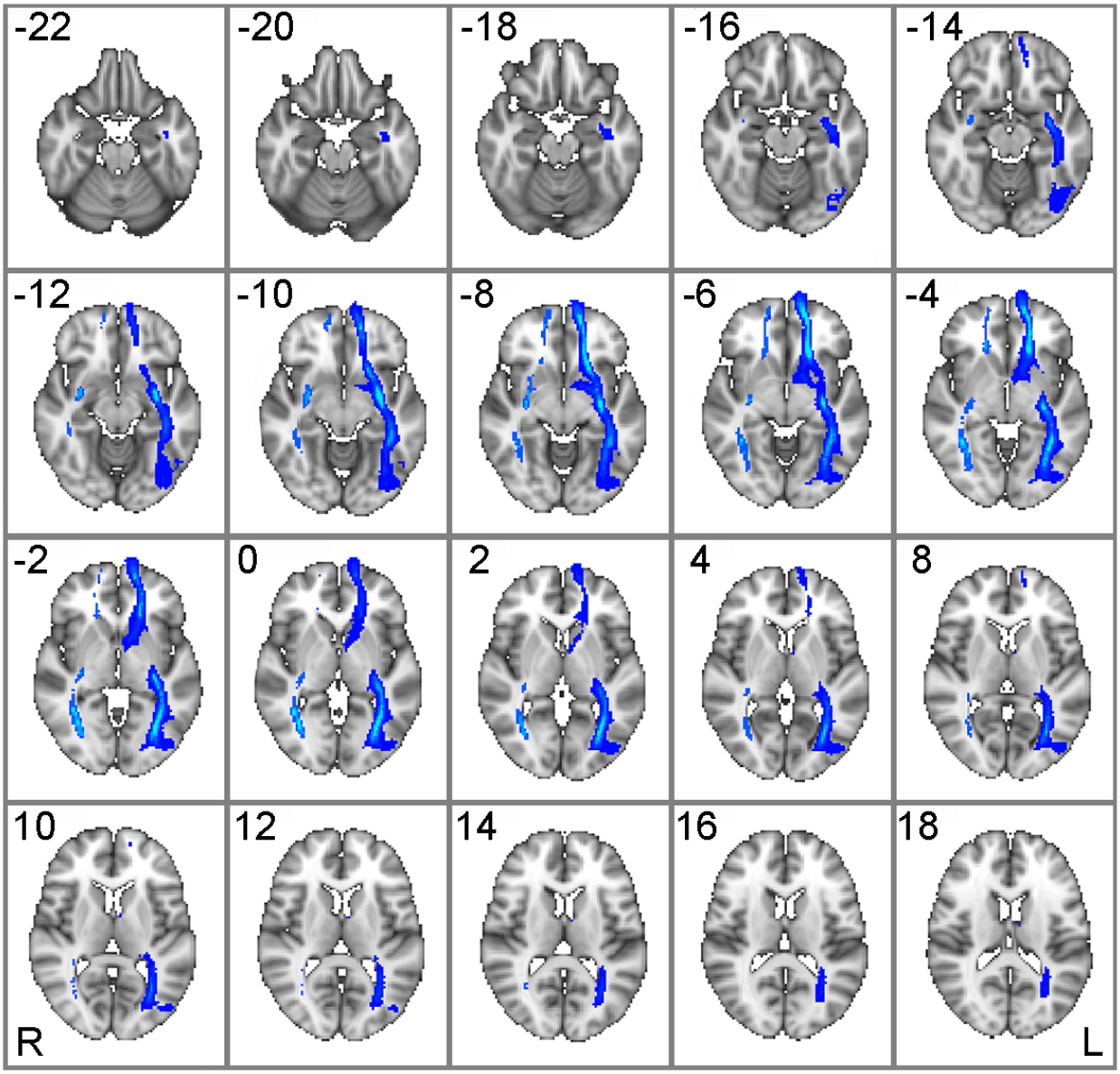

Figure 5. Chapter 2: White matter paths between vmPFC and bilateral LOC. (A) White matter paths for 108 subjects that did not participate in the task. The vmPFC ROI was defined by 12 mm radius sphere about the peak coordinate from the group IC20 t-map [0 62 4], and bilateral LOC was defined by 12 mm radius spheres about peak coordinates for object-sensitive LOC (left: [--46 -70 -4], right: [46 -68 -10], see table 3). Paths were thresholded to show voxels in which 50% or more subjects exhibited at least one or more waypoints from vmPFC to LOC (the maximum streamlines in the left pathway was 42, while the right pathway was 3). Maps are in Radiological convention (right=left, and top left numbers in each panel indicate z MNI coordinate.

Discussion

Here we show that 1) vmPFC is correlated with visual activity involved in search for an object embedded within a complex scene 2) there is bi-directional, positive functional and effective connectivity between vmPFC and LOC during the search task and 3) there exist white matter tracts between these interacting regions. These findings provide evidence of structural paths underlying task-related functional interactions between vmPFC and object-sensitive regions (LOC) during visual search.

A recent and related study applied search-light and multivoxel pattern analysis to reveal that activity patterns within the medial prefrontal cortex (whose peak MNI coordinates – [2, 43, 5] - were very close to ours, [0, 62, -4]) as well object-sensitive LOC showed a significant category-specific cue effect in anticipation of visual search for people or cars in subsequent briefly presented (100 ms) natural scenes (Peelen and Kastner, 2011). The authors conclude that medial prefrontal cortex may constitute a top-down source of preparatory activity observed in object-sensitive LOC. Here we extend these findings with the demonstration of increased effective connectivity between these regions during extended visual search lasting approximately 4-10 seconds.

To the authors' knowledge, this study is the first to characterize functionally-seeded, probabilistic white-matter paths between vmPFC and object-sensitive LOC. We propose that these structural paths underlie the observed fronto-occipital functional interactions during visual search. It is suggested that the vmPFC and its projections to visual cortex may mediate expectancy-related, stimulus-specific attentional mechanisms during visual discrimination and search, and may be more or less an enhanced feature of the human brain.

A recent DTI study used a spatial attention task to determine visuospatial attention-related regions of interest (ROIs) to functionally seed DTI analyses of a visuospatial attention network (Umarova et al., 2010). Dorsal connections that link temporoparietal cortex with frontal eye fields and area 44 of the inferior frontal gyrus (IFG) were described as well as the ventral connections, which traveled in the white matter between insular cortex and putamen parallel to the sylvian fissure. However, while this study used fMRI to inform structural DTI analyses, they did not focus on ventral prefrontal-occipital pathways.

Our observation of bidirectional positive effective connectivity between vmPFC and LOC during the search task is consistent with the theory of predictive coding, which postulates that bottom-up, degenerate sensory information is matched with top-down expectations (Mumford, 1992; Rosen et al., 1999), and that bottom-up and top-down analyses appear to occur in the cortex simultaneously (Grossberg, 1980; Lee and Mumford, 2003)friston 2002. Top-down modulation of visual processing during face recognition has been shown to involve positive effective connectivity between vmPFC and a fusiform area responsive to faces (FFA) during a face detection task (Summerfield et al., 2006). Similar top-down projections from orbital frontal cortex during object recognition have been shown using fMRI combined with magnetic encephalography (MEG) (Fenske et al., 2006b). These and other studies have also suggested that "bottom-up", coarse visual information is rapidly projected to areas within vmPFC in order to form an initial template for predictive codes that are subsequently projected to object-sensitive and face-sensitive visual processing regions during matching with more detailed bottom-up information.

Spatial-ICA extracted several independent spatial components that were significantly correlated to the task. IC25 was anticorrelated with the task and contained the putative default-

mode network (Greicius et al., 2003; Raichle et al., 2001), and IC23 contained task-related deactivation of the lingual and parahippocampal gyrus. IC6 contained an attentional, or 'task-positive' (Fransson, 2006; Kennedy and Courchesne, 2008) fronto-parietal network made up of parietal lobule, dorsolateral prefrontal cortex and tempero-occipital lobe. These areas are assumed to be associated with the mediation of spatial selective attention (Dosenbach et al., 2007; Hahn et al., 2006; Lawrence et al., 2003), as well as executive attention and cognitive control (Dosenbach et al., 2007). IC17 consisted of supplementary premotor and motor areas, thalamus and cerebellum and are consistent with spatial orienting, and saccade and response execution during the task (Ploran et al., 2007; Rosen et al., 1999; Seeley et al., 2007). The most highly task-related spatial component (IC20), which had the highest R2 value (0.41) from temporal sorting using the canonical HRF as a reference function, contained early visual areas (bilateral LGN, V1/V2/V3/V4), association visual areas (LOC, fusiform gyrus), ventral and dorsal stream visual areas (middle temporal and posterior parietal cortex), superior colliculus, SMA, M1 and vmPFC.

Conclusion: In the present study we employed a multivariate analysis of fMRI data obtained during a natural search and detection task to isolate a highly task related component that contained primary and association visual areas as well as vmPFC. The functional and structural connectivity of this visual and search-related vmPFC cluster with object-sensitive visual areas was tested using functional (PPI), effective (DCM) and structural (DTI) connectivity analyses. These analyses revealed increased functional and effective connectivity between vmPFC and LOC during visual search, as well as substantial white matter connectivity between them. These

data suggest a role of vmPFC during visual search which involves functional interactions with object-sensitive visual regions.

CHAPTER 3

DYNAMIC COUPLING BETWEEN VISUAL CORTEX, DEFAULT MODE AND FRONTOPARIETAL NETWORKS DURING BISTABLE PERCEPTION[2]

Summary

Mutually exclusive bistable percepts, referred to as "default" and "alternative", elicited by the well-known Schroeder Staircase figure differentially engaged the Default Mode Network and the FrontoParietal Network, respectively, during functional magnetic resonance imaging. These two networks exhibited percept-dependent cross-interactions and connectivity with the visual cortex. Interestingly, both visual cortex and FrontoParietal Network exhibited higher connectivity with the Default Mode Network during the "alternative" percept, suggesting increased coupling between incoming visual information and externally-oriented attentional control with internally-oriented processing and mental imagery. These findings advance neural models of bistable perception by implicating the default mode and frontoparietal networks during image segmentation.

Introduction

The mechanism by which the neural correlates of human vision segregate and bind features to form unified percepts from a complex visual world is a long standing central question that has also been linked to more general questions related to the neural correlates of awareness and consciousness (Leopold and Logothetis, 1999; Sterzer et al., 2009). A bistable figure presents a unique opportunity to investigate mechanisms involved in segmentation of visual input because one stimulus elicits two mutually exclusive percepts representing alternative organizations of the same visual input. Although neuroimaging studies have previously

[2] Karten, Ariel, Spiro Pantazatos, David Khalil, Xian Zhang, and Joy Hirsch. 2013. Dynamic Coupling between the Lateral Occipital Cortex, Default Mode and Frontoparietal Networks During Bistable Perception. *Brain Connect.*

confirmed the involvement of parietal and frontal brain regions in bistable perception (Kleinschmidt et al., 1998), there is no established framework to describe the underlying neural mechanisms of image segmentation.

In this study, fMRI was employed to identify neural substrates engaged during each of the mutually exclusive percepts elicited by a common bistable figure, the Schroeder Staircase (Fig 6). In the "default" percept the staircase is readily perceived as a normal staircase whereas in the "alternative" percept the staircase is less readily perceived and is seen as an inverted staircase. As is typical with bistable figures, the two percepts differ with respect to the volitional effort and attention required for their realization and maintenance and this variation suggests a putative role for the attentional control networks during percept maintenance. Prior investigations of bistable perception have considered the role that attention and the frontoparietal network (FPN) plays in forming and in switching between each of the percepts (Knapen et al., 2011; Meng and Tong, 2004; Slotnick and Yantis, 2005)}}. In this study we tested the hypotheses that FPN would exhibit increased connectivity with the visual processing stream (i.e. visual cortex) during maintenance of the "alternative" percept of the Schroeder Staircase figure. Suprisingly we instead observed increased connectivity of visual cortex with default mode network (DMN). To the authors' knowledge this is first implication of the default mode network during image segmentation.

The DMN, sometimes referred to as the task negative network, consists of temporal and midline structures that are more active during rest than during a task (Buckner et al., 2008; Greicius et al., 2003; Gusnard et al., 2001), and has been associated with internal stimuli or self-reflection as well as memory of past events (Andrews-Hanna, 2012). The FPN, sometimes referred to as the task-positive network, consists of dorsal and frontal regions, and is associated

with tasks that require attention to external stimuli (Corbetta and Shulman, 2002; Dosenbach et al., 2007; Kastner and Ungerleider, 2000). These two networks have also been identified on the basis of spontaneous correlations during resting states characterized by anti-correlations between them (Anderson et al., 2011; Fox et al., 2005) suggesting an intrinsic oppositional functional organization of neural processes that mediate cognitive tasks.

Methods

Subjects: A total of 12 volunteers participated in the functional imaging study (8 males and 4 females; ages 18-27 mean = 22.8). All subjects were informed about possible risks and provided consent according to the guidelines established by the Columbia University Institutional Review Board.

Stimulus: The stimulus was a black and white line drawing of a common bistable figure (Fig6) referred to as the Schroeder Staircase. The figure can be perceived as either a normal right-side up staircase, or an inverted upside-down staircase.

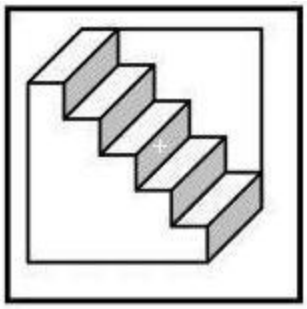

Figure 6. Chapter 3: Bistable Schroedinger staircase. Normal (default percept) and upside-down (alternative-percept) staircase.

Functional Imaging Procedures: The functional study was run as a block design in which the stimulus was presented for 12 fifteen second epochs, each of which was preceded by a fifteen

second baseline epoch that featured a black screen with a crosshair (+). Prior to scanning, the "default" and the "alternative" percepts were determined for each subject based on the percept that the subject reported as seen first and most automatically. For all subjects the "default" percept was the right-side up staircase most resembling a familiar staircase, and the "alternative" percept was the up-side down staircase that appears to be suspended in midair. The subject was instructed to hold the "default" percept for the first 15-second stimulus epoch, and then instructed to switch and hold the "alternative" percept for the following 15-second stimulus epoch, and to continue this alternation for the rest of the 6.0 minute run. The percepts were cued by indications of the targeted percept name (alternative or default) above the image, and the subjects were given a keypad to indicate the actual engaged percept and whenever a perceptual switch (voluntary or otherwise) occurred. Subjects practiced outside the scanner until they felt comfortable with this perceptual task.

Image Acquisition and Analysis: Functional images were acquired on a 1.5T GE MRI scanner located in the Columbia University fMRI Research Center, New York, NY. Whole brain Ecoplanar functional images (EPI) were collected with an 8 channel GE head coil in 25 contiguous axial slices obtained parallel to the AC/PC line (TR=3000 ms, TE=35 ms, Flip angle=84 degrees, FoV=19.2 x 19.2, Array Size=128 x 128, Spatial Resolution=1.5 x 1.5 x 4.5 mm). One hundred and twenty whole brain images were acquired during each of two 6-minute runs. High-resolution 3-D anatomical scans were also acquired with a T1-weighted SPGR sequence (TR=19 ms, TE=5 ms, Flip angle=20 degrees) FoV=220 x 200mm, A slice thickness of 1.5 mm, in-plane resolution of 0.86 x 0.86 mm, and 124 slices per image.

Image pre-processing and statistical analysis employed SPM5 software (Wellcome Department of Cognitive Neurology, University College London, UK). Functional T2*-images were slice-timing corrected and spatially realigned to the first volume of the first run. The SPGR scans were co-registered with the mean realigned EPI image, and normalization parameters to a standard T1 template image were computed, and combined realignment, inverse co-registration normalization parameters were applied to the functional images. Finally, images were smoothed with a Gaussian kernel of 8.0 x 8.0 x 8.0 mm full-width half-maximum, and a 128 s temporal high-pass filter was applied.

GLM analysis: Statistical analysis of the BOLD signal aimed to locate activity associated with each perspective. Perceptual onset times (according to subjects' button presses) for the "default" and "alternative" percepts were convolved with the canonical hemodynamic response function (HRF). Contrasts of resulting beta estimates ("Default">"Alternative" and "Alternative">"Default"), for each run separately (for independent ROI analyses, see below), averaged across both runs, and were passed to 2nd level random effects (RFX) analyses (one-sample t-tests). Beta estimates from each run were also passed to a 2nd level RFX analysis (paired t-test) in order to determine conjoined activation and deactivation common to both percepts in run 1, used for independent ROI analyses (see below).

PsychoPhysiological Interaction (PPI) analysis: The PPI analysis measures the extent to which regions are differentially correlated during a given task (Friston et al., 1997). Visual cortex, the primary seed-of-interest, was defined by the conjunction of "alternative" and "default" activity, at peak MNI coordinates for right [40 -70 -8] and left [-38, -78 -6], thresholded at $p < 0.0001$,

uncorrected corresponding to the lateral occipital complex. Activity was extracted from 6 mm spheres centered at the above coordinate locations. The BOLD signal throughout the whole-brain was then regressed on a voxel-wise basis against the product of this time course and the vector of the psychological variable of interest, (1*Default + -1*Alternative), with the physiological and the psychological variables serving as regressors of no interest. Resulting beta maps, within each run and averaged across both runs, were subsequently passed to 2nd level random effects analysis (one sample t-test). Results for left and right seeds were similar; hence the main text depicts results using the bilateral seed. GLM models that were used to extract seed region activity and to estimate PPI results included additional nuisance regressors, i.e. 6 motion parameters, mean white-matter, and mean csf signal.

Independent ROI analysis: To test whether the DMN and FPN were significantly more active and functionally connected with visual cortex during one percept vs. the other, we conducted an independent ROI analysis using the Marsbar Toolbox (http://marsbar.sourceforge.net/). For this, the FPN and DMN were defined using conjunction of both "default" and "alternative" conditions from Run 1 of each subject. These beta estimates were input to a 2^{nd} level RFX analysis (paired 2-sample t-test) in which positive and negative conjunction contrasts, thresholded at $p<0.0001$, uncorrected, defined the independent FPN and DMN ROIs. Contrast values (or beta estimates from PPI analyses) of "Default-Alternative" from Run 2 of each subject were then averaged over all voxels within the above ROIs, and submitted to two separate 2nd level RFX analysis (one-sample t-tests, one for each ROI).

Results

Activation results: Blood Oxygen Level Dependent (BOLD) signal in regions consistent with the DMN was relatively lower during the "alternative" percept ("default > alternative", Fig 7a), whereas signal in regions consistent with the FPN was relatively higher during the alternative percept ("alternative > default", Fig 7b). In particular, the "default > alternative" perspective contrast included the middle temporal cortex (mTC), anterior cingulate cortex (ACC), posterior cingulate cortex (PCC), inferior parietal lobule (IPL), medial prefrontal cortex (MPFC), lateral prefrontal cortex (LPFC), and precuneus (PC), which have been previously associated with the DMN (Raichle et al., 2001). In comparison, the "alternative > default" contrast include the lateral occipital cortex (LOC), middle occipital cortex (mOC), inferior frontal cortex (IFC), inferior parietal lobule (IPL), superior parietal lobule (SPL), middle frontal gyrus (mFG), and supplementary motor area (SMA), which have previously been associated with the FPN (Corbetta and Shulman, 2002). An independent ROI analysis confirmed that activation of the DMN, as a whole, was significantly greater during the "default" perspective ("default" > "alternative, $t=2.29$, $p<0.05$), while activation of the FPN, as a whole, was significantly greater during the "alternative" perspective ("alternative" > "default", $t=2.01$, $p<0.05$) (See Methods).

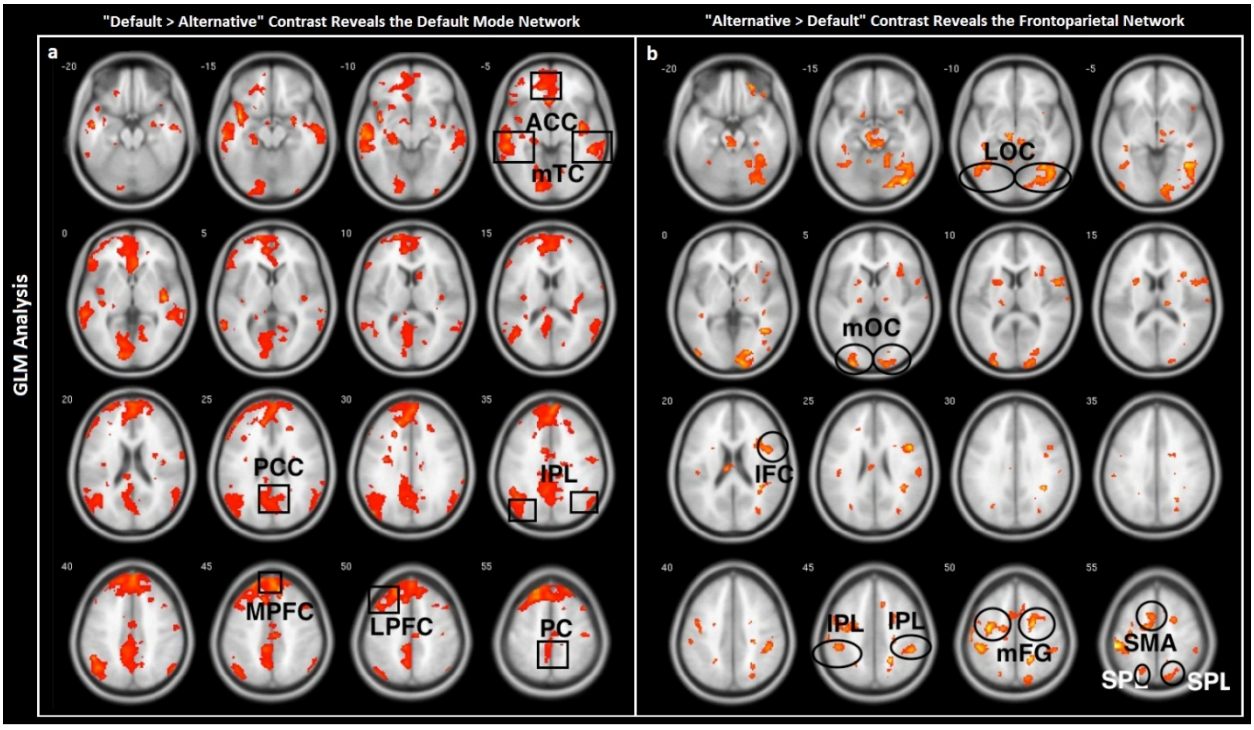

Figure 7. Chapter 3: Activation differences between "default" and "alternative" percepts. For display purposes maps are loosely threshold at $p<0.05$ uncorrected, $k=10$.

Functional connectivity with visual cortex: Whole-brain functional connectivity with bottom up visual processing stream (i.e. association visual cortex) was explored to distinguish between two possible models of interactions. In one model, the positive correlation model, incoming visual information is expected to be positively correlated with the attentional control network (i.e. FPN) during the "alternative" percept, consistent with the notions of increased attentional resources being devoted to processing of the visual stimulus. An alternative, and initially counter intuitive anti-correlation model, predicts that incoming visual information would decouple from the FPN, consistent with the notion of decreased external attentional resources being devoted to processing bottom-up visual information.

PPI analysis of connectivity between visual cortex and all other brain regions was employed to test these alternative models, and revealed findings consistent with the anti-correlation model; namely visual cortex decoupled from the FPN ("default" > "alternative", Fig 8a) and instead increased coupling with the DMN, (vmPFC in particular, "alternative > default, Fig 8b). An independent ROI analysis confirmed that connectivity with the FPN was significantly greater during the "default" perspective ("default" > "alternative, $t=4.80$, $p<0.05$), while connectivity with the DMN was greater during the "alternative" perspective ("alternative">"default", $t=5.39$, $p<0.05$) (See Methods).

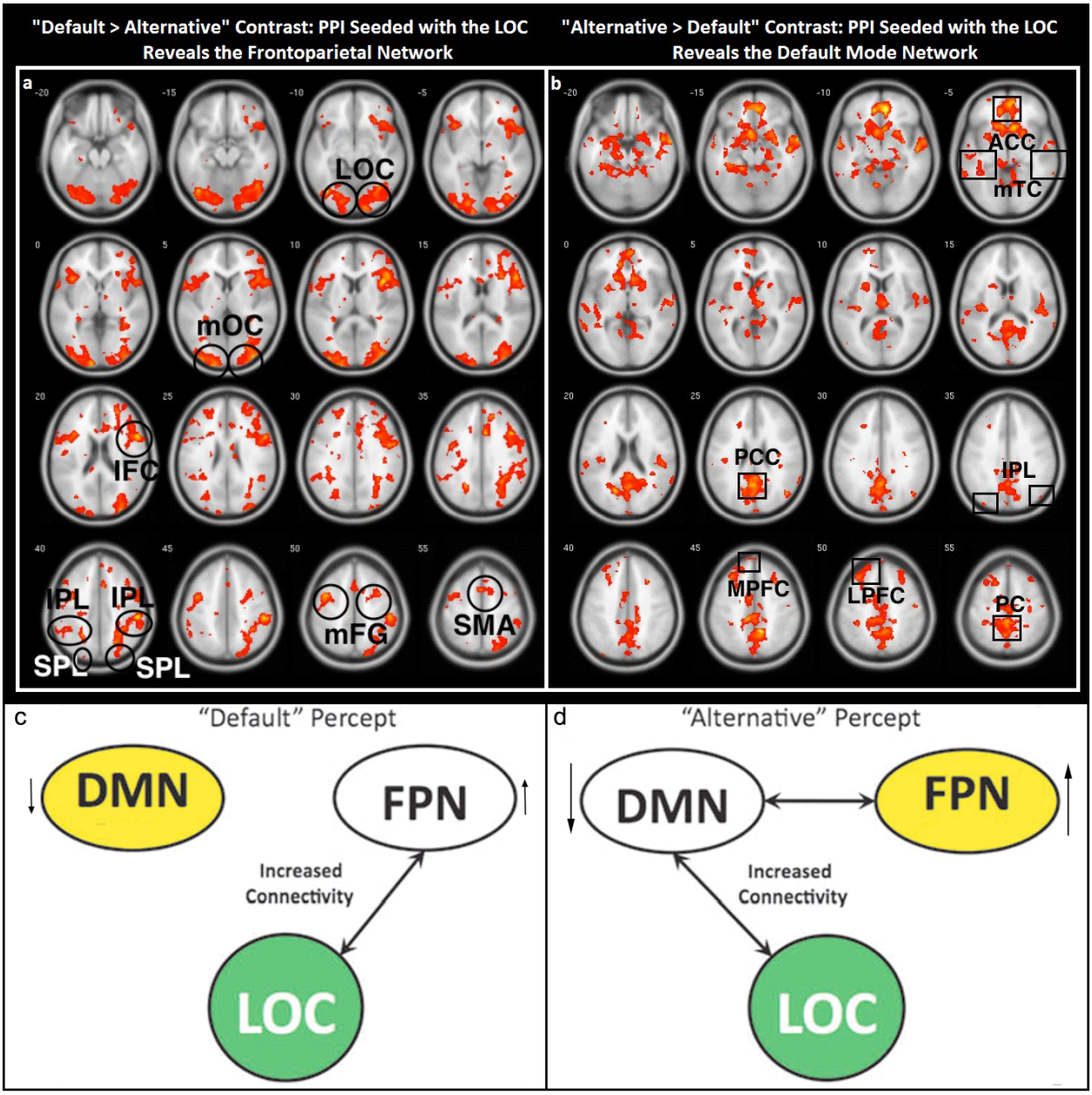

Figure 8. Chapter 3: Functional connectivity of visual cortex during default and alternative percepts. (A) The visual cortex (lateral occipital cortex) exhibited greater coupling with FPN regions during the "default" percept. (B) The visual cortex (lateral occipital cortex) exhibited greater coupling with DMN regions during the "alternative" percept. For display purposes, maps were thresholded at $p<0.05$, uncorrected, $k=10$. Note: for "default" > "alternative", core nodes of the DMN, vmPFC and PCC, survived cluster-extent threshold at $p<0.05$ corrected). (Lower panels) A conceptual summary of findings. (c) During the conscious default percept, functional connectivity increased between the LOC and the FPN. There was no evidence for cross network connectivity during this percept. (b)

During the conscious alternative percept, as revealed by the alternative > default contrast, the FPN was more engaged, while DMN de-activated even further, and the functional connectivity increased between the LOC and the DMN. Additionally, functional connectivity between the FPN and DMN was observed in this condition.

Connectivity between FPN and DMN: In addition to the connectivity between the visual cortex and the two networks, the connectivity between the DMN and FPN was also investigated using PPI analysis in order to observe possible cross-network connectivity and dynamic coupling. During the "default" relative to "alternative" percept, both the DMN and the FPN exhibited higher connectivity within their respective networks. Independent ROI analyses confirmed that connectivity within each network was significantly greater during the "default" perspective ("default" > "alternative, DMN $t=4.45$, $p<0.05$ and FPN $t=6.58$, $p<0.05$). During the "alternative" percept however, the two networks increased their connectivity to each other and the DMN was more connected to the FPN and the FPN was more connected to the DMN (data not shown). This "cross-network" connectivity that was observed most prominently during the "alternative" perspective was also confirmed by independent ROI analyses ("alternative">"default", DMN connectivity with FPN seed, $t=3.63$, $p<0.05$ and FPN connectivity with DMN seed $t=5.33$, $p<0.05$). In general, during the "default" percept, the individual networks tended to be more connected within themselves, whereas during the "alternative" percept, within-network connectivity decreased whilst cross-network functional connectivity increased.

Discussion

Here we show that bistable perception of the Shrodinger staircase differentially engages the FPN and DMN. Furthermore both visual cortex and FPN decouple from the FPN and increased coupling with the DMN (particular ACC/vmPFC and PCC) during the “alternative” percept (an upside down staircase in the case of the Schrodinger staircase). Increased coupling between association visual areas that process object recognition (LOC) with core components of the DMN such as vmPFC has been previously associated with visual imagery (Mechelli et al., 2004) and goal-oriented visual perception (Bar, 2003; Pantazatos, Yanagihara et al., 2012; Summerfield et al., 2006), implicating similar processes during bistable perception, and in particular the percept that is more "effortful" to maintain.

At rest FPN and DMN are anticorrelated; in particular activity in vmPFC is anti-correlated with parietal visual spatial and temporal attention networks, whereas PPC negatively predicts activity within with prefrontal-based motor control circuits (Uddin et al., 2009). FPN and DMN are also anti-correlated during performance of externally-oriented attention tasks; in fact individuals who displayed greater anti-correlation (phase closer to 180 degrees) between DMN and FPN exhibited greater consistency in behavioral performance during an externally oriented attention task (Eriksen flanker task) (Kelly et al., 2008). In addition a recent study observed that DMN and components of the FPN are positively correlated during performance of an internally oriented mental planning task, while uncorrelated during an externally-oriented mental planning task (Spreng et al., 2010). In the context of the current study, the above results suggest that the “alternative” percept engages neural processes related to internally oriented goals. In the case of the Shrodinger Staircase, the “alternative” percent is an upside down staircase (i.e. a relatively unfamiliar stimulus not normally encountered in one’s daily environment), and we speculate that the viewer is “shutting down” processes that treat a stimulus

as “externally-generated” (i.e. a functional staircase normally encountered in an everyday environment) and instead engage processes that “internally-generate” a percept that is less familiar to the viewer.

A conceptual summary of our findings is presented in Fig 3c and Fig 3d. The LOC (Fig. 3–green) was more highly correlated with FPN during the “default” percept (Fig 3c) and more highly correlated with the DMN during the alternative percept (Fig 3d). In addition, during the alternative percept, FPN BOLD activity increased, while DMN BOLD signal decreased even further. Variations in concurrent deactivations of irrelevant sensory input have been associated with a suppressive mechanism (Amedi et al., 2005; Shmuel et al., 2002; Wade, 2002). Accordingly, our finding of increased connectivity between the FPN and the deactivated DMN suggests that the FPN may suppress DMN activity during the alternative percept.

Variations in connectivity of association visual regions with FPN and DMN have previously been reported depending upon volitional (top-down) goals (Chadick and Gazzaley, 2011). Each visual stimulus in the task contained two superimposed objects from different stimulus categories (i.e. a face and a scene). When the scene stimulus was relevant to the task (i.e. visual activity in place-responsive regions (parahippocampal place area, PPA) was enhanced while connectivity with the FPN increased, whereas when the scene stimulus was irrelevant, activity of the PPA was suppressed while functional connectivity with the DMN increased. In the current study a (single) bistable image was presented, and the following pattern was observed: during the “alternative” percept when activity LOC was relative higher (Fig 6b), connectivity with the DMN increased. This may reflect the possibility that, instead of being up-regulated or suppressed for the purposes of an externally-oriented task goal, visual cortex increased engaging

with DMN reflecting increased integration of visual sensory information with internally-oriented mental imagery processes.

Recent EEG findings have reported that neural activity precedes the perceptual emergence of the "hidden" percept (Britz et al., 2009). While previously proposed models for bistable perception suggest that "fatigue" or "satiation" of the conscious percept allows for the subconscious percept to be expressed (Toppino and Long, 1987). Our data further suggest that these active stages of percept maintenance involve dynamic coupling between low and high levels of visual information processing and large-scale networks including the DMN. These new findings can be interpreted as reflecting a balance between suppressive and active interactions between the FPN and DMN networks and the visual cortex. Together, the cross-network and the visual cortex connectivity observed in this study are consistent with a model where active image segmentation is mediated by both suppressive and active top-down mechanisms originating with the DMN and FPN that may regulate and/or preferentially integrate with incoming visual information.

CHAPTER 4

DECODING UNATTENDED FEARFUL FACES WITH WHOLE-BRAIN CORRELATIONS: AN APPROACH TO IDENTIFY CONDITION-DEPENDENT LARGE-SCALE FUNCTIONAL CONNECTIVITY[3]

Summary

Processing of unattended threat-related stimuli, such as fearful faces, has been previously examined using group functional magnetic resonance (fMRI) approaches. However, the identification of features of brain activity containing sufficient information to decode, or "brain-read", unattended (implicit) fear perception remains an active research goal. Here we test the hypothesis that patterns of large-scale functional connectivity (FC) decode the emotional expression of implicitly perceived faces within single individuals using training data from separate subjects. fMRI and a blocked design were used to acquire BOLD signals during implicit (task-unrelated) presentation of fearful and neutral faces. A pattern classifier (linear kernel Support Vector Machine, or SVM) with linear filter feature selection used pair-wise FC as features to predict the emotional expression of implicitly presented faces. We plotted classification accuracy vs. number of top N selected features and observed that significantly higher than chance accuracies (between 90-100%) were achieved with 15-40 features. During fearful face presentation, the most informative and positively modulated FC was between angular gyrus and hippocampus, while the greatest overall contributing region was the thalamus, with positively modulated connections to bilateral middle temporal gyrus and insula. Other FCs that predicted fear included superior-occipital and parietal regions, cerebellum and prefrontal cortex. By comparison, patterns of spatial activity (as opposed to interactivity) were relatively uninformative in decoding implicit fear. These findings indicate that whole-brain patterns of

[3] Pantazatos, Spiro P, Ardesheer Talati, Paul Pavlidis, and Joy Hirsch. 2012a. Decoding unattended fearful faces with whole-brain correlations: an approach to identify condition-dependent large-scale functional connectivity. *PLoS Comput. Biol.*

interactivity are a sensitive and informative signature of unattended fearful emotion processing. At the same time, we demonstrate and propose a sensitive and exploratory approach for the identification of large-scale, condition-dependent FC. In contrast to model-based, group approaches, the current approach does not discount the multivariate, joint responses of multiple functional connections and is not hampered by signal loss and the need for multiple comparisons correction.

Introduction

Faces with a fearful expression are thought to signal the presence of a significant, yet undetermined source of danger within the environment, or 'ambiguous threat' (Ewbank et al., 2009). Evidence from fMRI and evoked potentials (ERPs) suggest that fearful face processing can strongly affect brain systems responsible for face recognition and memory during implicit (consciously perceived but unattended) presentation of these stimuli (Vuilleumier et al., 2002; Vuilleumier and Pourtois, 2007). Group-based fMRI studies have shown that the perception and processing of facial emotional expression engages multiple brain regions including the fusiform gyrus, superior temporal sulcus, thalamus, as well as affect-processing regions such as amygdala, insula, anterior cingulate cortex among others (Adolphs et al., 2003; Haxby et al., 2000; Ishai et al., 2005; Pessoa et al., 2002). However, to the authors' knowledge, no study to date has identified features of brain activity that contain sufficient information to reliably decode, or "brain-read", the threat-related emotional expression of unattended (implicitly perceived) faces within individual subjects. The identification of such features, though less well quantified as in group model-based studies, would have a greater capacity for representing distinctions between different cognitive-emotional perceptual states (Norman et al., 2006), and hence could contribute

in advancing our understanding of the neural mechanisms that underlie threat detection and facial emotion processing.

Most group fMRI approaches that have studied the neural correlates of emotional face perception have relied on univariate approaches (Bishop et al., 2007; Etkin et al., 2004; Haas et al., 2009) which identify regions correlated with a regressor-of-interest, but ignores any interactions with other regions. Bivariate approaches have been applied, but assess the interactivity (functional connectivity) of only one seed region (usually amygdala) with the rest of the brain (Etkin et al., 2006; Pezawas et al., 2005). Even though several notable studies have taken a multivariate approach in assessing the effective connectivity among multiple brain regions during emotional face processing (Fairhall and Ishai, 2007; Ishai, 2008; Stein et al., 2007), a limited number of nodes were included in the networks and they were selected based on a priori anatomical knowledge or on their activation in conventional, General Linear Model (GLM)-based mass univariate analyses. However, univariate GLM approaches make strong assumptions about the hemodynamic response (i.e. sustained periods of activation or deactivation relative to baseline), while functional connectivity offers a complementary and more data-driven and exploratory measure that makes use of temporal correlations to estimate functional connectivity (Li et al., 2009).

There has been a recent surge of interest in examining the large-scale (i.e. pair-wise connectivity throughout the whole-brain) functional network architecture of the brain as a function of various cognitive processes or individual variation (Smith et al., 2011). This is often done by first defining a set of functional "nodes" based on spatial ROIs and then conducting a connectivity analysis between the nodes based on their FMRI timeseries. Large-scale functional connectivity patterns have been successful in predicting age (Dosenbach et al., 2010a) as well as

subject-driven mental states such as memory retrieval, silent-singing vs. mental arithmetic (Shirer et al., 2011) and watching movies vs. rest (Richiardi et al., 2011). It remains to be determined however, whether whole-brain connectivity can be used to decode very similar stimuli that differ by only one or a few subtle characteristics, such as the emotional expression of an unattended face. If so, then functional connections that discriminate between the two conditions can be interpreted as being uniquely related to the parameter of interest that varies across both conditions.

Although multivariate pattern analyses are more sensitive than group, model-based approaches, one disadvantage is decreased interpretability and quantification of the precise relationship among features related to a certain condition (Norman et al., 2006). However, since this approach exploits the information inherent in the joint responses of many functional connections, an advantage is that pattern classification of similar conditions coupled with feature selection and identification can be used as a means to identify condition-dependent, large-scale functional connectivity, without the need to correct for tens of thousands of multiple comparisons. This approach can be used for hypothesis generation to identify groups of functional connections associated with a condition, which can then serve as connections and regions of interest for more rigorous and mechanistically revealing approaches such as effective connectivity (Marreiros et al., 2008).

Here we estimate the large-scale functional networks of implicit fear processing using a blocked design and Blood Oxygen Level Dependent (BOLD) image acquisition, during which subjects were instructed to identify the color of pseudo-colored fearful and neutral faces (Fig 9). We applied atlas-based parcellation to derive several hundred nodes throughout the whole-brain and computed thousands of pair-wise correlations (40 total time points, or 80s worth of fMRI

data) during each of two conditions: implicit processing of fearful and neutral faces. We then employed multivariate pattern analyses in conjunction with linear filter feature selection to identify functional connections whose pattern could distinguish between implicit processing of fearful and neutral faces within individual subjects, using training data from separate subjects. We plotted classification accuracy vs. number of included features to approximate the minimum number of informative features, and then identified these features (functional connections) on a neuroanatomical display. See Fig 10 for an outline of the analysis scheme.

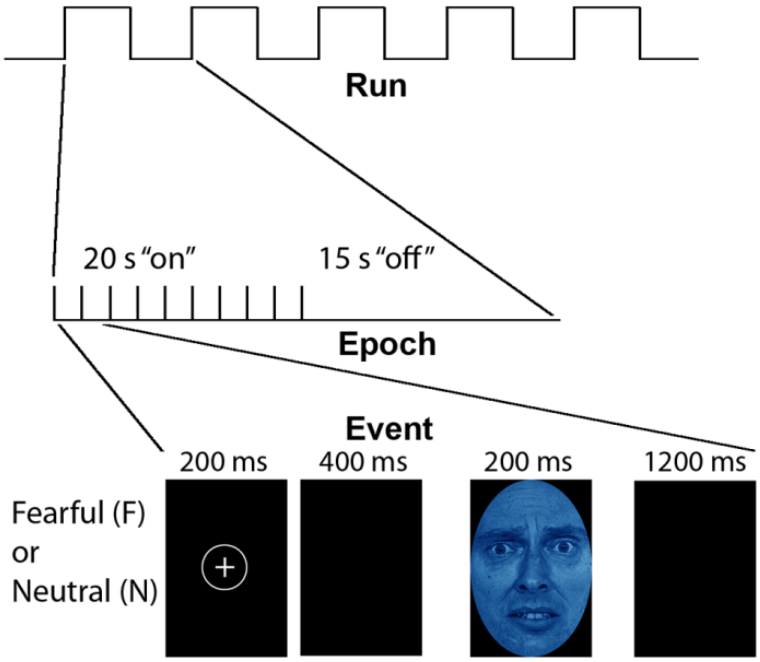

Figure 9. Chapter 4: Experimental paradigm for the interaction of attention and affect (adapted from Etkin, et. al. 2004). Stimuli were either fearful (F) or neutral (N) expression faces, pseudocolored in red, yellow,or blue. Each event was comprised of a face which was either masked (33 ms for a fearful or neutral face, followed by 167 ms of a neutral face mask of the same gender and color, but different individual; MF or MN, respectively), or unmasked (200 ms for each face; F or N) or masked. Ten events of the same type, spaced 2 seconds apart, were presented within each 20 second block, followed by 15 seconds of crosshair with black background. There were four blocks per condition, giving 40 time points in the correlation estimates per condition per subject. In view of our specific

hypotheses, only the unmasked conditions are discussed in the main text, while results for unmasked conditions are presented elsewhere (manuscript in preparation).

Our primary objective was to test the hypothesis that condition-specific, functional connectivity over the whole-brain (here Pearson correlation using 40 time points of fMRI data per example) contain enough information to discriminate between implicitly presented fearful and neutral faces, and to identify the functional connections that are most informative in this decoding task. A secondary objective was to compare the decoding accuracies achieved when using *interactivity* (pair-wise correlations) vs. *activity* (i.e. beta estimates from SPM maps). We show that a small subset of connections estimated across the whole-brain can predict, or "brain-read", implicitly presented fearful faces with high peak accuracies using training and testing data from separate subjects. We propose that this is a valuable, exploratory approach to estimate condition-dependent, large-scale functional connectivity and demonstrate that whole-brain patterns of *interactivity* are a sensitive and informative signature of cognitive-emotional perceptual states.

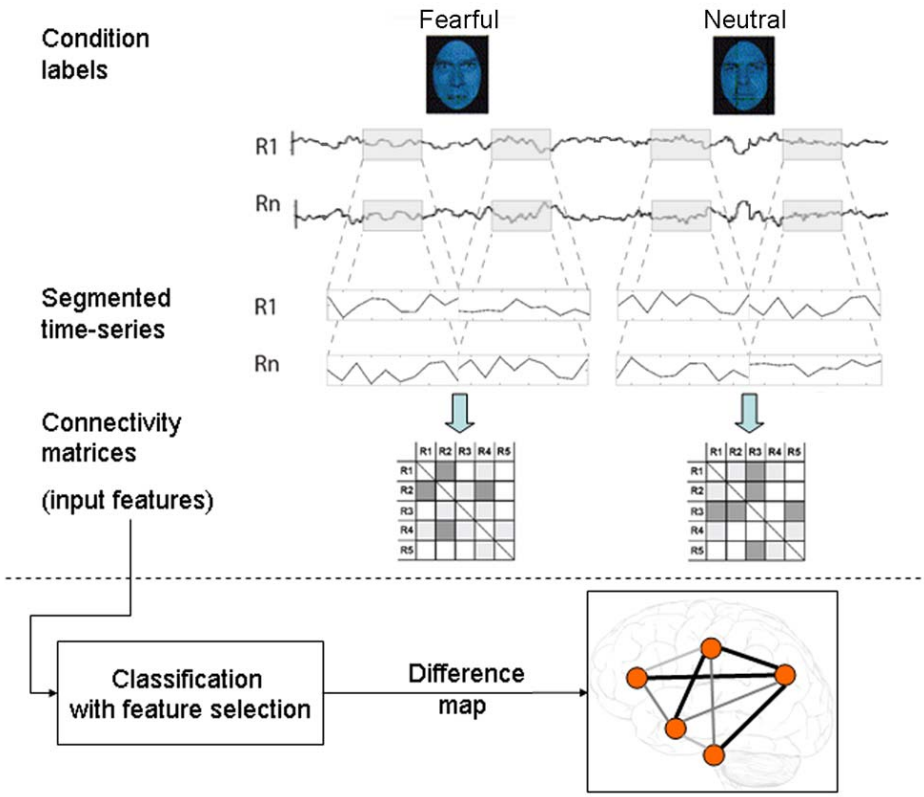

Figure 10. Chapter 4: Data analysis scheme. Time series from each condition (unmasked fearful and unmasked neutral, F and N) and for N regions (R1 though RN) were segmented from each subject's whole run and concatenated (concatenation of two blocks for each condition shown in figure). There were four 20 second (10 TR) blocks of each condition; hence each example was comprised of 40 time points per condition per subject. For each of example, correlation matrices were estimated, in which each off-diagonal element contains Pearson's correlation coefficient between region i and region j. The lower triangular region of each of these matrices were used as input features in subsequent classifiers that learned to predict the example (i.e. F or N) based on their observed patterns of the correlations. Here, we used a filter feature selection based on t-scores in the training sets during each iteration of leave-two-out cross validation. The difference map consists of the set of most informative features (those that are included in the most rounds of cross-validation and have the highest SVM weights.)

Methods

Ethics Statement: All procedures and tasks were reviewed for ethical concerns and protection of human subjects by appropriate local IRB boards prior to subject recruitment and data collection.

The procedures described in this study of healthy adults have been approved by the Columbia University Morningside IRB (#IRB-AAAA3690, PI: Joy Hirsch) and IRB (#IRB5290, PI: Myrna M. Weissman)

Subjects: A total of 38 (19 female) healthy volunteers (mean age = 29, SD = 6.9) with emmetropic or corrected-to-emmetropic vision participated in the study in accordance with institutional guidelines for research with human subjects. All subjects were screened to be free of severe psychopathology including Bipolar Disorder and Psychotic Disorders.

Stimulus Presentation Paradigm: Subjects performed a previously described task (Etkin et al., 2004) which consists of color identification of fearful and neutral faces (F and N respectively). Although backwardly masked (subliminal) fearful and neutral faces were also presented, here we discuss results based on the unmasked (supraliminal) conditions. Results based on comparisons of masked conditions are presented elsewhere (manuscript in preparation). *Stimuli:* Black and white pictures of male and female faces showing fearful and neutral facial expressions were chosen from a standardized series developed by Ekman and Friesen (Ekman and Friesen, 1976). Faces were cropped into an elliptical shape that eliminated background, hair, and jewelry cues and were oriented to maximize inter-stimulus alignment of eyes and mouths. Faces were then artificially colorized (red, yellow, or blue) and equalized for luminosity. For the training task, only neutral expression faces were used from an unrelated set available in the lab. These faces were also cropped and colorized as above.

Behavioral task: Each stimulus presentation involves a rapid (200 ms) fixation to cue subjects to fixate at the center of the screen, followed by a 400 ms blank screen and 200 ms of face presentation. Subjects have 1200 ms to respond with a key press indicating the color of the face. Behavioral responses and reaction times were recorded. Unmasked stimuli consist of 200 ms of a fearful or neutral expression face, while backwardly masked stimuli consist of 33 ms of a fearful or neutral face, followed by 167 ms of a neutral face mask belonging to a different individual, but of the same color and gender (see Fig 9). Each epoch consists of ten trials of the same stimulus type, but randomized with respect to gender and color. The functional run has 16 epochs (four for each stimulus type) that are randomized for stimulus type. To avoid stimulus order effects, we used two different counterbalanced run orders. Stimuli were presented using Presentation software (Neurobehavioral Systems, http://nbs.neuro-bs.com), and were triggered by the first radio frequency pulse for the functional run. The stimuli were displayed on VisuaStim XGA LCD screen goggles (Resonance Technology, Northridge, CA). The screen resolution was 800X600, with a refresh rate of 60 Hz. Prior to the functional run, subjects were trained in the color identification task using unrelated neutral face stimuli that were cropped, colorized, and presented in the same manner as the nonmasked neutral faces described above in order to avoid any learning effects during the functional run. After the functional run, subjects were shown all of the stimuli again, alerted to the presence of fearful faces, and asked to indicate whether they had seen fearful faces on masked epochs.

fMRI Acquisition: Functional data were acquired on a 1.5 Tesla GE Signa MRI scanner, using a gradient-echo, $T2^*$-weighted echoplanar imaging (EPI) with blood oxygen level-dependent (BOLD) contrast pulse sequence. Twenty-four contiguous axial slices were acquired along the

AC-PC plane, with a 64 × 64 matrix and 20 cm field of view (voxel size 3.125 × 3.125 × 4 mm, TR = 2000, TE = 40, flip angle = 60). Structural data were acquired using a 3D T1-weighted spoiled gradient recalled (SPGR) pulse sequence with isomorphic voxels (1 × 1 × mm) in a 24 cm field of view (256 × 256 matrix, ~186 slices, TR 34 ms, TE 3 ms).

GLM analysis: Functional data were preprocessed and processed in SPM8 (Wellcome Department of Imaging Neuroscience, London, UK). For preprocessing, the realigned T2*-weighted volumes were slice-time corrected, spatially transformed and resampled to a standardized brain (Montreal Neurologic Institute, 2x2x2 mm^3 cube resolution) and smoothed with a 8-mm full-width half-maximum Gaussian kernel. 1st-level regressors were created by convolving the onset of each block (MF, MN, F and N) with the canonical HRF with duration of 20 seconds. Additional nuisance regressors included 6 motion parameters, white matter and csf signal, which were removed prior to time-series extraction. For the current work, the same GLM analysis served three purposes: 1) facilitate removal of nuisance effects from time series prior to FC estimation using structurally (atlas-based) and functionally defined ROIs, 2) produce beta-estimates of each condition for classification analysis of spatial activity patterns and 3) functionally define ROIs (nodes) prior to FC calculation (used for comparing results of structural vs. functional definition of nodes).

Node definitions: Brain regions were parcellated according to bilateral versions of the Harvard-Oxford Cortical and sub-cortical atlases and the AAL atlas (cerebellum) and were trimmed to ensure no overlap with each other and to ensure inclusion of only voxels shared by all subjects (Fig 11, left panel). For each subject, time-series across the whole run (283 TRs) were extracted

using Singular Value Decomposition (SVD) and custom modifications to the Volumes-of-Interest (VOI) code within SPM8 to retain the top 2 eigenvariates from each atlas-based region. Briefly, the data matrix for each atlas-based region is defined as A, an n x p matrix, in which the n rows represent the time points, and each p column represents a voxel within an atlas-based region. The SVD theorem states:

$$A_{nxp} = U_{nxn}\, S_{nxp}\, V^{T}_{pxp,}$$

where $U^{T}U = I_{nxn}$ and $V^{T}V = I_{pxp}$ (i.e. U and V are orthogonal). The columns of U are the left singular vectors (eigenvariates, or summary time courses of the region), S (the same dimensions as A) has singular values, arranged in descending order, that are proportional to total variance of data matrix explained by its corresponding eigenvariate, and is diagonal, and V^{T} has rows that are the right singular vectors (spatial eigenmaps, representing the loading of each voxel onto its corresponding eigenvariate). Here we retain the top two eigenvariates (nodes) from each region.

For each atlas-based region, we opted to apply SVD over the entire time-series from each subject and *then* segment and concatenate the eigenvariates according to the conditions/comparisons of interest (rather than segment and concatenate all the masks' voxels *first* and then apply SVD) in order to maximize the total number of observations (time points) per region and also to avoid potentially introducing any artifact and unnatural variation caused by the splicing together of signal from disparate time points, which could possibly bias the SVD results. However, a potential disadvantage of this approach is that important sub-regions and associated eigenvariates within a particular atlas-based region could be missed due to variation in other conditions/blocks within the run that are not considered in the current work. This is an additional motivation to retain the top two eigenvariates from each atlas-based region, as opposed to just one.

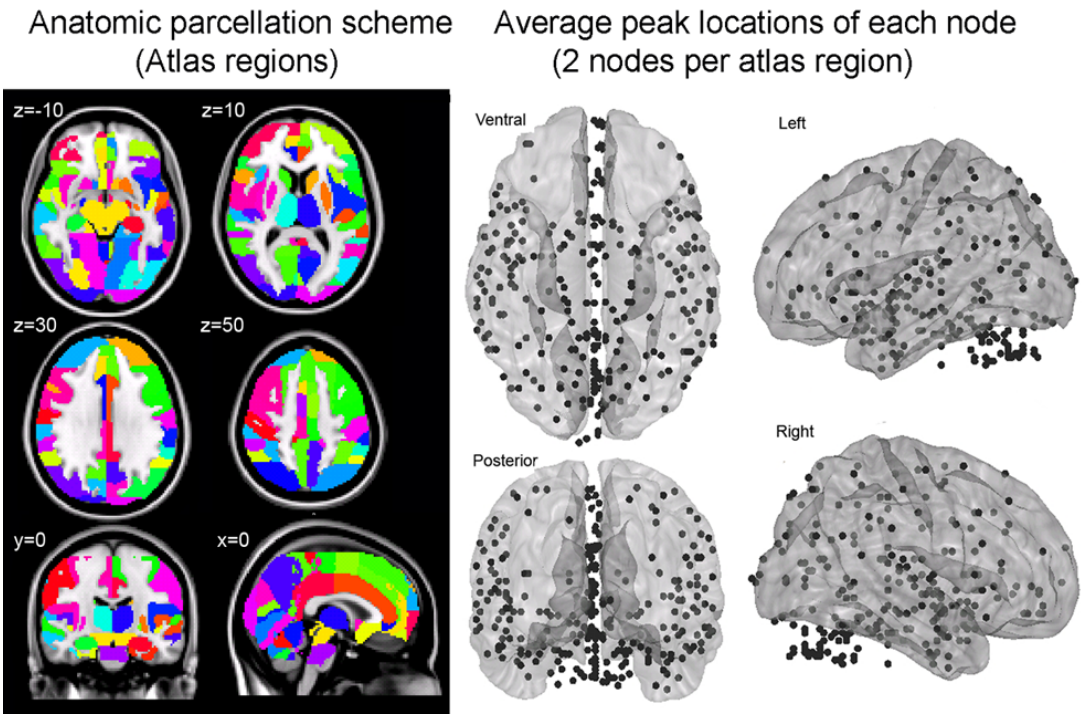

Figure 11. Chapter 4: Node definitions and anatomical locations**.** Cortical and subcortical regions (ROIs) were parcellated according to bilateralized versions of the Harvard-Oxford Cortical and subcortical-atlases, and the cerebellum was parcellated according to AAL (left panel). ROIs were trimmed to ensure there was no overlap between them and that they contained voxels present in each subject. The top two eigenvariates from each ROI was extracted, resulting in 270 total nodes throughout the brain (right panel). For display purposes, node locations (black spheres) correspond to the peak loading value from each time-course's associated eigenmap averaged over all subjects.

The above step resulted in a total of 270 nodes with an associated time course (i.e. eigenvariates) and spatial eigenmaps from the 135 initial atlas-based regions. Thus, each atlas-based region was comprised of two nodes. Interestingly, when extracting only one eigenvariates per region, maximum accuracy did not surpass 46% (data not shown). This is possibly due to the fact that larger, atlas-based regions encompassed other functional sub-regions which were not included in the analysis. Another possible reason is that for many regions, the 1st eigenvariate

may reflect artifact global or mean grey matter signal (while white matter and csf signal were regressed out from nodes' time-series, global and mean grey matter signals were not), or it may reflect variation caused by other conditions/blocks within the run that were not considered in the current classification analyses (see paradigm task description above), or a combination of all the above. Therefore we extracted two eigenvariates from each region. We note that this means it is likely that node 2 of a particular region shows functional connectivity that differentiates between conditions and node 1 of the same region has no differential connectivity. For clarity we therefore label each node using its Harvard-Oxford atlas label appended by either "_PC1" for the first eigenvariate and "_PC2" for the second. For display purposes, we calculated the MNI coordinates of the peak loading weight (locations averaged across subjects) for each eigenvariate from its associated eigenmap (Fig 11, right panel). Supplementary Table 1 from (Pantazatos et al., 2012a) lists these average MNI coordinates for each node.

Functional connectivity networks for implicit fearful and neutral face processing: For each subject, functional connectivity matrices (i.e. where cell *i,j* contains the Pearson correlation between region *i* and region *j*) were generated for implicit fearful (F) and neutral (N) conditions. The above time-series were segmented and concatenated according to conditions of interest (40 total time points per condition, incorporating a lag of 2 or 3 s from the start of each block) before generating the correlation matrices. Fisher's R to Z transform was then applied to each correlation matrix. Finally for the binary classification of interest (i.e. F vs. N), correlation matrices were demeaned with respect to the average between the two conditions in order to remove the effects of inter-subject variability. The lower diagonal of the above preprocessed

correlation matrices (38 subjects X 2 conditions total) were then used as input features to predict viewed stimuli in subsequent pattern recognition experiments.

Differences in functional connectivity between implicit fearful and neutral face processing: We first tested for significant differences between the primary conditions of interest (i.e. F > N) while correcting for multiple comparisons (False Discovery Rate, FDR). This yielded no significant results when multiple comparison correction was applied (FDR, $p < 0.05$ and 0.1). This was not surprising, as multiple comparison correction was expected to be too conservative given the exceedingly high number of independent comparisons (36,315).

Pattern analysis of large-scale functional connectivity to predict implicit fear perception: Support vector machines are pattern recognition methods that find functions of the data that facilitate classification (Vapnik, 1999). During the training phase, an SVM finds the hyperplane that separates the examples in the input space according to a class label. The SVM classifier is trained by providing examples of the form $<x,c>$, where x represents a spatial pattern and c is the class label. In particular, x represents the fMRI data (pattern of correlation strengths) and c is the condition or group label (i.e. $c = 1$ for F and $c = -1$ for N). Once the decision function is determined from the training data, it can be used to predict the class label of new test examples.

For all binary classification tasks, we applied a linear kernel support vector machine (SVM) with a filtering feature selection based on t-test and leave-two-out cross validation (LTOCV). There were 38 examples for each condition (2 from each subject, 76 total). During each iteration of 38 rounds of LTOCV, both examples (1 from each class) from one subject were withheld from the dataset and 1) a 2-sample t-test was performed over the remaining training

data (N=37 in each group) 2) the features were ranked by absolute t-score and the top N were selected 3) these selected features were then used to predict the class of the withheld test examples during the classification stage. The full feature set for each example consisted of 36,315 correlations.

If the classifier predicted all trials as positive or negative, the resulting accuracy would be 50% since the number of examples are equal for each class. We therefore report classification accuracy (number of true positives and negatives over all trials) vs. number of included features that have been ranked by their t-score. We assessed the significance of decoding results by computing the frequency in which actual values surpassed those from null distributions derived by randomly permuting class labels based on the method proposed by (Golland and Fischl, 2003), with the a slight modification to account for the dependence between pairs of examples from each subject. Briefly, to derive this null distribution, class labels within each pair conditions from each subject were randomly flipped with a probability of 0.5 over 2000 iterations for each number of included features. P-values for the peak decoding accuracies (F vs. N: 100%, top 25 features) were also calculated with respect to classification results when shuffling labels 10,000 times, and then subjected to Bonferroni correction for the number of total Top N comparisons (in this case 20).

For SVM learning and classification we used the Spider v1.71 Matlab toolbox (http://people.kyb.tuebingen.mpg.de/spider/) using all default parameters (i.e. linear kernel SVM, regularization parameter C=1. Graphical neuro-anatomical connectivity maps of the top N features were displayed using Caret v5.61 software (http://brainvis.wustl.edu/wiki/index.php/Caret:About). We note that different features could be selected during the feature selection phase of each round of cross-validation. Therefore in

ranking the top 25 features, we first rank by total number of times that feature was included in each round of cross-validation, and then among these features, we sort by absolute value of the average SVM weight.

Our intent is not to estimate the true accuracy of prediction given a completely new data set, but rather to test whether there exists information in the pattern of functional connections relevant to unattended emotion perception, and to approximate the optimal number of features that containing this information. We note that our approach (plotting accuracy vs. number of top N features) is not biased, since for each number of top N features, and for each round of leave-two-out cross validation, the top N features were selected from a training set that was completely independent from the testing set. If there is a true signal present in the data, we expect, and in the current data in general observe, that there is an initial rise in accuracy as more informative features are added to the feature set, and a dip in accuracy as less informative features (i.e. noise) are added to the feature set. Therefore in reporting classification results, we report the range of features at which accuracies first reach maximum accuracy-10% (positive slope) to which they reach maximum accuracy-10% (negative slope), and also correct for multiple comparisons (i.e. number of top N features tested) using Bonferroni when reporting the p-value for the maximum accuracy achieved.

For assessing the significance of the differences between decoding results (i.e. FC as features vs. beta estimates) we used the Accurate Confidence Intervals MATLAB toolbox for assessing whether the parameter *p* (probability of correct prediction) from two independent binomial distributions was significantly different (http://www.mathworks.com/matlabcentral/fileexchange/3031-accurate-confidence-intervals). Briefly, these methods search for confidence intervals using an integration of the Bayesian

posterior with diffuse priors to measure the confidence level of the difference between two proportions (Ross, 2003). We used the code prop_diff(x_1,n_1,x_2,n_2,delta), (available from the above website) returning Pr($p_1 - p_2 > \delta$), where x_1, n_1, x_2, n_2, are number of correct responses and total predictions in two distributions being compared, and delta (zero in our case) is the null hypothesis difference between the probabilities.

Results

Behavioral results: The average response rate in the color discrimination task was 98% (σ=4.6%), mean accuracy was 97% (σ=3.5%), and mean reaction time was 0.65 s (σ=0.12), indicating that subjects performed the color discrimination task as instructed.

Discriminating between implicit processing of fearful and neutral faces with patterns of functional connectivity: We applied atlas-based parcellation (see Fig 11) and computed pair-wise correlations between 270 nodes (derived from 135 atlas-based brain regions) using 40 total time points of fMRI data that were segmented and concatenated from two conditions; unattended and nonmasked (i.e. implicit) fearful (F) and neutral (N) faces (Figure 1). This resulted in 36,315 total functional connections (z-transformed Pearson correlations) for each condition of interest (F and N).

We quantified the extent to which a subset of these functional connections could decode, or predict, the conditions from which they were derived by submitting them as features into a pattern classifier. We used a linear kernel Support Vector Machine (SVM) with a filter feature selection based on the t-score of each feature (functional connectivity) in each training set. Decoding accuracies for implicit fearful vs. neutral classifications (F vs. N) were plotted against

the number of included features (ranked in descending order by t-score) in order to approximate the number of informative features relevant to the emotional expression of the facial stimulus.

For implicit fearful vs. neutral (F vs. N) classification, maximum accuracies of 86-96% ($p < 0.0001$) were achieved with the top 10-20 features (Fig 12A). Anatomical display of the top 16 overall features that differed between F and N conditions revealed functional connections among occipital regions, middle and superior temporal gyrus, lateral and medial prefrontal regions, thalamus, cerebellum and insula (Fig 12B-D, Table 4). The connections that carried the most weight in the linear SVM classifier was included right angular gyrus and left hippocampus, and left thalamus and left planum polare, which exhibited a greater correlation in the F vs. N condition (Table 4, F# 1-3). To identify regions whose overall functional connectivity was greater during fear, the size of each node was made proportional to the sum of SVM weights of each of its connections. The node with the most positive functional connectivity during fear was the thalamus (Figure 4B-D, large red sphere in center), which exhibited positively modulated functional connections with bilateral middle temporal gyrus and right insula.

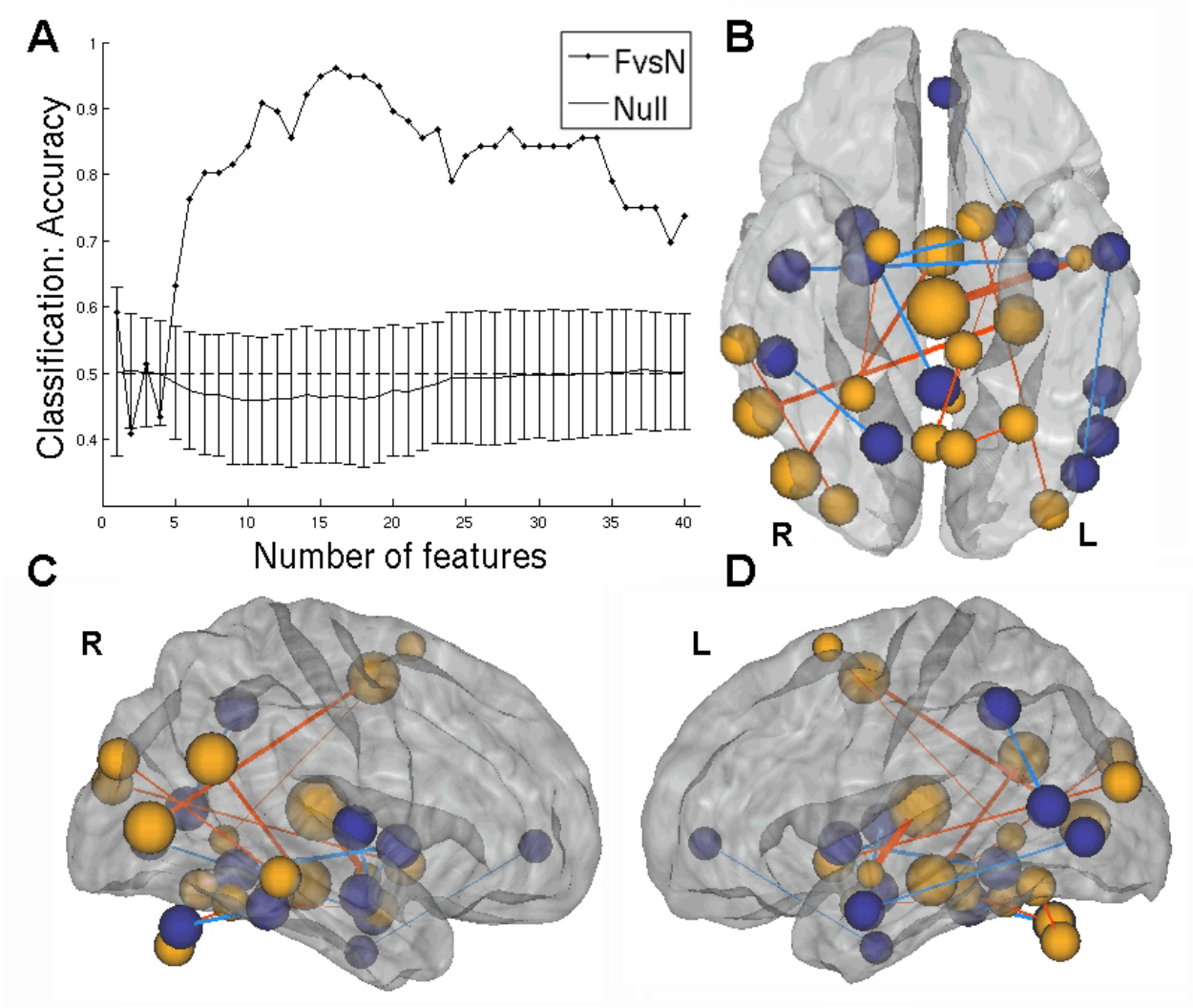

Figure 12. Chapter 3: Large-scale functional connectivity discriminates between unattended, conscious processing of fearful and neutral faces. (A) Decoding accuracy when classifying F vs. N as a function of the number of features (1 to 40) included ranked in descending order by their absolute t-score. Maximum accuracy for F vs. N classification (100%, $p < 0.002$, corrected) was achieved when learning was based on the top 25 features in each training set. Mean accuracy scores for shuffled data are plotted along the bottom, with error bars representing standard deviation about the mean. Posterior (B), ventral (C) and right lateralized (D) anatomical representation of the top 25 features when classifying supraliminal fearful vs. supraliminal neutral face conditions (F vs. N). The thalamus (large red sphere in the center of each view) is the largest contributor of connections the differentiate the F from N. Red indicates correlations that are greater in F, and blue represents correlations that are greater in N. For display purposes, the size of each sphere is scaled according to the sum of the SVM weights of each node's connections,

while the color of each sphere is set according to the sign of this value; positive sign, red, F > N and negative sign, blue, N > F. In addition, the thickness of each connection was made proportional to its SVM weight.

Table 4. Chapter 4: F vs. N, Top 16 features. Consensus features are shown in bold.

Edge label	Mean R Fear	Mean R Neutral	T-value	SVM weight	FSets
Left_Thalamus_PC2 - Left_Planum_Polare_PC1	**0.061307**	**-0.082794**	**4.3082**	**1.7364**	**38**
Right_Lateral_Occipital_Cortex_inferior_division_PC2 - Left_Juxtapositional_Lobule_Cortex_Supp_Motor_cortex_PC1	**0.09372**	**-0.071973**	**4.3893**	**1.3856**	**38**
Right_Angular_Gyrus_PC1 - Left_Hippocampus_PC2	**0.089644**	**-0.043317**	**4.7277**	**1.3773**	**38**
Vermis_4_5_PC1 - Right_Putamen_PC1	-0.052167	0.068933	-4.0958	-1.1339	17
Right_Central_Opercular_Cortex_PC1 - Left_Planum_Polare_PC1	0.101	0.24164	-4.141	-1.1261	25
Right_Amygdala_PC2 - Left_Putamen_PC1	**0.018875**	**0.14839**	**-4.7533**	**-1.116**	**38**
Left_Supramarginal_Gyrus_posterior_division_PC2 - Left_Lateral_Occipital_Cortex_inferior_division_PC2	0.013263	0.15074	-3.9791	-1.112	11
Right_Inferior_Temporal_Gyrus_posterior_division_PC1 - Cerebelum_6_R_PC2	**-0.02189**	**0.11678**	**-4.521**	**-1.1031**	**38**
Left_Ventral_Lateral_Occipital_Cortex_superior_division_PC2 - Left_Accumbens_PC2	**0.039594**	**-0.10233**	**4.6239**	**1.0477**	**38**
Right_Ventral_Lateral_Occipital_Cortex_superior_division_PC2 - Right_Middle_Temporal_Gyrus_posterior_division_PC2	**0.041073**	**-0.063035**	**5.3268**	**1.0433**	**38**
Left_Middle_Temporal_Gyrus_anterior_division_PC2 - Left_Lateral_Occipital_Cortex_inferior_division_PC1	-0.028552	0.062753	-4.1191	-1.0078	23
Left_Temporal_Occipital_Fusiform_Cortex_PC2 - Cerebelum_8_L_PC1	0.040634	-0.098713	4.2072	1.0032	35
Vermis_7_PC2 - Midbrain_PC1	**0.12648**	**-0.001608**	**4.5083**	**0.99178**	**38**
Right_Temporal_Occipital_Fusiform_Cortex_PC1 - Right_Amygdala_PC1	**0.23713**	**0.10776**	**4.9032**	**0.90304**	**38**
Left_Temporal_Fusiform_Cortex_anterior_division_PC1 - Left_Paracingulate_Gyrus_PC1	-0.14323	-0.016626	-4.2079	-0.77203	34
Left_Superior_Frontal_Gyrus_PC2 - Left_Cingulate_Gyrus_posterior_division_PC2	**0.069026**	**-0.074108**	**4.4018**	**0.67325**	**38**

In addition to parcelating the brain and defined nodes based on an atlas, we also functionally defined nodes using two approaches 1) using the same 160 MNI coordinates as used in Dosenbach et. al., 2010 (Dosenbach et al., 2010b) which were selected and defined based on

separate meta-analyses of the fMRI literature, and 2) a biased approach based on 92 nodes (2 eigenvariates from each of 49 ROIs defined as 6 mm radius spheres centered at peak coordinates) that were based on the GLM results from the same, whole dataset (for F contrast F > N thresholded at p=0.05, k=30). For 1) achieved accuracies were 63-73% when using 75 to 130 features, and for 2) accuracies between 76-86% were obtained when using 80 to 140 features (data not shown). Approach 2) is biased in that we defined our nodes based on the GLM results of the whole data set, and as such provides an upper bound on the expected accuracies when functionally defining nodes based on the GLM results in separate training sets during each iteration of LTOCV. Therefore we conclude that the above whole-brain, atlas-based approach, which achieved 86-96% accuracy with 10-20 features when using unbiased feature selection, is optimal to using functionally defined nodes.

Discriminating between F and N faces using spatial patterns of activation: To compare the information content of patterns of interactivity (i.e. functional connections used above) vs. patterns of activity we also attempted F vs. N classifications using beta estimates, which are considered summary measures of activation in response to each condition. In order to make feature-selection/LTOCV and SVM learning more computationally tractable, preprocessed functional data were resized from 2x2x2 mm voxel resolution to 4x4x4 mm resolution, and subject-specific GLM models were re-estimated, resulting in a reduction of total feature space per example from ~189,500 betas to ~23,500. Feature selection, LTOCV and SVM learning proceeded exactly as above for FC data. We observed accuracies of 66%-76% with ~500 to 2600 features, with peak accuracy at 76% ($p = 0.0044$, uncorrected) at ~1900 features (Fig 13A). The most informative voxels encompassed many distributed regions that included dorsolateral

prefrontal/opercular cortex, fusiform gyrus, lateral occipital cortex, superior temporal gyrus, anterior cingulate, amygdala, parahippocampal gyrus, ventrolateral prefrontal cortex, pulvinar, precuneus, cerebellum, inferior parietal lobe and insula (Fig 13B). Although significantly above chance, and despite the involvement of many more regions, maximum accuracy using betas was significantly less than the maximum accuracy achieved with FC (76% < 100%, p=5.37x10-7).

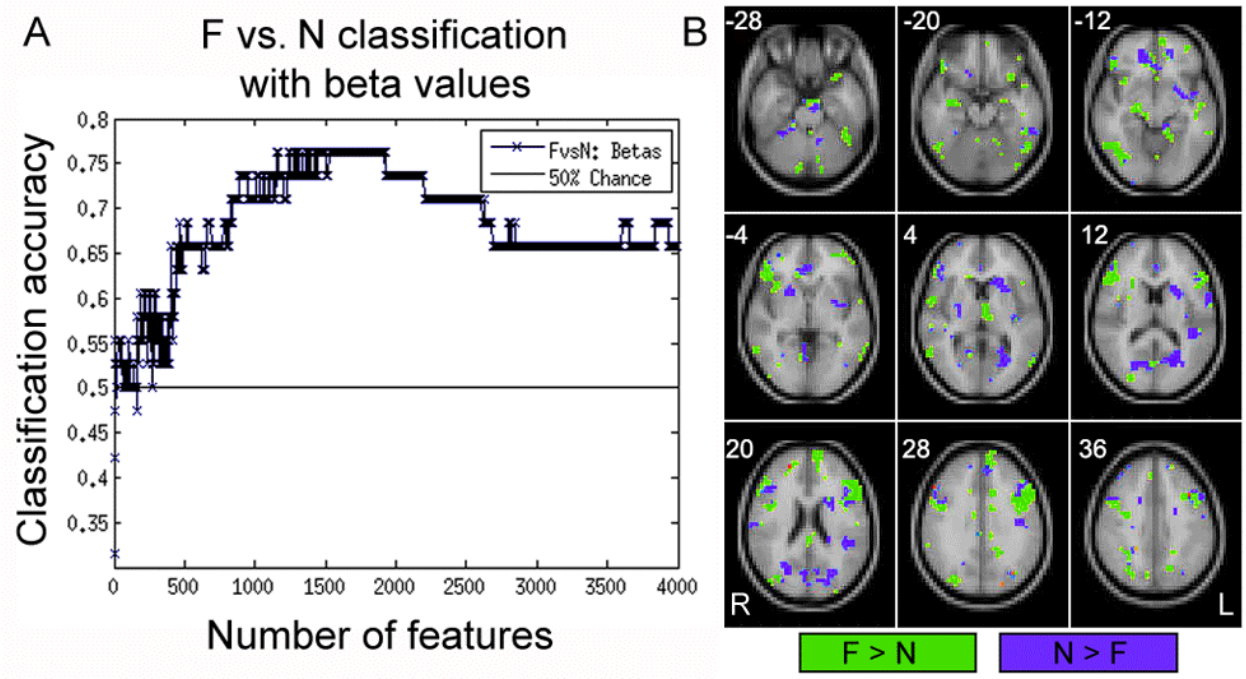

*Figure 13.*Chapter 4: Classification results using beta estimates as features. (A) Feature selection, cross-validation and SVM learning were performed exactly the same as for FC, but over the range of 1 to 4000 ranked features (voxels). Accuracies for F vs. N classification reached 66-76% with ~500-2500 features, with maximum accuracy (76%, p = 0.0044, uncorrected) at ~1,900 features. (B) The most informative voxels with positive SVM weights (F > N, yellow) included fusiform gyrus (-28,-20,-12), cerebellum (-28, -20), amygdala (-20), insula (-12), orbital and ventrolateral prefrontal cortex (-20, -12, -4), midbrain (-12), parahippocampal gyrus (-12), middle temporal gyrus and superior temporal sulcus (-12,-4,4), thalamus/pulvinar (4), dorsolateral prefrontal/opercular cortex (12,20,28), dorsomedial prefrontal cortex (20,28), and superior occipital cortex (20,28) and inferior parietal lobe (36). Informative voxels with negative SVM weights (N > F, blue) included temporal-occipital cortex (-20), subgenual

anterior cingulate (-12,-4), striatum (-4,4), lingual gyrus (4,12), precuneus (20) and dorsolateral prefrontal cortex (28,36). (B). Brain images are displayed using Neurological convention (i.e. L=R), and top left number in each panel represents the MNI coordinate (z) of depicted axial slice.

We performed additional classifications using betas derived from the original, smaller voxel-sizes and with the addition of an initial (positively biased) feature selection step over the whole-dataset for the same issues of technicality stated above. This also served to estimate an upper bound on the expected accuracy when using beta-values: if maximum accuracy achieved was still less than when using functional connectivity with unbiased feature selection, then we can more readily conclude that functional connectivity features are more "informative" than beta estimates (when using the Canonical Hemodynamic Response Function (HRF) to model activation). For this analysis, the initial (biased) feature selection employed an F-test of the contrast F>N thresholded at $p<0.01$, cluster threshold=20, resulting in 4,226 total initial features. Feature selection/LTOCV and classification again proceeded as above across the range of 1 to 4000 features. In spite of initially biased feature selection, F vs. N classification reached 92% maximum accuracy (data not shown).

In addition to using beta maps throughout the whole-brain, we derived beta weights using the same summary time courses (eigenvariates) that were extracted and used to compute pair-wise FC (270 total betas per condition per subject). For this, the GLM analysis was kept the same as above except that previously included nuisance regressors (6 motion, mean white and mean csf) and a low-pass filter were not included, since they were already removed from the time courses during extraction. Resulting estimated beta weights were then used as features to predict fearful vs. neutral faces using the exact same procedure when using whole-brain FC. Accuracies of between 69-79% were achieved with between 40 to 150 features (data not shown).

Discussion

Here we demonstrate that pattern analysis of large-scale functional connectivity can reliably decode the emotional expression of implicitly perceived faces, and that pair-wise functional connections are modulated by implicit fear perception. This work also demonstrates a whole-brain, large-scale and exploratory approach for the identification of condition-specific, functional connectivity that avoids correcting for multiple comparisons among thousands of connections (discussed more below).

One of the more significantly modulated functional connections during implicit presentation of fearful faces was between left hippocampus and right angular gyrus. The left hippocampus is a key region for memory (i.e. autobiographical memory retrieval) and the right angular gyrus has been implicated in mentalizing, or inferring the thoughts and feelings of others (Spreng and Mar, 2010). Interestingly, during resting states, these two regions were found not to correlate with each other, but instead correlated with other regions that substantially overlapped, such as superior temporal sulcus (STS), anterior temporal lobe, posterior cingulate cortex, dorsomedial and ventral prefrontal cortex, inferior frontal gyrus, and the amygdala. It has been proposed that this functional overlap facilitates the integration of personal and interpersonal information and provides a means for personal experiences to become social conceptual knowledge (Spreng and Mar, 2010). Here, we observed the left hippocampus and right angular gyrus were correlated during implicit emotion (fear) perception, suggesting the integration of autobiographical memory with mentalizing during implicit perception of emotional faces.

Other connections that discriminated between implicitly presented fearful and neutral faces included thalamus, superior and lateral occipital, superior frontal gyrus, precentral gyrus,

cerebellum, striatum, parietal and posterior and anterior temporal regions (in the vicinity of the superior temporal sulcus, STS). This latter observation is consistent with previous models and group studies that identify the STS and middle temporal gyrus as a primary neural substrate for processing the emotional expression of faces (Engell and Haxby, 2007; Haxby et al., 2002; Sabatinelli et al., 2011), and recent work demonstrating that multivariate pattern analyses applied to these regions could decode explicit emotional face recognition (Peelen et al., 2010; Said et al., 2010; Tsuchiya et al., 2008). Importantly, the current findings suggest that interactions of temporal regions and STS with areas such as cerebellum, thamalus, lateral occipital cortex and central opercular cortex (Table 4 F# 1, 5, 8 and 10) are also involved in implicit emotion perception.

An amygdala-FG interaction did appear among the top features for discriminating between implicit fearful and neutral faces and also was a consensus feature (Table 4, F#14): this is predicted by previous studies have shown that emotional faces modulate amygdala-fusiform (FG) interactions (Fairhall and Ishai, 2007; Sabatinelli et al., 2005; Vuilleumier et al., 2004)}} and further contributes face validity in the ability of the current approach to not only identify informative, but also neurophysiologically meaningful, features in decoding fear. The structure with the overall highest weight in discriminating between the fear and neutral conditions was thalamus (Fig 12C and D, largest red sphere in center), which exhibited greater correlation with left superior gyrus (STS) during the fear condition (Table 4 F#1). This observation is consistent with its purported role as a hub integrating cortical networks during the evaluation of the biological significance of affective visual stimuli (Pessoa and Adolphs, 2010), and with the observation of direct structural connectivity between several sub-regions of the thalamus with the

STS (Yeterian and Pandya, 1991). The current results suggest that functional connectivity between thalamus and STS play a prominent role during implicit fear perception.

Interestingly, functional connections of the cerebellum were also significantly modulated during the fear condition. In particular, functional connections of the cerebellum with midbrain (Table 4 F# 13) and fusiform gyrus (F# 12) were increased during fear, while connections with putamen (F# 4) and inferior temporal gyrus (F#8) were decreased. Although cerebellum has been frequently reported to be activated or involved during emotion processing (Fusar-Poli et al., 2009; 2010; Karama et al., 2011), the specific roles the various subregions play during affective processing remain to be elucidated (Stoodley and Schmahmann, 2010).

Large-scale functional network of fear processing: It is clear that fearful emotion processing and its behavioral consequences involve the complex interactions among many distributed regions (Coplan and Lydiard, 1998; Gorman et al., 2000; Kent and Rauch, 2003). Among these, the amygdala and its interactions with the frontal and visual cortex are critically involved in attended and pre-attentive threat and emotion processing (Banks et al., 2007; Bishop et al., 2004; Etkin et al., 2004; 2006). Numerous previous studies have examined functional interactions between amygdala and several other regions in the fear and facial emotion processing pathway. Usually these have used Psycho-Physiological Interaction (PPI) analysis to study the functional connectivity of a seed region, often the amygdala, with the rest of the brain during a fearful relative to non-fear perceptual or cognitive state (Banks et al., 2007; Pezawas et al., 2005). Other studies employed effective connectivity measures such as structural equation modeling (SEM) and dynamic casual modeling (DCM) to examine multiple interactions among a more limited set of a priori defined regions (Fairhall and Ishai, 2007; Stein et al., 2007)

In contrast to the above-mentioned studies, the current approach is relatively model-free in that we estimate functional connectivity throughout the whole-brain without a priori restrictions based on anatomically defined areas or seed regions. We estimate network connections using simple correlation measures, similar to a previous study that demonstrated condition dependent modulations in large-scale (41 nodes) functional connectivity across various syntactical language production tasks (Dodel et al., 2005) but on a much larger scale (270 nodes in the current analysis). We then identified a subset of functional connections whose pattern could discriminate between implicit fearful and neutral face processing.

An approach to estimate condition specific large-scale functional connectivity: There is considerable interest in examining the large-scale functional network architecture of the brain as a function of various cognitive processes or individual variation (Smith et al., 2011). This is often done by first defining a set of functional "nodes" based on spatial ROIs and then conducting a connectivity analysis between the nodes based on their FMRI timeseries. Group-based statistical parametric mapping can then be applied to resulting connections (Ginestet and Simmons, 2011). However, as the number of nodes (N) increases, the number of connections increases exponentially (# connections = (N*(N-1))/2) resulting in a multiple comparisons problem, and hindering the exploration-based query of condition-specific whole-brain functional connectivity on a large-scale. The equivalent of cluster-extent thresholding for graphs has been proposed, such as the Network Based Statistic (Zalesky et al., 2010), which estimates the probability of observing groups of linked, suprathreshold edges based on chance. However, inferences can only be made on groups of interconnected edges, not individual ones. In addition, there is a substantial loss of information in model-based approaches when conducting statistical

inference on signals (functional connections) averaged over a group of subjects, and discounting the joint responses among many functional connections.

Here, we present a novel alternative to identify functional connections of interest based on their information content in machine-learning based multivariate pattern analyses that attempt to discriminate between two conditions that differ based on a parameter of interest (in this case the emotion expression of a presented face). For this we used linear filter feature selection and plotted classification accuracy vs. number of included features in order to determine the number of features required to distinguish between conditions, and then identified the top N features on neuroanatomical display.

"Information content" of neural activity vs. neural interactivity: Large-scale functional connectivity and network analysis has been increasingly used as the tool of choice for extracting meaningful and understanding complex brain organization (Smith et al., 2011). In the current work we applied simple Pearson correlation to estimate the large-scale functional connectivity of implicit threat-related emotion and ambiguous facial processing using a block-design. Previous work based on simulations has indicated that correlation-based methods, including Pearson correlation, are in general quite successful in capturing true network connections (Smith et al., 2011). Here we "validated" the estimated connections by testing whether a subset of features could be used to decode ("brain-read") the emotional expression of the facial stimulus that was presented during each block. For this we applied Multivariate Pattern Analyses (MVPA) techniques similar to those used previously to decode categories of viewed stimuli (Cox and Savoy, 2003; Hanson et al., 2004; Haxby et al., 2001; Mourao-Miranda et al., 2005; O'Toole et

al., 2005) orientation (Haynes and Rees, 2005; Kamitani and Tong, 2005) and the decisions made during a near-threshold fearful face discrimination task (Pessoa and Padmala, 2007).

In contrast to the above-mentioned studies, which applied MVPA to the activity of spatially distributed regions and/or voxels, in the current work we applied pattern analysis to the correlations, or interactivity, between regions distributed throughout the whole-brain. We compared the decoding accuracy when using correlations as features versus beta estimates, (i.e. summary measures of activation amplitudes for each condition for each voxel). We observed that the peak classification rate when using betas (76%, ~1900 features) was significantly lower than that achieved using FC (96%, ~16 features). Even with an additional, initial feature-selection based on the entire data set which positively biased results, peak decoding accuracies when using ~4,000 beta values (92%) were lower than those reached when using only ~16 correlations as features and unbiased feature selection (96%). This suggests that there is substantially more information, relevant to cognitive-emotional neural processing, that is contained in the interactions between regions than is typically realized through standard univariate approaches. However, it should be noted that this requires enough TRs (time-points) to compute meaningful correlations between brain regions for a particular condition, and would thus in general be impractical for decoding single-trial or event-related data.

We observed that using whole-brain, anatomically defined ROIs to define nodes for whole-brain FC estimation yielded much higher classification rates than using nodes that were functionally defined (either from other meta-analyses or coordinates defined from GLM analysis of these same data). This was not too surprising, as these functionally defined ROIs were smaller (6 mm radius spheres centered around peak F-value coordinates from the contrast of F > N obtained from the GLM vs. atlas-based masks), and hence provided considerably less

coverage of the brain. In addition, the GLM framework relies on multiple assumptions (i.e. model/shape of hemodynamic response function, effects add linearly, etc.) (Monti, 2011) and regions that show activation to a stimulus (i.e. sustained increase in signal amplitude during the duration of a block) may not necessarily exhibit differential functional connectivity and vice versa. These observations further the notion that there exists substantial information in whole-brain large-scale functional connectivity patterns, the nodes of which may not be captured or revealed adequately through standard GLM approaches.

Limitations: Previous simulations have raised concerns regarding the use of atlas-based approaches for parcellating the brain (Smith et al., 2011). Because the spatial ROIs used to extract average time-series for a brain region do not likely match well the actual functional boundaries, BOLD time-series from neighboring nodes are likely mixed with each other. While this hampers the ability to detect true functional connections between neighboring regions, it has minimal effect on estimating functional connectivity between distant regions. This perhaps explains why in this study most of the functional connections that discriminated between fearful and neutral faces are long-distance. Future experiments using non-atlas based approaches would likely lead to better estimates of shorter-range functional connections. We also note that the current atlas-based approach may have under-sampled the prefrontal cortex, and that possible future improvements could break up the prefrontal regions into smaller pieces in order to sample more nodes from this area.

Using Pearson correlation, it is possible that any association between two brain regions is the result of a spurious association with a third brain region. Another limitation of the current study is the required amount of data used to extract quality features of brain activity. Our use of

correlations as features required a substantial number of time points (i.e. 40 scans per condition per subject) relative to previous studies of decoding emotion perception. Given this, it was not feasible to sample enough examples within a single or few subjects as is typical in multivariate pattern analysis studies, and we instead pooled examples across multiple subjects. On the other hand, the fact that reliable classifiers could be learned using examples from separate subjects speaks to the generalizability of our obtained results.

CHAPTER 5

CORTICAL FUNCTIONAL CONNECTIVITY DECODES SUBCONSCIOUS, TASK-IRRELEVANT THREAT-RELATED EMOTION PROCESSING[4]

Summary

It is currently unclear to what extent cortical structures are required for and engaged during subconscious processing of biologically salient affective stimuli (i.e. the 'low-road' vs. 'many-roads' hypotheses). Here we show that cortical-cortical and cortical-subcortical functional connectivity (FC) contain substantially more information, relative to subcortical-subcortical FC (i.e. 'subcortical alarm' and other limbic regions), that predicts subliminal fearful face processing within individuals using training data from separate subjects. A plot of classification accuracy vs. number of selected whole-brain FC features revealed 92% accuracy when learning was based on the top 8 features from each training set. The most informative FC was between right amygdala and precuneus, which increased during subliminal fear conditions, while left and right amygdala FC decreased, suggesting a bilateral decoupling of this key limbic region during processing of subliminal fear-related stimuli. Other informative FC included angular gyrus, middle temporal gyrus and cerebellum. These findings identify FC that decodes subliminally perceived, task-irrelevant affective stimuli, and suggest that cortical structures are actively engaged by and appear to be essential for subliminal fear processing.

Introduction

The human brain has evolved specialized neural mechanisms for recognizing and processing the emotional expressions of faces (Adolphs, 2001). Of particular importance are

[4] Pantazatos, Spiro P, Ardesheer Talati, Paul Pavlidis, and Joy Hirsch. 2012b. Cortical functional connectivity decodes subconscious, task-irrelevant threat-related emotion processing. *NeuroImage.*

faces with fearful expressions, which are thought to signal the presence of a source of danger within the environment (Ewbank et al., 2009). It is commonly assumed that threat-related and other biologically salient affective signals are processed automatically, without the requirement of awareness or attention, by a sub-cortical pathway involving the superior colliculus, pulvinar and amygdala (i.e. 'subcortical alarm' system, or 'low road' hypothesis) (Liddell et al., 2005; Tamietto and de Gelder, 2010). However, recent evidence has initiated debate regarding the extent to which these stimuli engage and rely upon cortical networks that are coordinated by sub-cortical regions such as the amygdala and thalamus (i.e. the 'many roads' and related hypotheses) (Pessoa and Adolphs, 2011).

Evidence arguing for the 'many-roads' hypothesis includes anatomical and physiological data in animal models, and behavioral, non-invasive neurophysiology and lesion studies in humans, while data to support the 'low-roads' hypothesis in humans has included group neuroimaging studies that have reported greater activation in sub-cortical "alarm" regions for subliminal affective stimuli relative to non-affective stimuli (Liddell et al., 2005) as well as increased covariation of right amygdala with pulvinar and superior colliculus during masked fear conditioning using Positron Emission Tomography (PET) imaging (Morris et al., 1999) see ((Pessoa and Adolphs, 2010; 2011; Tamietto and de Gelder, 2010; de Gelder et al., 2011)for detailed reviews and perspectives).

Compared to multivariate pattern analyses which take into account the joint responses (or covariations) of multiple brain regions, group GLM neuroimaging approaches are relatively insensitive due to loss-of-signal from averaging across many sessions and subjects (Cox and Savoy, 2003; Norman et al., 2006). An alternative and complementary approach, that could reduce signal-loss and the risk of false positives is to apply multivariate pattern analysis to

identify regions of the brain that contain enough information to distinguish between subconscious presentation of biologically salient affective and non-affective stimuli, such as masked fearful and neutral faces.

Although the neural correlates of subliminal (both either task- and task-irrelevant) and threat-related emotional face processing have been extensively investigated using group fMRI studies (Etkin et al., 2004; Fusar-Poli et al., 2009; Kouider et al., 2009; Liddell et al., 2005; Pessoa, 2005) as well as group EEG (Kiss and Eimer, 2008; Pegna et al., 2011), features of brain activity that contain sufficient information to reliably decode, or "brain-read", the emotional expression of subliminally processed faces remain to be identified. Identifying such features could be a crucial step towards understanding the subconscious encoding and processing of affective facial stimuli, since these features would have a greater capacity (though less well quantified) for representing distinctions between fear- and non-fear- related cognitive-emotional perceptual states than those previously identified through standard brain mapping approaches (Norman et al., 2006). This is a particularly important goal given that deficits in facial affect processing are thought to underlie psychiatric disorders such schizophrenia, autism, and anxiety (Harms et al., 2010; Machado-de-Sousa et al., 2010).

Decoding, or predicting, a presented stimulus or cognitive state based on brain activity has mostly relied on multi-voxel pattern analysis (MVPA) approaches that take into account the joint, multivariate response of multiple voxels and/or brain regions (see (Norman et al., 2006) for a review). The above approaches have been increasingly applied toward the problem of identifying features of brain activity that can decode explicit emotional face perception (see discussion for a brief review). Statistically significant, albeit modest, decoding accuracies have been demonstrated when using activation (i.e. either instantaneous, time-averaged activity or

summary measures of activation such as beta estimates derived from SPM maps) of spatially distributed voxels or regions as input features when predicting the emotional expressions of perceived faces. However, like most other complex brain processes, threat-related stimuli and face perception consists of the coordinated functional connectivity among distributed cortical and sub-cortical brain regions (Ishai et al., 2005; Kober et al., 2008; Vuilleumier and Pourtois, 2007). Hence, whole-brain functional connectivity patterns may be more informative than spatial activation patterns when decoding subliminally processed facial emotion.

The current fMRI study employed a blocked design in which subjects were instructed to identify the color of pseudo-colored masked fearful and neutral faces (Etkin et al., 2004). Our primary objective was to test the hypothesis that whole-brain functional connectivity (here Pearson correlation using 40 or 10 time points of fMRI data per example) can discriminate between task-irrelevant and subliminally presented (backwardly masked) fearful and neutral faces, and to identify the functional connections that are most informative in this decoding task. Our secondary objective was to directly assess and compare the decoding ability of correlations that were restricted to regions of the 'sub-cortical alarm pathway' and other limbic regions.

Finally, we compared the decoding accuracies achieved when using *functional connectivity* (FC, or pair-wise correlations) vs. *activity* (i.e. beta estimates from SPM maps). We show that a small subset of connections estimated across the whole-brain (most of which are cortical-subcortical and cortical-cortical that include temporo-parietal regions), can "brain-read" subliminally presented fearful faces with significantly higher accuracies than subcortical-subcortical functional connections restricted to 'subcortical alarm' and other limbic regions. In addition, patterns of spatial activity were significantly less informative than whole-brain FC in discriminating between these two conditions. These findings support the notion that the cortex

plays an active and essential role in subliminal affect processing, and that this neural processing is sub-served by complex interactions among distributed brain regions.

Methods

Subjects: A total of 38 (19 female) healthy volunteers (mean age = 29, SD = 6.9) with emmetropic or corrected-to-emmetropic vision participated in the study in accordance with institutional guidelines for research with human subjects. All subjects were screened to rule out severe psychopathology.

Stimuli Presentation Paradigm: Subjects performed a previously reported task (Etkin et al., 2004) which consists of color identification of masked and unmasked fearful and neutral faces (Fig 9). Results for unmasked conditions, which were used to address separate questions about processing of supraliminal fearful stimuli from those considered here, were presented in Chapter 3. See Chapter 3 Methods for more details regarding stimuli.

Behavioral task: See Chapter 3 Methods for details. Additionally, while still in the scanner and after the main presentation paradigm, subjects were administered a forced-choice test under the same presentation conditions as the functional run and asked to indicate whether they saw a fearful face or not. These data were used to determine d-prime (d′) values using the formula: d' = z(hit rate) – z(false alarm rate), where z represents transformation to z-scores. After the imaging session, subjects were shown the stimuli again, alerted to the presence of masked faces, and asked to indicate whether they had been aware of fearful faces.

fMRI Data Acquisition: See Chapter 3 Methods.

GLM analysis: See Chapter 3 Methods.

Node definitions: Whole-brain parcellation was similar to Chapter 3, and is recapitulated in Fig 15A and 15B below, while sub-cortical alarm parcellation included bilateral masks for hippocampus, dorsal and ventral amygdala, insula and caudate, anterior cingulate, pulvinar and superior colliculus were defined using WFU_pickatlas with the exception of superior colliculus and locus ceruleus, which were manually drawn using FLSview (amygdala was manually separated into dorsal and ventral regions along z=0) (Fig 15C). These regions produced 32 nodes (not shown) and 496 total features. Average MNI locations for each node are listed in Supplementary Table 2 of (Pantazatos, Talati et al., 2012b).

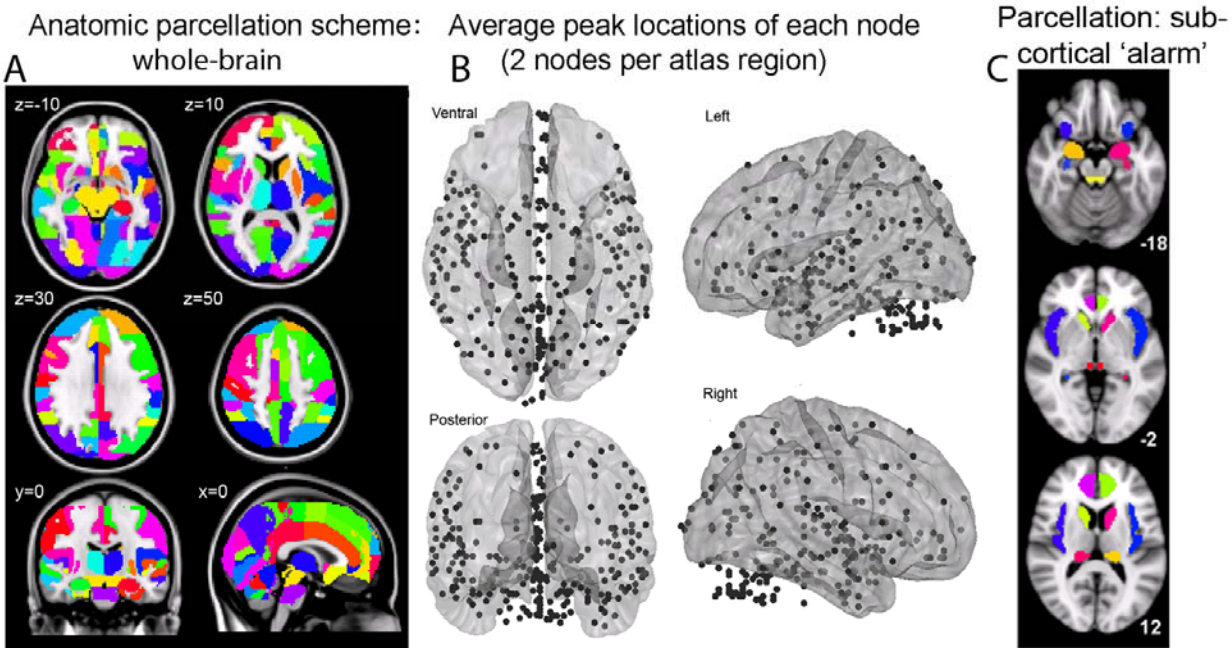

Figure 14. Chapter 5: Whole-brain and "sub-cortical alarm" parcellation. (A) Cortical and subcortical regions (ROIs) were parcellated according to bilateralized versions of the Harvard-Oxford Cortical and Subcortical-atlases, and the cerebellum was parcellated according to the Automated Anatomical Labeling (AAL) atlas ROIs were trimmed to ensure there was no overlap between them and that they contained voxels present in each subject. (B)

The top two eigenvariates from each ROI was extracted, resulting in 270 total nodes throughout the brain. For display purposes, node locations (black spheres) correspond to the peak loading value from each time-course's associated eigenmap averaged over all subjects. (C) Bilateral masks for hippocampus, dorsal and ventral amygdala (left top slice; middle ROIs), insula and caudate (left middle slice; middle ROIs), anterior cingulate, pulvinar and superior colliculus (left bottom slice; top, middle and bottom ROIs respectively) were defined using WFU_pickatlas with the exception of superior colliculus and locus ceruleus, which were manually drawn using FLSview (amygdala was manually separated into dorsal and ventral regions along z=0).

Functional connectivity networks for subliminal fearful and neutral face processing: See Chapter Methods. For the current binary classification of interest (i.e. MF vs. MN), correlation matrices were demeaned with respect to the average between the two conditions in order to remove the effects of inter-subject variability. The lower triangle of the above preprocessed correlation matrices (38 subjects X 2 conditions total) were then used as input features to predict viewed stimuli.

Pattern analysis of large-scale functional connectivity to predict subliminal (and implicit) fear perception: See Chapter 3 Methods. We plotted classification accuracy vs. every 5 features from the top 1 through 200 (the maximum number was chosen heuristically based on (Dosenbach et al., 2010b)). Other than a peak near 10 features, accuracies hovered near 50%. Therefore we changed the range to every single feature from top 1 through 20. For sub-cortical 'alarm' FC we used the same initial range (5 to 200) to confirm that accuracies also hovered near 50% beyond 10 features, and then plotted results using 1 to 20 features as above. We also plotted the null distribution and assessed the significance of peak decoding results by computing the frequency in which actual values surpassed those from null distributions derived by randomly permuting

class labels. To derive this null distribution, class labels within each pair conditions from each subject were randomly flipped with a probability of 0.5 over 10000 iterations (top N features at which peak accuracy was achieved) or 50 iterations (for plots at each number of included features). Uncorrected p-values were reported, and unless otherwise stated, p-values were also corrected at $p<0.05$ for multiple comparisons using Bonferroni procedure. For plots, 95% Confidence Intervals (95% CI) of the accuracy score were calculated using the normal approximation interval of the binomial distribution: $(p\pm Zc*\sqrt{[p(1-p)/n]}$, where $p=TP+TN/(TP+FP+TN+FP)$, $Zc=97.5$ percentile of a standard normal distribution, and n=sample size. This formula was used as it is the simplest and most commonly used to approximate confidence intervals for proportions in a statistical population, and because there was adequate sample size and proportions were not extremely close to 0 or 1(Newcombe, 1998).

SVM learning and classification followed similar procedures as in Chapter 3. For assessing the significance of the differences between decoding results (i.e. whole-brain FC as features vs. subcortical FC) we used the Accurate Confidence Intervals MATLAB toolbox for assessing whether the parameter p (probability of correct prediction) from two independent binomial distributions was significantly different (http://www.mathworks.com/matlabcentral/fileexchange/3031-accurate-confidence-intervals). Briefly, these methods search for confidence intervals using an integration of the Bayesian posterior with diffuse priors to measure the confidence level of the difference between two proportions (Ross 2003). We used the code prop_diff(x_1,n_1,x_2,n_2,delta), (available from the above website) returning $\Pr(p_1-p_2\geqslant\delta)$, where x_1, n_1, x_2, n_2, are number of correct responses and total predictions in two distributions being compared, and delta (zero in our case) is the null hypothesis difference between the probabilities.

Results

Behavioral results: The average response rate in the color discrimination task was 98% (stdev=4.6%), mean accuracy was 97% (stdev=3.5%), and mean reaction time was 0.65 s (stdev=0.12), indicating that subjects performed the task as instructed. In the task used to determine d' scores (see methods), twelve subjects reported that no masked fearful face had been presented). In the remaining subjects, mean observed d' score was 0.13, std = 0.35, and the max was 0.71 (~65% accuracy). A one-sample t-test confirmed these scores were not significantly different than zero (p=0.07). We also included the twelve subjects who only responded with misses and correct rejections. In order to do so we had to slightly adjust their hit rate and false alarm from 0 and 1 to 0.01 and 0.99 respectively, since the z-transform is undefined at 0 and 1. These subjects' d' scores thus all became -4.65, and when they were included in a new one-sample t-test the overall scores were significantly negative (p=0.0006). Taken together, the above results indicate that backward masking was successful.

Discriminating between subliminal processing of fearful and neutral faces with whole-brain patterns of functional connectivity: We applied atlas-based parcellation and computed pair-wise correlations between 270 cortical and sub-cortical brain regions, or nodes, using 40 total time points of fMRI data that were segmented and concatenated from two conditions; task-unrelated viewing of backwardly masked fearful (MF) and neutral (MN) faces (similar to Fig 10 in previous chapter). This resulted in 36,315 total functional connections (z-transformed Pearson correlations) for each condition (MF, MN). The atlas-based parcellation scheme and average node locations are shown in Fig 14A and B, while MNI coordinates and labels corresponding to each node are listed in Supplementary Table 1 in (Pantazatos, Talati et al., 2012b).

The extent to which a subset of these functional connections could decode, or predict, the conditions from which they were derived was quantified by submitting them as features into a linear kernel SVM pattern classifier using filter feature selection based on the t-score of each feature (functional connectivity) in each training set. Decoding accuracies for subliminal fearful vs. neutral classifications (MF vs. MN) were plotted against the number of included features (ranked in descending order by t-score) in order to approximate the number of informative features relevant to the emotional expression of the facial stimulus. For MF vs. MN classification, accuracy reached a maximum of 82% ($p < 0.0001$) when learning was based on the top 9 features in each training set, while accuracies remained above 75% from 10-20 features

(Fig 14A). Features were display neuroanatomically Fig 14B-D and are listed in Table 5.

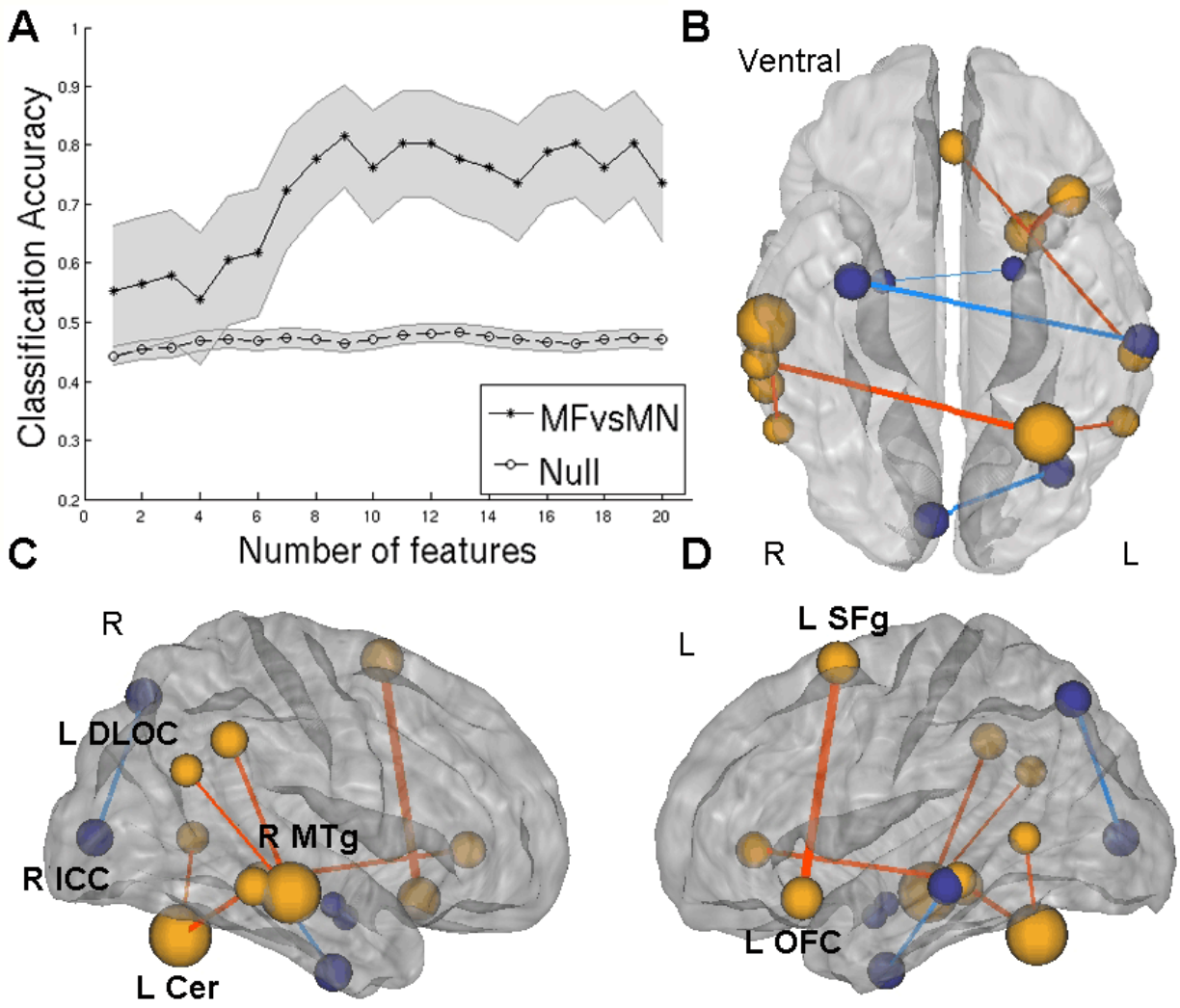

Figure 15. Chapter 5: Large-scale functional connectivity discriminates between processing of masked fearful and neutral faces. (A) Decoding accuracy when classifying MF vs. MN as a function of the number of features (1 to 20) ranked in descending order by their absolute t-score. Maximum accuracy for MF vs. MN classification (82%, $p < 0.0001$) was achieved when learning was based on the top 9 features in each training set. Ventral (B), right (C) and left (D) lateralized anatomical representation of the top 9 overall features. Red indicates correlations that are greater in MF, and blue represents correlations that are greater in MN. For display purposes, the color of each sphere is set according to the sign of the sum of the SVM weights of each node's connections; positive sign, red, MF > MN and negative sign, blue, MN > MF, and the thickness of each connection was made proportional to its weight. Abbreviations: L SFg = Left Superior Frontal Gyrus PC2, L OFC = Left Frontal Orbital Cortex PC2, R MTg =

Right Middle Temporal Gyrus PC2, L Cer = Left Cerebellum, R ICC = Right Intracalcarine Cortex, L DLOC = Left Dorsal Lateral Occipital Cortex.

Table 5. Chapter 5: MF vs. MN, Top 9 features. Consensus features are shown in bold, and Fsets refers to number of training sets in which that feature was selected.

Edge label	Mean R MF	Mean R MN	T-value	SVM weight	FSets
Left_Superior_Frontal_Gyrus_PC2 - Left_Frontal_Orbital_Cortex_PC2	**-0.0079881**	**-0.12867**	**4.5835**	**1.9781**	**38**
Right_Middle_Temporal_Gyrus_posterior_division_PC2 - Cerebelum_6_L_PC1	**0.068222**	**-0.09052**	**5.0103**	**1.6945**	**38**
Right_Temporal_Fusiform_Cortex_anterior_division_PC1 - Left_Middle_Temporal_Gyrus_posterior_division_PC2	-0.091167	0.079443	-4.4287	-1.6638	23
Right_Supramarginal_Gyrus_posterior_division_PC1 - Right_Middle_Temporal_Gyrus_posterior_division_PC1	0.067526	-0.10074	4.5524	1.6333	36
Right_Intracalcarine_Cortex_PC2 - Left_Dorsal_Lateral_Occipital_Cortex_superior_division_PC1	-0.031813	0.10989	-4.3699	-1.6219	20
Left_Middle_Temporal_Gyrus_posterior_division_PC1 - Left_Cingulate_Gyrus_anterior_division_PC1	0.17677	0.019301	4.6431	1.601	37
Left_Middle_Temporal_Gyrus_temporooccipital_part_PC1 - Cerebelum_6_L_PC1	**0.1089**	**-0.037114**	**4.7473**	**1.3721**	**38**
Right_Middle_Temporal_Gyrus_posterior_division_PC1 - Right_Angular_Gyrus_PC1	0.14702	0.0068463	4.3078	1.3644	15
Right_Amygdala_PC2 - Left_Amygdala_PC1	**-0.057707**	**0.055489**	**-4.5929**	**-0.96079**	**38**

Although time-series were high-pass filtered and white-matter and csf signal was removed, it is possible that slow frequency drifts (just below periods of 128 s and manifesting within global grey matter signal) remained, and that these drifts could have artificially increased the variance in (and hence affect the correlation between) the concatenated time series. Given our use of counterbalanced designs, this effect should not have been enhanced in the concatenated time-series from one condition over the other, and hence any differences in FC

between conditions should be attributed to differences in stimulus features of subliminally presented faces, not the above-mentioned potential artifacts.

Discriminating between MF and MN faces using functional connectivity among 'sub-cortical alarm' system and other limbic regions: Previous work in animal models confirms a sub-cortical "alarm" pathway for fast and subliminal fear processing through the superior colliculus, pulvinar and amygdala (Tamietto and de Gelder, 2010). However, direct evidence for this pathway in humans is sparse (Pessoa and Adolphs, 2010). We tested whether functional connectivity among these and other sub-cortical and limbic ROIs could discriminate between masked threat-related and neutral facial stimuli using masks for left and right dorsal and ventral amygdala, pulvinar, insula, anterior cingulate, hippocampus, caudate and bilateral superior colliculus and locus ceruleus (Figure 14C). Classifications used pair-wise functional connections among the above regions (32 nodes, 496 total features) and were performed as above. In contrast to peak decoding results obtained when using functional connections across the whole-brain (82%), MF vs. MN discrimination using features restricted to 'sub-cortical alarm' and limbic regions did not surpass 45% (data not shown). Thus classification accuracy using only subcortical 'alarm' and limbic ROIs was less effective than using ROIs throughout the whole-brain.

Discriminating between MF and MN faces with patterns of activation: To compare the information content of patterns of *functional connectivity* (i.e. functional connections used above) vs. patterns of neural *activity*, we also performed MF vs. MN classification using beta estimates, which are scaling factors estimated from the General Linear Model and can be considered a summary measure of activation to each condition. Our primary goal was to assess

the relative classification performances when using "betas" as features under "best-case scenario" conditions. Thus we employed a single, biased feature-selection step in which features (voxels) were chosen based on an F-test conducted over the entire data set. An inclusion mask was defined from an F-test of the contrast MF > MN ($p < 0.05$, k=30: 6,248 total features, Figure 3A, yellow). Accuracies were plotted against the number of included features ranging from 1 to 6000. In spite of biased feature selection, MF vs. MN classification only reached a maximum of 78% accuracy (data not shown).

Top FC features that discriminated between MF and MN faces: We formally compared the "information content" of whole-brain FC vs. subcortical alarm FC and whole-brain betas when used as features in predicting MF vs. MN faces. For this we tested for significant differences between the maximum classification accuracies achieved for whole-brain FC vs. the other two (see methods). The maximum accuracy for whole-brain FC (82%) was significantly greater that maximum accuracy achieved with sub-cortical 'alarm' FC (45%) ($p < 0.001$) and greater than the peak accuracy achieved with whole-brain beta values under biased feature selection (78%).

Anatomical display of the top 9 overall whole-brain FC features that discriminated between MF and MN conditions revealed functional connections among regions in right middle temporal gyrus, superior frontal gyrus, orbitofrontal cortex, angular gyrus, amygdala, cerebellum, precuneus and anterior cingulate (Figure 15, Table 5). The connection that carried the most weight in the linear SVM classifier was between left superior frontal gyrus and left orbitofrontal cortex, which exhibited a greater correlation in the MF vs. MN condition.

Discussion

The current work demonstrates that patterns of *functional connectivity* (pair-wise cortical-cortical and subcortical-cortical functional connections) contain sufficient information to decode the emotional expression of task-irrelevant, subliminally presented faces. The connections that discriminated between subliminally presented fearful and neutral faces included cerebellum, superior frontal and orbitofrontal cortex, amygdala, temporo-occipital and temporo-parietal regions, with the majority of connections involving the posterior and anterior middle temporal gyrus (in the vicinity of the superior temporal sulcus, STS). This is consistent with models and studies of emotional face recognition that identify the STS and middle temporal gyrus as a primary neural substrate for suprathreshold processing of the emotional expression of faces (Haxby et al., 2002; Sabatinelli et al., 2011; Said et al., 2010). Importantly, the current results suggest these cortical regions are also engaged and required during *subliminal* and task-irrelevant emotional face processing, and furthermore, that functional interactions of STS with temporo-parietal, temporo-occipital and cerebellar regions are also critically involved in subliminal emotional face processing. In addition, we observed that functional connections restricted to the 'sub-cortical alarm' pathway were not sufficient to decode subliminal emotion perception. Taken together, these observations support the notion that the cortex plays a more important role in the processing of subliminal affective visual information than is typically acknowledged (Pessoa and Adolphs, 2010)}}

Interestingly, the only observed functional connection among the top 9 informative features which included two sub-cortical regions was between left and right amygdala. This FC decreased during during fear, suggesting bilateral decoupling of this key limbic region during the MF condition. This observation is consistent with previous studies suggesting that the right

amygdala is more involved during automatic, subliminal and unintentional mood induction, whereas the left amygdala is more involved during supraliminal perception and intentional, cognitive mood induction engaged during explicit reflection processes (Dyck et al., 2011; Williams et al., 2006).

"*Information content" of neural activity vs. functional connectivity:* Multi-voxel pattern analysis (MVPA) methods have been successful in decoding categories of viewed stimuli (Cox and Savoy, 2003; Hanson et al., 2004; Haxby et al., 2001; Mourao-Miranda et al., 2005; O'Toole et al., 2005), orientation (Haynes and Rees, 2005; Kamitani and Tong, 2005), the decisions made during a near-threshold fearful face discrimination task (Pessoa and Padmala, 2007), and decoding explicit emotion perception (Peelen et al., 2010; Said et al., 2010; Tsuchiya et al., 2008). However, complex and subtle cognitive and affective processes such as those that are engaged by subliminally presented emotional faces, and which entail interactions among many distributed regions, may not be adequately captured or represented by patterns of spatial activation, when using typical imaging parameters used for whole-brain imaging and particularly when the activity in each region is averaged over several or more time points to increase signal to noise. Instead, the pattern of *functional connectivity*, (i.e. pair-wise correlations or other measures of large-scale functional connectivity), may be a relatively more sensitive and informative representation of such brain-states compared to patterns of *activity*. (However, we speculate that with the increasing sensitivity, spatial and temporal resolution of fMRI, decoding subliminal emotion perception based on fine-grained activity patterns within key regions (i.e. amygdala, fusiform, superior-temporal sulcus), and particularly within single subjects, should be feasible.)

Large-scale functional connectivity (i.e. thousands of pair-wise function connections) and network analysis has been increasingly used as the tool of choice for extracting meaningful and understanding complex brain organization (Li et al., 2009; Smith et al., 2011). A previous group study, which did not apply MVPA but instead averaged each connection over multiple subjects in a univariate fashion, demonstrated condition dependent modulations in pair-wise (41 nodes) functional connectivity across various syntactical language production tasks (Dodel et al., 2005). More recently, pattern analysis on large-scale functional connections obtained from resting state data were used to predict individual maturity (Dosenbach et al., 2010b) as well as subject-driven mental states such as memory retrieval, silent-singing vs. mental arithmetic and watching movies vs. rest (Richiardi et al., 2011). Here we used stimulus-associated, condition-dependent functional connectivity to discriminate between subconscious cognitive-emotional processing states within individual subjects.

Previous work based on simulations has indicated that correlation-based methods, including Pearson correlation, are in general quite successful in capturing true network connections (Smith et al., 2011). Here we show that Pearson correlation can be used to estimate connections that decode ("brain-read") the emotional expression of a face that was subliminally presented during each block from which they were derived. We also compared the decoding accuracy when using correlations as features versus beta estimates (i.e. summary measures of activation to each condition at each voxel). We observed that, even with feature-selection based on the entire data set which positively biased results, peak decoding accuracies for betas were lower than those reached when using correlations as features (betas: MF vs. MN peak accuracy 78%, MF vs. MN peak accuracy 82%). This suggests that there is more information, relevant to subliminal cognitive-emotional neural processing, that is contained in the interactions between

regions than is typically realized through standard univariate approaches. However, it should be noted that this requires enough time-points to compute meaningful correlations between brain regions for a particular condition, and would thus in general be impractical for decoding single-trial or event-related data.

Subliminal vs. supraliminal fearful face processing: The same method used here was recently applied to decode supraliminal (200 ms presentation prior to backward masking), as opposed to subliminal (67 ms presentation prior to backward masking, fearful vs. neutral faces (Pantazatos et al., 2012a). As expected, supraliminal emotional stimuli were more distinguishable than subliminal stimuli, as evidenced by higher maximum accuracies (86-96%) achieved across a wider range of features (10-20) for supraliminal stimuli. As in the current work, many of the connections that distinguished between supraliminal emotion stimuli included STS and middle temporal gyrus. However, by and large, there was little to no overlap between the most informative connections that discriminated between subliminal fearful and neutral faces presented in the current work and the most informative features that discriminated between supraliminal fearful and neutral faces. For supraliminal stimuli, the most positively modulated FC was between left thalamus and STS, while thalamus was not included in the current results. This is consistent with the observation that the thalamus (pulvinar) is relatively more active for attended and consciously-perceived affective stimuli (Pessoa and Adolphs, 2010), and also with the idea that separable and largely non-overlapping neural regions and mechanisms may underlie conscious vs. non-conscious processing of affective stimuli (Etkin et al., 2004; Tamietto and de Gelder, 2010).

Limitations: Using Pearson correlation, it is possible that any association between two brain regions is the result of a spurious association with a third brain region. Likely candidates for this third region are the pulvinar (located in the posterior thalamus) and amygdala, which are proposed to act as hubs integrating the activity of multiple cortical areas during sub-threshold emotional stimulus processing (Pessoa and Adolphs, 2010; de Gelder et al., 2011). The current analysis may have neglected to account for functional contributions of the pulvinar since we extracted the top two principal components from the whole thalamus; thus possible future experiments would explicitly define the pulvinar separately from the rest of the thalamus.

Another possible limitation of the current study is the required amount of data used to extract quality features of brain activity. Our use of correlations as features required a substantial number of time points (i.e. 40 time points per condition per subject) relative to previous studies of decoding emotion perception. Given this, it was not feasible to sample enough examples within a single or few subjects as is typical in multivariate pattern analysis studies, and we instead pooled examples across multiple subjects. On the other hand, the fact that reliable classifiers could be learned using examples from separate subjects speaks to the generalizability of our obtained results.

Previous simulations have raised concerns regarding the use of atlas-based approaches for parcellating the brain (Smith et al., 2011) Because the spatial ROIs used to extract average time-series for a brain region do not likely match well the actual functional boundaries, BOLD time-series from neighboring nodes are likely mixed with each other. While this hampers the ability to detect functional connections between neighboring regions, it has minimal effect on estimating functional connectivity between distant regions. This perhaps explains why in this study most of the functional connections that discriminated between fearful and neutral faces are

long-distance. Future experiments using non-atlas based approaches would likely lead to better estimates of shorter-range functional connections.

In addition to the choice of parcellation schemes, decoding results were also affected by the number of eigenvariates extracted from each region. Extracting only one eigenvariate from each region did not contain sufficient information to decode subliminal fear (data not shown), whereas extracting two eigenvariates did. Extracting three and four eigenvariates resulted in a decrease in decoding accuracies (data not shown), probably because the exponential increase in estimated edges among the nodes led to increased likelihood of "false-positives" being selected during the linear filter feature selection. Future studies should explore more sophisticated methods of feature selection that could better exploit and select informative features from higher-dimensional feature spaces.

Conclusions: The current work demonstrates that large-scale functional connections between cortical-cortical and cortical-sub-cortical regions are sensitive features of brain activity that can decode task-irrelevant, subliminal emotion processing. In contrast, sub-cortical-sub-cortical functional connections, particularly among 'sub-cortical alarm' regions, contained less information for this decoding task, as did patterns of spatial activity. These data are consistent with the notion that *interactions* that include cortical regions are employed for the subconscious processing of biologically salient affective stimuli. In addition, the pattern of connections (edges of a weighted graph) between regions is an informative and sensitive signature of subconscious cognitive-emotional brain states.

CHAPTER 6

LARGE-SCALE FUNCTIONAL CONNECTIVITY DURING SPEECH AND SONG IN AUTISM[5]

Summary

A prominent aspect of neurobiological accounts of autism is significantly reduced strength of long-range, and in particular frontal-posterior, neural connections. This largely comes from functional connectivity MRI during resting-state or language and speech comprehension, and is interpreted as a deficit in the formation and maintenance of long-range structural and functional connections, particular frontal-posterior connections involved in language and social communication. Despite language disabilities in autism, however, music abilities are frequently preserved. Paradoxically, brain regions associated with these functions typically overlap, suggesting domain-specificity in autism such that stronger long-range functional connectivity would be observed during song (vs. speech) perception. This hypothesis was tested with large-scale functional network analyses of both song and speech processing in autistic and control subjects. In support of this hypothesis, in autistic children, we observed significantly stronger long-range frontal-posterior connectivity during music stimulation when compared to speech stimulation, suggesting that in autism, long-range, frontal-posterior functional connections are more effectively engaged for song than for speech. These observations may provide at least a partial neurobiological account for the observed effects of music therapy in autism.

[5] Lai, Grace, Spiro P Pantazatos, Harry Schneider, and Joy Hirsch. 2012. Neural systems for speech and song in autism. *Brain.*

Introduction

Autism is a complex developmental disorder currently estimated to affect approximately 1 in 100 children (Kogan et al., 2009). It is defined by reduced social interaction, impaired communication, and restricted interests and behavior. One prevailing characterization of autism is that it is a disorder associated with atypical brain connectivity affecting distributed neural systems (Belmonte et al., 2004; Courchesne and Pierce, 2005; Just et al., 2004; Minshew and Williams, 2007). Neuroimaging studies of language in high-functioning autistic subjects have reported decreased activation in Broca's area (left inferior frontal gyrus, IFG as well as decreased functional connectivity between frontal and posterior language processing regions (Fletcher et al., 2010; Harris et al., 2006; Just et al., 2004; Kana et al., 2006; Sahyoun et al., 2010). However, while these findings support disconnection models for autism that propose under-connectivity between distant brain regions (Just et al., 2004; Kana et al., 2006), disconnection models do not explain the frequently observed preservation of related functions such as music (Allen et al., 2009; Mottron et al., 2000) where, in healthy adults, neural systems engaged during music and language functions tend to be highly coincident (Koelsch et al., 2002; Limb, 2006; Patel, 2011; Schön et al., 2010). Here we examine the large-scale functional architecture of music and language perception in autistic children and healthy controls, and tested the hypothesis that music engages longer-range functional connections in autism. Positive findings would imply that long-range disconnection, it in of itself, is not a sufficient account for impairment in autism, but rather that long-range disconnection is instead an outcome and result of domain-specific deficits in language and social processing, which may occur more locally in the brain.

Methods

Subjects: Thirty-six patients with autism participated in this study, all recruited by physician referral. Twelve of these patients (mean age = 12.40 SD = 4.70, range = 7.01-22.47; males = 10; right-handed = 10) were imaged while alert. Images from an additional 27 patients (mean age = 8.62, SD = 3.14, range = 5.41-17.93; males = 22; right-handed = 15) who received MRI evaluations (structural, functional, and DTI scans) for medical purposes under light propofol sedation were also included in this study, following parental consent. Twenty-one non-autistic controls (mean age = 10.72, SD = 4.42, range = 3.57-17.78; males = 14; right-handed = 19) were imaged alert and recruited via flyers distributed within the Columbia University Medical Center and Columbia University campuses. Due to excessive head movement, several additionally recruited subjects (two control and four autistic subjects) were excluded from the final dataset. All parents provided consent for their child to participate, or to include their clinical MRI examinations in this research study as approved by the Columbia University Medical Center Institutional Review Board. When possible, assent was also obtained from the subjects. A subset of data from these same subjects were used in a previous study investigating the potential application of fMRI for identification of autism (Lai et al., 2011).

Comparisons between autistic and control groups were based on subsets of age-matched subjects and functional MRI comparisons between autistic and control groups included only images acquired during alert conditions. Patients and controls were not matched on IQ since patients were low-functioning. Within-group contrasts for the autism group included sedated and non-sedated subjects. Additionally, DTI comparisons included data from both non-sedated and sedated subjects for the benefit of an increased sample size. DTI images from 5/12 alert patients were excluded due to visible movement. Table 1 provides a summary of demographic information (age, gender, and handedness) for subjects included in all DTI and fMRI

comparisons.

Autistic children were eligible for the study if they met diagnostic criteria for autism on the DSM-IV and the Autism Diagnostic Interview – Revised (ADI-R). Language impairment was measured using the Language and Communication subscale of the ADI-R and clinical observation (see supplemental methods). Control subjects were eligible to participate if they did not have a diagnosis of autism, a psychiatric disorder, or siblings diagnosed with autism. Levels of normal social and academic functioning for controls were confirmed via scholastic performance at grade-level and parent report. Both autistic and control children were without co-morbid neurological or developmental disorders, as determined by clinical evaluation performed by the referring physician for autistic subjects and parent report for control subjects.

Music Affinity ratings: Due to the severity of impairment of autistic subjects in this study, a formal assessment of music function was not performed. Rather, parents were asked to rate how receptive their child was to different kinds of music on a scale from 0-10. "0" was defined as *Not at all - does not orient to music when playing, may as well be random noise*. "5" was defined as *Moderately - will listen to and enjoy if playing, but will not request it*. "10" was defined as *Extremely - will request it to be played frequently and listen attentively for long periods of time*. Parents rated their child's affinity for the child's specific song selection.

Alert autistic and control subjects: We employed a "silent video" technique to help minimize head-movement and distractibility in young children . A familiar video was shown (on mute) throughout the scan duration. The silent video was presented via a rear-projection screen or MRI compatible goggles depending on the child's preference. Comparisons between auditory epochs

and baseline revealed brain activity related to the auditory stimulus rather than the video that occurred continuously during both stimulus and baseline epochs.

Sedated autistic patients: Patients imaged under conventional clinical conditions were imaged to rule out organic disease while sedated with propofol for neurologic assessment in accordance with the medical requisition of the referring physician. Although sedation has been associated with reduced amplitude of the fMRI signal during auditory stimulation (Davis et al., 2007) it is indicated to map language systems in children under clinical conditions (Souweidane et al., 1999). See Supplemental Methods for description of anesthesia management. Parents of eligible patients provided permission to include these medical scans.

fMRI Stimulation: Each fMRI acquisition (run) was 2 min and 29 sec in duration, consisting of a 24 sec period of background scanner noise, followed by four 15 sec presentations of the auditory stimulus alternating with 15 sec when the auditory stimulus was not presented. Two runs for each stimulus type (speech and song) were presented consecutively. The order of presentation was randomized across subjects. Auditory stimuli were pre-recorded by parents and presented passively to subjects via MR-safe headphones. Although passive language stimulation primarily engages receptive processes, it is necessary for use with low-functioning children who cannot comply with task instructions during an imaging procedure. Activation in typical language areas has been previously reported during routine clinical assessments for alert (Hirsch et al., 2000) and sedated patients (Souweidane et al., 1999) using similar stimulation techniques.

Speech stimuli were recordings of each child's own parents speaking in a natural and conversational manner to their child. All parents were instructed to talk about the same topics

(i.e. being in the scanner, recent events, plans after the scan) although the test was not scripted in order to assure familiarity with each parent's conversational style. Song stimuli were selected as each child's favorite or preferred song containing vocals. Since autistic children often have fixed interests and are particularly receptive to familiar stimuli, it was necessary that speech and song stimuli were familiar and preferred for each subject. For the speech recordings, two independent raters judged whether the 15 sec clips of voice recordings from autistic and control parents could be distinguished. Both raters judged the child's diagnosis with only 55% accuracy (11/20) with a 43% (9/20) correspondence. Close-to-chance levels of performance indicate that narratives from autistic parents did not differ perceptibly from controls. Audio stimuli were power-normalized across subjects to ensure similar acoustic properties across subjects.

MRI acquisition: Alert autistic and control children were imaged using a research-dedicated 1.5 T GE Twin Speed magnetic resonance scanner located in the Functional MRI Research Center at Columbia University Medical Center. Clinical structural and functional images were acquired at the MR Imaging Center of the Morgan Stanley Children's Hospital of New York-Presbyterian Hospital on a similar 1.5 T GE Twin Speed magnetic resonance scanner using identical sequences.

In both cases, fMRI images were acquired using an echo planar T2*-weighted gradient echo sequence (TE = 51 ms, TR = 3000 ms, flip angle = 83 deg). Twenty-seven contiguous axial slices covering the full brain were acquired along the AC-PC plane, with a 192 x 192 mm field of view (FOV) imaged on a 128 x 128 grid yielding an in-plane resolution of 1.56 x 1.56 mm and slice thickness of 4.5 mm. High-resolution structural images were acquired using a 3D SPGR sequence (124 slices, 256 x 256, FOV = 220 mm), with a total scan time of 10 min and 38

sec. Diffusion tensor imaging (DTI) images were acquired using a echo-planar sequence (TR = 8500 ms, TE = 81.9, 25 directions, b = 1000 s/mm^2). Twenty-seven slices were acquired with a resolution 1.02 mm x 1.02 mm and slice thickness of 5.00 mm on a 128 x 128 grid. The total scan time for the DTI acquisition was 3 min and 58 sec. Although the use of 25 diffusion directions constrains the ability to detect crossing fibers for tractography analyses, the shorter run time achieved by using fewer diffusion directions was necessary to minimize image acquisition time for children.

Preprocessing: Realigned T2*-weighted volumes were slice-time corrected, spatially transformed to the standard MNI brain and smoothed with a 8-mm full-width half-maximum Gaussian kernel. First-level regressors were created by convolving the onset of each stimulus epoch with the canonical HRF with duration of 15 seconds. Additional nuisance regressors included motion, global white matter and CSF signal. Prior to extraction, each voxel's time-series were adjusted for effects of interest by removal of the above nuisance effects.

ROI definition: Brain regions were parcellated by the Harvard-Oxford Cortical and Subcortical atlases and the AAL (cerebellum) atlas and were trimmed to ensure no overlap (Figure 16a). The time-series from each voxel in each region was extracted, segmented according to condition onsets and durations (incorporating a lag of 1 TR, or 3s, to account for the HRF), and concatenated across all conditions and subjects. Singular Value Decomposition (SVD) was then applied to the m x n data matrix to reduce data dimensionality, where m = number of voxels in each region, and n = number of time points across all subjects and conditions (4080). For each region, eigenvariates that accounted for greater than 5% of the total variance across all subjects

and conditions were used as ROIs for the whole-brain connectivity analysis. This resulted in 298 total time courses (eigenvariates) and ROIs (spatial eigenmaps) from the 133 initial regions. Concatenation across subjects was performed prior to data reduction in order to ensure that each ROI had identical, normalized spatial locations across all subjects. ROI locations were defined in MNI coordinates at the peak value of each eigenmap.

Large-scale functional connectivity analyses: Images were preprocessed using SPM8 software (see above) (Wellcome Department of Imaging Neuroscience, London, UK). Pair-wise functional connectivity (Fisher's R-to-Z transformed Pearson correlations) was computed between 298 total cortical, subcortical, and cerebellar ROIs for each subject and condition (Figure 16a, see above section). We performed an initial filter step to filter out noise (~38,000 positive and negative correlations hovering near zero) and increase the likelihood of only including real functional connections in comparisons between conditions and groups. Connections that were either positive or negative over all subjects and conditions were analyzed separately (thresholded using a one-sample t-test, $p < 0.001$ uncorrected). There were 5,879 positive connections and 4959 negative connections. A paired t-test was then applied to identify connections that were greater for song relative to speech (song > speech), and those greater for speech relative to song (speech > song) across a range of p-thresholds ($p=0.05$ to $p=0.001$, x-axis of Figure 16b) in order to ensure that results of subsequent comparisons were not specific to or dependent upon particular p-value thresholds. The mean length (Euclidean distance between the end points) of these identified connections was then compared between song>speech and speech<song using two-sample t-tests. Correlations that survived $p<0.05$ uncorrected thresholds

(for the paired comparisons) were used to define the connections between ROIs displayed in Figure 16c.

Results

Behavioral Results: All autistic subjects scored in the high range of impairment on all three ADI-R sub-sections (Reciprocal Social Interaction: mean = 21.18, SD = 1.66, range = 17-24; Language and Communication: mean = 18.87, SD = 2.62, range = 12-26; Restricted, Repetitive, and Stereotyped Behavior: mean = 6.00, SD = 1.15, range = 4-9). A diagnosis of autism is made when a child scores higher than a specified minimum on all three sections (Social: >10; Language: >8; Repetitive Behaviors: >3). In particular, scores on the language and communication domain for all patients in this study (range=12-26) were well above the diagnostic minimum (>8) for autism.

Clinical observations of words uttered during a 30 minute free-play session ranged from 0–250. Mean number of words uttered in response to a physician's prompt was 46.4 (SD = 76.16, median = 14), and the mean number of spontaneously produced words was 16.29 (SD = 42.70, median = 4). Breakdown of the percentage of children with zero to over 50 words (Figure 1a) document the limited verbal output in a majority of our patients (over 50% of them produced under 5 spontaneous words during the session). Breakdown of verbal output by age (Figure 1b) fails to suggest a relationship between number of words and age. Linguistic comprehension was limited to simple (subject, verb, object) grammatical relationships in all subjects except for one child who was able to comprehend more complex constructions, such as the use of the passive voice or hierarchical structures. Verbal output for controls could not be assessed in the same way as the autistic patients due to the absence of standardized instruments appropriate for both low-functioning language-impaired autistic children and typically developing controls. Behavioral

milestones reported by the National Institute on Deafness and Other Communication Disorders, (NIDCD. (2001). Retrieved from http://www.nidcd.nih.gov/health/voice/speechandlanguage.asp#mychild.) for typically developing children include understanding of approximately 2000 words, production of more than 300 words, and use of grammatically correct compound and complex sentences by the age of five.

Despite language impairments, the autism group did not differ from the control group on ratings of music affinity. Parent ratings (on a scale of 1-10) of how receptive their child was to the familiar song showed no significant group differences between the autistics and controls in their affinity for familiar songs (autism mean = 8.20 SD = 2.16, control mean = 9.05 SD = 1.10, t = -1.56, p = 0.126).

Large-scale functional connectivity results: Large-scale functional connectivity between song and speech stimulation was assessed using the mean lengths (Euclidean distance) of pair-wise functional connections across ROIs of the whole-brain (Figure 16a) that differed between conditions. In the autism group, positive pair-wise correlations that were greater in song relative to speech ($p < 0.05$) had a grater mean Euclidean distance (length) than those greater for speech relative to song (song > speech, mean length = 63 mm, speech > song, mean length = 49 mm, p = 0.0009). This was significant over a range of thresholds used to define song > speech and speech > song connections (Figure 16b, top). No differences were observed in controls (song > speech, mean length = 59 mm, speech > song, mean length = 60 mm, p = 0.79, Figure 16b, bottom), consistent with the lack of song vs. speech differences in the PPI analysis for the control group (see (Lai et al., 2012) for activation, PPI and DTI results and discussion). Anatomical display of

these connections (defined at p-value threshold of 0.05) illustrates greater fronto-posterior connectivity during song relative to speech in autistic subjects (Figure 16c, top, orange connections) but not controls (Figure 16c, bottom). Greater fronto-posterior connections for song > speech relative to speech > song is consistent with PPI results of greater functional connectivity between left IFG and posterior brain regions during song relative to speech stimulation in autistic patients (see (Lai et al., 2012)). Overall numbers of increased versus decreased connections were comparable between the two groups, but interestingly in autism there were slightly fewer connections during song relative to speech, and vice versa in controls (Autism: song > speech = 127; speech > song = 186; Total=313; Control: song > speech = 181; speech > song = 156; Total = 337). This suggests fewer, but longer distance connections during song, and greater, short distance connections during speech in autistic subjects.

In contrast to positive functional connections, negative functional connections exhibited no significant differences in the Euclidean length of pair-wise correlations that were greater in song relative to speech in either group: autism, song > speech, 141 connections, mean length = 79 mm, speech > song, 128 connections, mean length = 81 mm, $p = 0.76$; Control, song > speech, 149 connections, mean length = 79 mm, speech > song, 151 connections, mean length = 86 mm, $p = 0.10$). Taken together, these results suggest that in autism, song induces increased long-range positive, but not negative, functional connectivity.

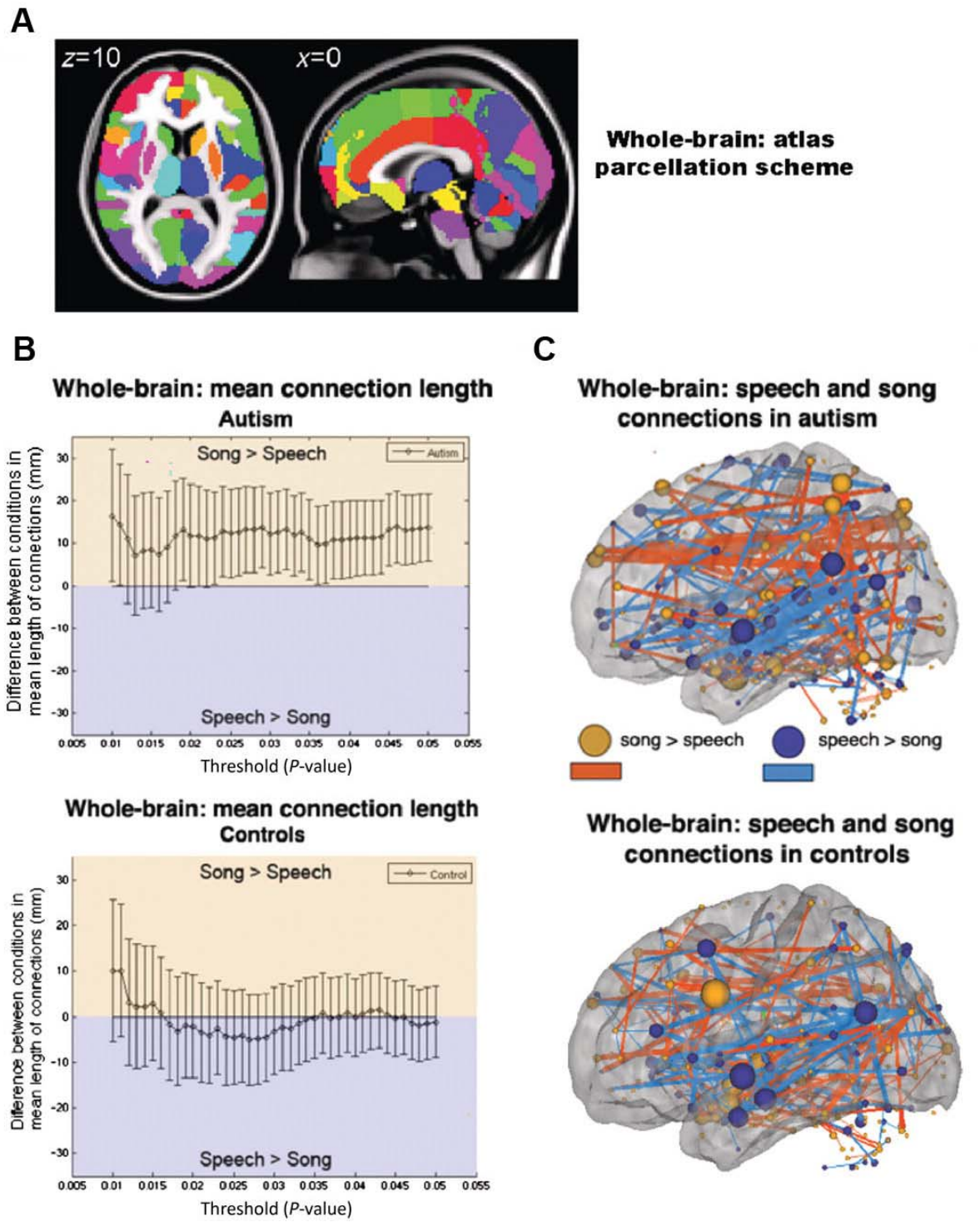

Figure 16. Chapter 6: Song vs. speech large-scale functional connectivity in autism and healthy controls. (**A**) Atlas used to parcellate regions for large-scale whole-brain analysis. (**B**) Large-scale whole-brain analysis showed that in autism (*top*), connections that are stronger for song relative to speech are longer on average than connections

stronger for speech relative to song (plotted with 95% CI). In controls (*bottom*), connections stronger for speech did not differ in length to connections stronger for song. (**C**) Anatomical representation of functional connections (lines) between regions (spheres) stronger in song relative to speech (red, $P < 0.05$ uncorrected) and speech relative to song (blue, $P < 0.05$ uncorrected) in autistic (*top*) and control (*bottom*) subjects (left hemisphere shown). Size of each sphere represents the sum of the lengths of all its connections. For display purposes, the thickness of connections was made proportional to their lengths.

Discussion

Using fMRI, the large-scale functional networks during language and music perception in autistic patients was investigated. Consistent with previous studies and models of neural disconnection (Just et al., 2004; Kana et al., 2006), we observed decreased long range functional connectivity, and increased short range functional connectivity, in response to speech (vs. song) stimulation in autistic subjects. In addition, reduced activation and functional connectivity in core components of the language system (left IFG, or inferior frontal gyrus, also known as Broca's area, and secondary auditory cortex) during speech perception was observed in these same data (Lai et al., 2012) However, during music perception there was a significant increase in long-range functional connectivity relative to the speech condition, as well as increased left IFG activation and increased functional connectivity with angular gyrus (Wernicke's area) relative to speech stimulation (Lai et al., 2012). Together, these findings support the hypothesis that long-range disconnection may not be a sufficient account for language impairment in autism.

One possibility for discrepancies between music and language functions in autism and models that propose long-range disconnection may be a speech-specific (and in general, social-information-specific) attentional deficit (Groen et al., 2008). Whereas typically developing individuals prefer speech to non-speech stimuli and are automatically inclined to process higher-level linguistic and semantic information in speech stimuli, there is evidence that autistic subjects

do not appear to exhibit the typical bias towards social stimuli (Ceponiene et al., 2003; Järvinen-Pasley and Heaton, 2007).

In summary, the current findings imply that long-range disconnection alone is not a sufficient account for impairment in autism, and that long-range disconnection may instead be an outcome and result of domain-specific deficits in language and social processing, which may occur more locally in the brain. These results also highlight the fact that large-scale functional networks may be more or less anomalous in a particular psychiatric disorder depending on the conditions under which they are measured. For the development of functional connectivity-based diagnostic neurobiological markers, which has largely relied on resting-state paradigms, these results further motivate the use of stimuli or conditions in which there is a disorder-dependent increase (or decrease) in attentional bias. The next chapter investigates whether large-scale functional connectivity during the processing of facial affect, particularly harsh or ambiguous emotions, can be used for diagnostic classification of social anxiety disorder.

CHAPTER 7

REDUCED ANTERIOR TEMPORAL AND HIPPOCAMPAL FUNCTIONAL CONNECTIVITY DURING FACE PROCESSING DISCRIMINATES INDIVIDUALS WITH SOCIAL ANXIETY DISORDER FROM HEALTHY CONTROLS AND PANIC DISORDER, AND INCREASES FOLLOWING TREATMENT[6]

Summary

Group functional magnetic resonance imaging (fMRI) studies suggest anxiety disorders are associated with anomalous brain activation and functional connectivity (FC). However, brain-based features sensitive enough to discriminate individual subjects with a specific anxiety disorder and that track symptom severity longitudinally, desirable qualities for putative disorder-specific biomarkers, remain to be identified. BOLD fMRI during emotional face perceptual tasks and a new, large-scale and condition-dependent FC and machine-learning approach was used to identify features (pair-wise correlations) that discriminated patients with social anxiety disorder (SAD, N=16) from controls (N=19). We assessed whether these features discriminated SAD from panic disorder (PD, N=16), and SAD from controls in an independent replication sample which performed a similar task at baseline (N: SAD=15, controls=17) and following 8-weeks paroxetine treatment (N: SAD=12, untreated controls=7). High SAD vs. HCs discrimination (Area under the ROC Curve, AUC, arithmetic mean of sensitivity and specificity) was achieved with two FC features during implicit neutral face perception (AUC=0.88, $p<0.05$ corrected). These features also discriminated SAD vs. PD (AUC=0.82, p=0.0001) and SAD vs. HCs in the independent replication sample (FC during implicit angry face perception, AUC=0.71, p=0.01). The most informative FC was left hippocampus-left temporal pole, which was reduced in both SAD samples (replication sample p=0.027). This FC increased following effective treatment

[6] Pantazatos, Spiro P, Ardesheer Talati, Franklin Schneier, and Joy Hirsch. 2013. Anterior temporal, hippocampal functional connectivity during face processing discriminates individuals with social anxiety disorder and normalizes following treatment. (submitted).

(post > pre, t(11)=2.9, p=0.007), with greater increases correlating with greater decreases in symptom severity (ΔLSAS vs. ΔFC, R=-0.55, p=0.008). In conclusion, SAD is associated with reduced FC between left temporal pole and left hippocampus during face perception, and results suggest promise for emerging FC-based biomarkers for SAD diagnosis and SSRI treatment effects.

Introduction

There is an increasingly recognized need for biomarkers in neuro-degenerative and psychiatric disorders for both early and differential diagnosis, personalized prediction of treatment response, and treatment and drug discovery (Gordon and Koslow, 2010). Biomarker research for anxiety disorders has received relatively little attention, despite the fact they are the most common psychiatric condition, with a lifetime prevalence of 29% (Kessler et al., 2005). Social anxiety disorder (SAD) is the most common of these disorders (Jefferys, 1997), with a 7% to 13% lifetime prevalence (Kessler et al., 1994). SAD is characterized by heightened anxiety and avoidance during social interactions. It has an early onset (80% of cases occur before age 18 years) (Otto et al., 2001), and often precedes other anxiety, mood, and substance abuse/dependence disorders (Lampe et al., 2003; Randall et al., 2001). SAD is associated with significant functional impairment and distress in work and social domains and usually persists unless treated (Lochner et al., 2003; Schneier et al., 1994).

Models of SAD (Clark and McManus, 2002; Rapee and Heimberg, 1997) have highlighted the role of sensitivity to perceived social threats, which is triggered by biased appraisals of social situations. These maladaptive appraisals transform innocuous social cues into interpersonal threats that induce a cascade of fears of negative evaluation, somatic concerns, inhibited behavior, and negative emotional reactivity. Behavioral studies have shown a negative

interpretation bias in SAD, such that ambiguous facial expressions are more likely to be deemed as threatening (Mohlman et al., 2007; Veit et al., 2002; Yoon and Zinbarg, 2007a). A meta-analysis of neuroimaging studies of anxiety (using tasks that mostly involved emotional face viewing) found overall greater activation of amygdala and insula, structures linked to negative emotional response, in SAD subjects relative to matched comparison subjects (Etkin and Wager, 2007).

Neuroimaging studies have typically used emotional face paradigms to contrast average activation between patients and healthy control subjects, identifying significant differences in particular brain regions. However, clinical application of neuroimaging for the diagnosis and treatment of anxiety would require a quantitative measure of brain activity that can distinguish single patients with a specific disorder (e.g. SAD) from healthy individuals as well as from individuals with a related disorder (e.g. Panic Disorder (PD), which is characterized by panic attacks and anxiety symptoms that overlap those of SAD but are not exclusively related to social stimuli). To accomplish this we shifted the focus of our data analysis from average differences (or similarities) in regional brain activity between groups to features of brain activity that maximize the probability of predicting the correct diagnosis within a single subject.

A novel approach based on multivariate machine learning-based pattern analysis of large-scale, condition-dependent functional connectivity (FC) recently demonstrated increased sensitivity of patterns of interactivity (i.e. pair-wise FC from hundreds of nodes) relative to patterns of activity (i.e. beta or contrast activation maps) in predicting subliminal and implicit viewing of fearful vs. neutral faces in healthy subjects (Pantazatos et al., 2012a; Pantazatos, Talati et al., 2012b) . Based on this and previous evidence that SAD subjects exhibit anomalies in the cognitive-emotional processing of emotional and ambiguous social stimuli, we

hypothesized that such patterns of interactivity during fearful and neutral face processing would be sensitive in discriminating whether an individual subject has SAD. The current work examined 1) whether pattern classification of FC during implicit or subliminal processing of emotional or neutral faces can predict SAD diagnosis (control vs. SAD, and SAD vs. PD), 2) whether discriminating features from the above were also replicated in an independent sample and 3) whether these same discriminating features tracked symptom severity in subjects undergoing 8 weeks of treatment with the selective serotonin reuptake inhibitor (SSRI) paroxetine. A secondary objective compared the classification performance achieved when using interactivity (pair-wise correlations) vs. activity (i.e. beta estimates from SPM maps). If FC-based features can be shown to reliably categorize subjects with a diagnosis of SAD, discriminate them from subjects with a closely related disorder such as PD, and demonstrate normalization following effective treatment, this would represent an important advance in the development of biomarkers for psychiatric diagnosis and treatment effects.

Methods

Ethics Statement: All procedures and tasks were reviewed for ethical concerns and protection of human subjects by the Columbia University and New York State Psychiatric Institute Institutional Review Boards prior to subject recruitment and data collection.

Subjects

Primary Sample: Twenty healthy control subjects (HC), 18 subjects (ages 18-50) diagnosed with SAD and 16 patients diagnosed with PD were recruited through web advertisements (except for seven of the SAD subjects recruited from a genetic study of anxiety (Talati et al., 2008). Functional scans of two subjects (1 control and 1 SAD) were unusable due to scanner technical

issues, while a third subject was excluded because she was diagnosed with both SAD and PD. Recruitment and clinical procedures have been detailed elsewhere (Talati et al., 2013).

Replication Sample: Eighteen medication-free adults with a primary diagnosis of GSAD (age 20–52) and 17 age, sex and race-matched HCs were recruited through media notices and clinical referrals. Diagnoses were based on psychiatric interview and confirmed by the Structured Clinical Interview for DSM-IV Axis I disorders. Data from four GSAD patients were excluded from analyses due to technical issues (described more below), yielding 14 GSAD patients and 17 HCs used for diagnostic classification analysis. Twelve GSAD patients and seven HCs completed a second scan following 8-weeks paroxetine treatment (or non-treatment for HCs).

Exclusion criteria for GSAD participants included having a current Axis I disorder (other than secondary diagnoses of generalized anxiety disorder, dysthymia, or specific phobia), major depressive episode in the past year, substance abuse in the past 6 months, and clinically significant general medical conditions. HCs did not meet criteria for any lifetime Axis I disorder. Health status was confirmed by a physical examination including drug toxicology screen. All subjects were free of psychotropic medications for at least 4 weeks prior to study entry.

Data from four GSAD patients were excluded from analyses (one subsequently revealed a recent history of major depression, one failed to follow imaging task instructions, and the functional scans of the others suffered from technical issues), yielding 14 GSAD patients. Secondary comorbid diagnoses in participants with GSAD consisted of current generalized anxiety disorder (N=3), past major depression (N=6), and past alcohol abuse (N=1). Six GSAD subjects had taken medication for anxiety or depression prior to the past 4 weeks. All subjects in both samples provided written informed consent after discussion of study procedures.

Behavioral task

Primary Sample: Subjects performed a previously described task from our group (Etkin et al., 2004; Pantazatos et al., 2012a) which consists of color identification of fearful, neutral, masked fearful and mask neutral faces (F, N, MF and MN respectively) with in a blocked paradigm (four 20 second blocks for each condition, 15 second baseline between each block). See Chapter 3 methods for further details regarding the task paradigm and stimuli.

Replication Sample: Subjects performed gender identification of angry, happy and neutral faces (A, H, and N respectively) drawn from the same standard series as above (Ekman and Friesen, 1976), and within a blocked paradigm (four 20 second blocks for each condition, 12-14 second baseline between each block). Stimuli consisted of faces of both genders expressing neutral, high valence angry or happy expressions during explicit and implicit viewing conditions. During the explicit processing condition, subjects were asked to judge the emotional facial expression (angry, neutral, happy) by using a keypad, and reaction times were recorded. During implicit processing, subjects were asked to identify gender of each face (male/female), responding via keypad. The stimuli were presented in a block design consisting of two 6 min and 48 sec. runs (one run implicit, one run explicit) each containing 4 blocks of angry (A), neutral (N) and happy (H) faces. Each block lasted 20 seconds, followed by 12-14 seconds of baseline (white crosshair against black backgroun d). Within each block, 10 stimuli (faces) were presented for 1 second, followed by 1 second crosshair between each stimulus presentation. At the start of each run, an instruction screen was presented for 10 seconds, with instructions for using the keypad. Subjects had been trained prior to the scanning session in the use of the keypad. Given that our primary

sample performed an implicit task (i.e. identification of colors overlaid on emotional faces), we conducted the replication analysis using the implicit runs from the replication sample.

Due to a minor programming error, during the implicit runs, 11 baseline (pre-treatment) subjects (6 controls, 5 cases) received a distribution (in no particular order) of 5/4/3 blocks of each condition, with 5 blocks tending to occur slightly more often for the A condition, and 3 blocks slightly more often for N (over all subjects, mean #blocks per condition: A-4.22, H-3.91, N-3.88). Five (1 control, 4 cases) post-treatment runs were similarly affected (over all subjects, mean # blocks per condition: A-3.95, H-4.11, N-3.95).

Image Acquisition and Analyses

fMRI Acquisition: Functional data were acquired on a 1.5 Tesla GE Signa MRI scanner in the functional MRI Research Center at Columbia University Medical Center, using a gradient-echo, T2*-weighted echoplanar imaging (EPI) with blood oxygen level-dependent (BOLD) contrast pulse sequence. Twenty-four contiguous axial slices were acquired along the AC-PC plane, with a 64 × 64 matrix and 20 cm field of view (voxel size 3.125 × 3.125 × 4 mm, TR = 2000, TE = 40, flip angle = 60). Structural data were acquired using a 3D T1-weighted spoiled gradient recalled (SPGR) pulse sequence with isomorphic voxels (1 × 1 × mm) in a 24 cm field of view (256 × 256 matrix, ~186 slices, TR 34 ms, TE 3 ms).

GLM analysis: Functional data were preprocessed and processed in SPM8 (Wellcome Department of Imaging Neuroscience, London, UK). For preprocessing, the realigned T2*-weighted volumes were slice-time corrected, spatially transformed and resampled to a standardized brain (Montreal Neurologic Institute, 2x2x2 mm3 cube resolution) and smoothed

with a 8-mm full-width half-maximum Gaussian kernel. 1st-level regressors were created by convolving the onset of each condition (primary sample: MF, MN, F and N, replication sample: A, H, and N) with the canonical HRF with duration of 20 seconds. Additional nuisance regressors included 6 motion parameters, white matter and csf signal, which were removed prior to time-series extraction. For the current work, the same GLM analysis served two main purposes: 1) facilitate removal of nuisance effects from time series prior to FC estimation using structurally (atlas-based) defined ROIs, and 2) produce beta-estimates of each condition for case vs. control classification analyses (primary sample) using spatial activity patterns.

Functional connectivity estimation: Atlas-based parcellation was applied and pair-wise correlations between 248 nodes (derived from 124 atlas-based brain regions) were computed using 40 total time points of fMRI data that were segmented and concatenated from four conditions; unattended and non-masked (i.e. implicit) fearful (F) and neutral (N) faces, and subliminal, masked fearful (MF) and neutral faces (MN) (see (Pantazatos et al., 2012a; Pantazatos, Talati et al., 2012b) for more details and analysis schematic. Correlations over the full run were also computed (Full). This resulted in 30,628 total functional connections (z-transformed Pearson correlations) for each condition of interest (F, N, MF, MN and Full), which were used as features for diagnostic classification.

Pattern analysis of large-scale functional connectivity to predict SAD diagnosis: For all binary classification tasks, a linear kernel SVM (Vapnik, 1999) with a filter feature selection (t-test) and leave-one-out cross validation was used. During each iteration of leave-one-out cross validation (primary sample), one subject was withheld from the dataset and 1) a 2-sample t-test was

performed over the remaining training data 2) the features were ranked by absolute t-score and the top N were selected 3) these selected features were then used to predict the class of the withheld test examples during the classification stage. For classification in the replication sample, the SVM model was learned from the whole primary sample using the top 2 features identified in the analysis above, and this same model was used to predict SAD vs. controls in the replication sample. Prior to learning, the effects of age and gender were regressed out from the features using a general linear model, and features were z-scored. Classification, performance assessment and confidence interval estimation followed previously described procedures (Pantazatos et al., 2012a; Pantazatos, Talati et al., 2012b).

Univariate replication analyses: Features identified in the primary analysis were subjected to univariate statistical tests in the replication sample. SAD vs. HC (pre-treatment) was assessed with Mann-Whitney U test, pre-post group changes in FC were assessed using paired t-test, and longitudinal pre-post correlations (decrease ΔLSAS vs. increase ΔFC) were assessed using Spearman's Rho (rank correlation coefficient). Our hypotheses were based on the directions observed in the primary sample, so reported p-values are one-tailed.

Results

Behavioral results: The average response rates in the color discrimination task were: HCs 96.4% (σ=6.2%), SAD 99.9% (σ=0.15%), PD 98.1% (σ=4.2%). Mean accuracies were: HCs 96.3% (σ=4.4%), SAD 99.1% (σ=0.96%), PD 97.0% (σ=4.3%). Mean reaction time were: HCs 0.66s s (σ=0.09 s), SAD 0.64 (σ=0.16 s), PD 0.70 s (σ=0.11 s) indicating that subjects performed the

color discrimination task as instructed. The groups did not differ significantly in RT ($F_{50}=1.75$, $p=0.18$) or accuracy ($F_{47}=0.46$, $p=0.63$, one-way ANOVA).

Discriminating between SAD and HCs with patterns of functional connectivity: For SAD (n=16) vs. HC (n=19) classification in the primary sample (see Table 6 for demographics), a peak AUC of 0.88 ($p< 0.004$ corrected, 0.81,1.0 90% CI) was achieved when learning was based on the top 2 features in each training set, derived from the N condition (Figure 17A; results from all conditions not shown). The accuracy decreases with three or more features as presumably less informative features (i.e. noise) are added to the feature set. Anatomical display of these two features revealed functional connections between Left Hippocampus and Left Temporal Pole, and between Right Anterior Middle Temporal gyrus and Left Orbitofrontal Cortex (Figure 17B, Table 7A). When comparing classification performance of each feature alone, Left Hippocampus-Left Temporal Pole was more discriminating than Right Anterior Middle Temporal gyrus-Left Orbitofrontal Cortex (AUC=0.77 vs. 0.68, data not shown).

Table 6. Chapter 7: Demographics table

Cross-sectional	**SAD**	**PD**	**Control**	
Primary Sample	**N = 16**	**N = 16**	**N = 19**	*statistic*
Age (Mean Years, sd)	33.6 (7.1)	32.2 (11)	31.7 (8)	*F(2,49)= 0.21, p = 0.81*
Gender (Number, % Female)	14 (88%)	12 (75%)	8 (42%)	*ChiSq = 8.7, p = 0.01*
LSAS Score, (mean, sd)	n/a	n/a	n/a	
Replication Sample	**N = 14**	**n/a**	**N = 17**	*statistic*
Age (Mean Years, sd)	27.3 (7.5)		31 (10.7)	*t(29)= 1.17, p = 0.25*
Gender (Number, % Female)	10 (71)		10 (58)	*Chi-Sq = 0.53, t = 0.46*
LSAS Score, (mean, sd)	86.7 (18.1)		7.8 (5.3)	*t(29) = 17.1, p < 0.0001*
Longitudinal				
Replication Sample Subset	**N = 12**	**n/a**	**N = 7**	*statistic*
Age (Mean Years, sd)	28.3 (7.8)		35 (13.0)	*t(17) = 1.43, p = 0.17*
Gender (Number, % Female)	8 (66)		2 (29)	*ChiSq = 2.6, p = 0.11*
LSAS Score pre, (mean, sd)	85.8 (15.3)		7.7 (6)	*t(17) =12.7, p < 0.0001*
LSAS Score post, (mean, sd)	44.5 (25.3)		8.25 (8.1)	*t(17) = 3.6, p = 0.0004*
LSAS Score post-pre, (mean, sd)	-41.3 (28.9)		0.57 (3.4)	*t(17) =3.4 p = 0.003*

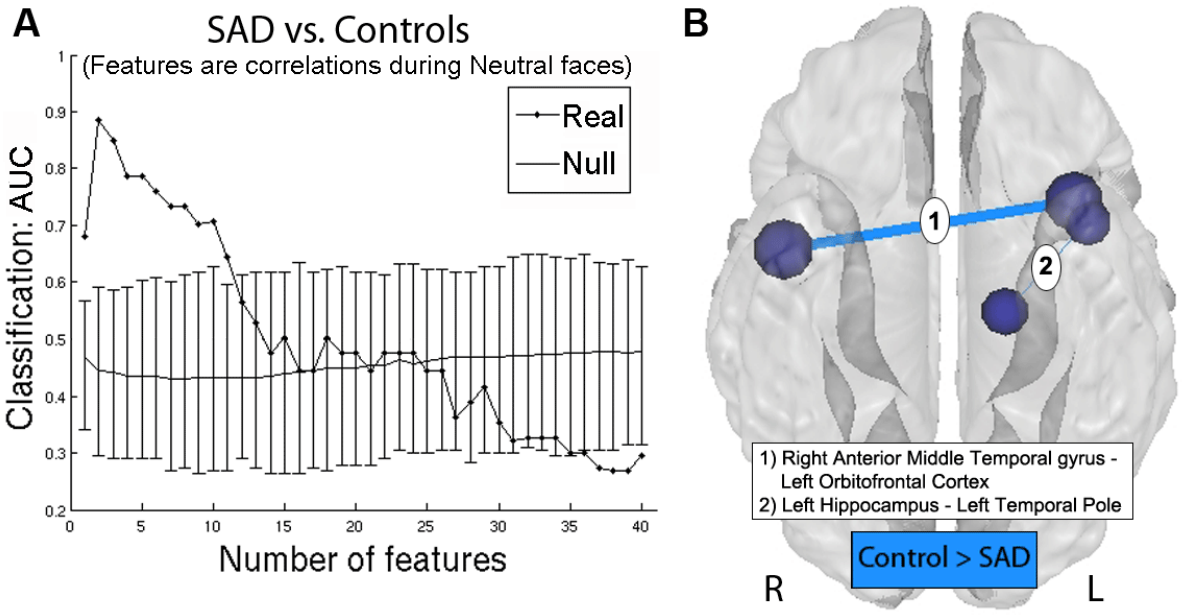

Figure 17. Chapter 7: Functional connectivity that discriminates SAD in primary sample. **(A)** Classification performance (AUC) when predicting SAD (n=16) vs. controls (n=19) as a function of the number of features (1 to 40) included ranked in descending order by their absolute t-score. Features were Pearson correlations using segmented and concatenated time-series during the implicit neutral face condition ("N", black dots, see text for results when using correlations over other stimulus conditions). The peak performance for SAD vs. Control classification using "N" correlations (sensitivity=0.88, specificity=0.89, AUC=0.89, $p < 0.002$, corrected) was achieved when learning was based on the top 2 features in each training set. Mean AUC for shuffled data are plotted along the bottom, with error bars representing 90% CI. Ventral **(B)** anatomical representation of the top 2 features when classifying SAD vs. control subjects using "N" correlations. The largest contributing FCs were between R Anterior Middle Temporal gyrus and L Orbitofrontal Cortex, and L Hippocampus and L Temporal Pole which were both reduced in SAD (shown in blue). For display purposes, the size of each sphere is scaled according to the sum of the SVM weights of each node's connections. In addition, the thickness of each connection was made proportional to its SVM weight.

Specificity of these features to the SAD diagnosis was tested by classifying SAD vs. subjects with panic disorder (PD, n=16). Using only the above two features (no feature selection), an AUC of 0.81, p=0.0001 uncorrected was achieved in discriminating between SAD

and PD patients (Table 7B), suggesting relative specificity of these features to SAD. These two features did not discriminate HCs from panic disorder (AUC=0.47, data not shown).

We note that that this primary sample was not balanced for gender (HCs: 11 males, 8 females; SAD: 2 males, 14 females). We therefore tested whether the top 2 features identified above could predict gender among the combined group (13 males vs. 22 females). Classification was not any greater than chance for this classification (AUC=0.50), verifying that classification performance was not an artifact of a sample mismatched for gender. In addition, there was only a slight decrease in performance after applying multiple regression to each feature and removing the effects of age and gender: original AUC/adjusted AUC=0.88/0.80. Importantly, replication of these findings (described more below) was tested in a sample that was matched for age and gender.

Examining previous SAD-related FC reported in the literature: In addition to the exploratory, data-driven approach above, we examined FC previously identified to be anomalous in SAD, in particular reduced aINS-dACC (Klumpp et al., 2012) and amygdala-dACC and amygdala-dlPFC (Prater et al., 2012) in SAD during fear. Using PPI analysis, a recent study observed less aINS-dACC FC during fearful (> happy) in gSAD relative to controls (Klumpp et al., 2012). All FC during both F and N conditions between bilateral Insula and Anterior Cingulate Gyrus was queried at $p < 0.05$ uncorrected, and the following was observed: Control > SAD, Left_Insular_Cortex_PC2-Left_Cingulate_Gyrus_anterior_division_PC1 t(33)=2.22/2.96 F/N, and Right_Insular_Cortex_PC2-Left_Cingulate_Gyrus_anterior_division_PC1 t(33)=1.82/Not significant F/N. The average peak location for Left Insula was anterior ([-36 16 2]), while peak

MNI location for the right was middle insula ([42 -4 6]). These results are consistent with the aforementioned study.

A related study (Prater et al., 2012) used PPI and observed less connectivity between amygdala-dACC and amygdala-dlPFC in SAD during fearful faces perception. As above, we interrogated FC between these regions during F and N conditions at $p<0.05$ uncorrected, Control > SAD and observed: Right_Amygdala_PC2-Right_Cingulate_Gyrus_anterior_division, t(33)=2.53/Not significant F/N and Right_Ventral_Frontal_Pole_PC1 - Right_Amygdala_PC1 = t(33) = 1.9208/Not significant F/N consistent with (Prater et al. 2012). However, many FC differences between amygdala and dlPFC/precentral gyrus were in the opposite direction (i.e. greater in SAD): Control > SAD, Right_Ventral_Frontal_Pole_PC1 - Right_Amygdala_PC2 = -1.94 Right_Ventral_Frontal_Pole_PC1 - Left_Amygdala_PC2 = -1.67, Left_Amygdala_PC1-Left_Middle_Frontal_Gyrus_PC1, t(33)=-3.08, Left_Precentral_Gyrus_PC1-Left_Amygdala_PC1, t=-2.63, Right, t=-1.72, Right_Ventral_Frontal_Pole_PC2 - Left_Amygdala_PC1 , t=-2.5082.

Although FC differences were mostly consistent with these studies, including the above connections (RAmygdala-RACC, Right_Ventral_Frontal_Pole_PC1-Right_Amygdala_PC1, Left Insula-dACC) with the top 2 connections identified in the main text did not improve classification performance (data not shown), while including only these connections resulted in poorer classification performance (AUC=0.53). It is important to note that FC was measure here using Pearson correlation, while these previous studies applied "seed" based regression analyses, which are different approaches for measure functional connectivity and their differences. See (Kim and Horwitz, 2008) for further discussion.

Discriminating between SAD and healthy control subjects with patterns of spatial activity: To compare the information content of patterns of interactivity (i.e. functional connections used above) vs. patterns of activity, SAD vs. control classification was also conducted using beta estimates, which are considered summary measures of activation in response to each condition. This approach is conceptually similar to a recent study that used pattern classification of whole-brain activity (BOLD averaged over several TR's of an event minus baseline activity immediately preceding the event) during sad face viewing to predict diagnosis (normal vs. clinically depressed) (Fu et al., 2008). In order to make feature-selection/leave-one-out cross validation and SVM learning more computationally tractable, preprocessed functional data were resized from 2x2x2 mm voxel resolution to 4x4x4 mm resolution, and subject-specific GLM models were re-estimated, resulting in a reduction of total feature space per example from ~189,500 betas to ~23,500. Feature selection, leave-one-out cross validation and SVM learning proceeded exactly as above for FC data. When using the contrast F-N, we observed a peak AUC of 0.88 ($p<0.0001$ uncorrected) with 8 voxels (within cerebellum and middle occipital gyrus), and when using the F beta weights, a peak AUC=0.83, $p=0.0008$ uncorrected was observed with ~170 voxels (Figure 19). However the AUC using F betas dropped to 0.49, and AUC using F-N contrast dropped to 0.58 after regressing out the effects of age and sex prior to classification.

Classification of SAD vs. PD using the same features as above was then attempted, and a decrease in classification performance was observed; when using F>N contrasts, AUC=0.59, $p=0.03$ uncorrected, and when using F beta weights, AUC=0.56 $p=0.26$ uncorrected, data not shown). Classification of SAD vs. PD using top 10:10:500 F-N contrast estimates over the whole-brain only achieved a peak AUC of 0.66 (data not shown). Thus, although peak classification performance for SAD vs. Controls using contrast estimates as features matched

that of using pair-wise functional connectivity, under the current analysis these activation differences appear to be less specific to SAD.

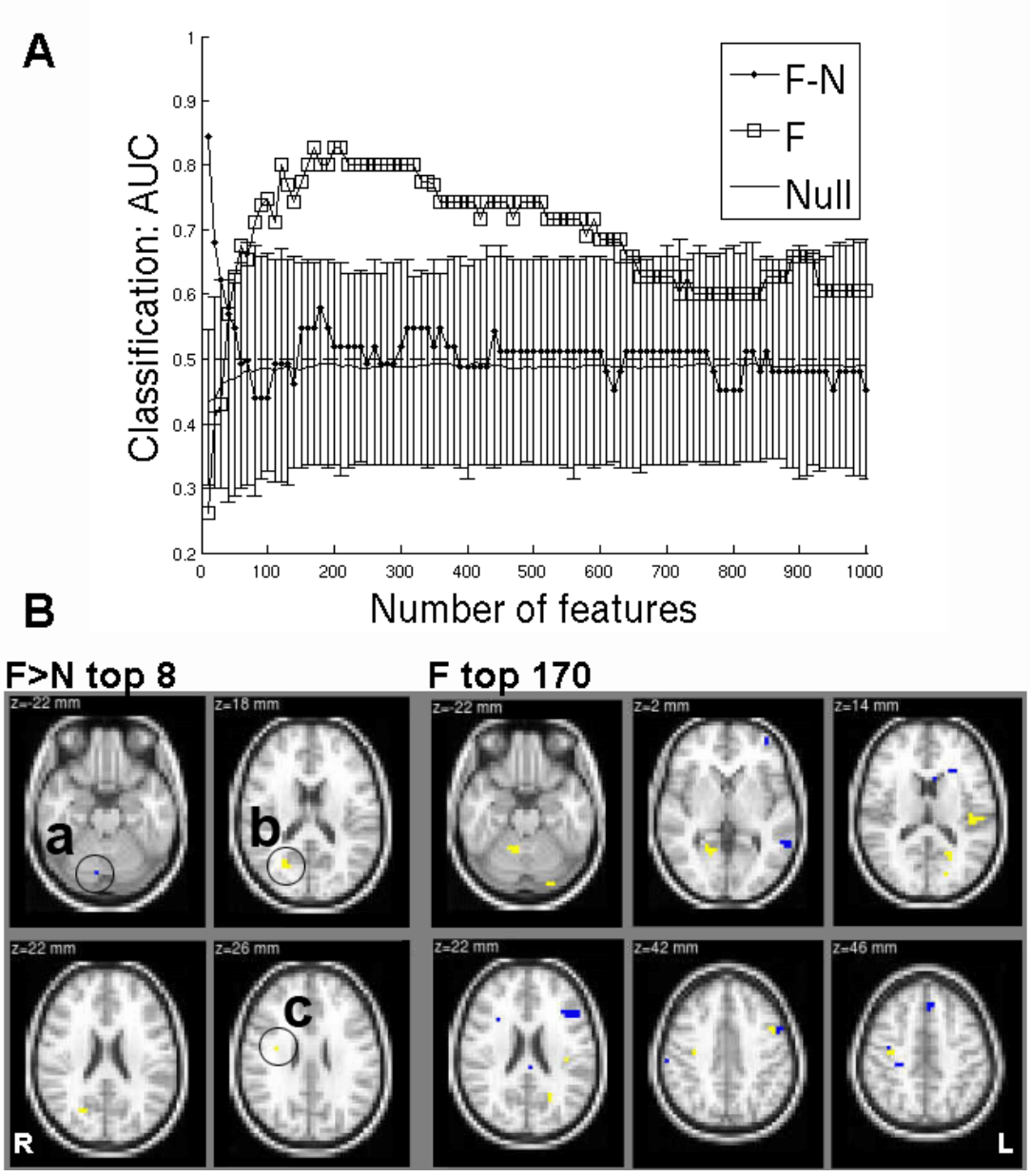

Figure 18. Chapter 7: Predicting SAD vs. Controls using beta and contrast estimates as features**.** (A) Feature selection, cross-validation and SVM learning were performed exactly the same as for FC, but over the range of 10 to 1000 ranked features (every 10 voxels). High SAD vs. control classification rates was observed when using the top 10 F > N contrast values (dots) in each training set, with high classification rates were observed with using the top 170-200 F beta values (squares) in each training set. (B, left) For F>N contrast values, classification was performed again with the top 1 to top 20 features, and the peak was identified at 8 features (sensitivity=0.74 , specificity=1.0 , AUC=0.88, $p<0.0001$ uncorrected). The most informative F>N contrast voxels with negative SVM weights (F>N,

Controls > SAD, blue) was in the cerebellum (a), while the most information voxels with positive SVM weights (F > N, SAD > controls, yellow) included middle occipital gyrus (b) and a voxel in the vicinity of precentral gyrus (c). (B, right) For F beta values, classification was performed again with the top 150 to top 200 features, and the classification performance first peaked with 170 features (sensitivity=0.81 , specificity=0.84 , AUC=0.83, p=0.0008 uncorrected). The most informative F beta voxels with negative SVM weights (F, Controls > SAD, blue) included regions in the left frontal pole and middle temporal gyrus (z=2mm), left inferior frontal gyrus (z=22mm), dorsomedial prefrontal cortex (z=46mm), while the most informative voxels with positive SVM weights (F, SAD > controls, yellow) included cerebellum (z=-22mm), superior occipital gyrus (z=22mm) and supramarginal gyrus (z=14mm). Brain images are displayed using Neurological convention (i.e. L=R), and top left number in each panel represents the MNI coordinate (z) of depicted axial slice.

Table 7. Chapter 7 Most informative features discriminating SAD. A) Top 2 FC features (during Neutral face blocks) discriminating SAD vs. HCs, B) Same 2 FC features (during Neutral face blocks) when predicting SAD vs. PD subjects C) Same 2 FC features (during Angry Faces) predicting SAD vs. HCs in an independent replication sample. All reported p-values are uncorrected.

A) Primary Sample: SAD (n=16) vs. Controls (n=19) Top 2 features, Neutral Faces Sensitivity=0.88; specificity=0.89; AUC=0.88, p<0.0001 (0.81,1.0) 90% CI	**SAD Mean R**	**Controls Mean R**	**T-value**	**SVM weight**	**Fsets (35)**
Right_Middle_Temporal_Gyrus_anterior_division_PC1 - Left_Frontal_Orbital_Cortex_PC1	-0.07	0.41	-5.81	-2.26	35
Left_Temporal_Pole_PC1 - Left_Hippocampus_PC1	-0.08	0.58	-5.39	-1.74	35
B) Primary Sample: SAD (n=16) vs. PD (n=16) Above 2 features, Neutral Faces Sensitivity=0.81; specificity=0.81; AUC=0.81, p=0.0001	**SAD Mean R**	**PD Mean R**	**T-value**	**SVM weight**	**Fsets**
Right_Middle_Temporal_Gyrus_anterior_division_PC1 - Left_Frontal_Orbital_Cortex_PC1	-0.07	0.24	-3.12	-2.25	N/A
Left_Temporal_Pole_PC1 - Left_Hippocampus_PC1	-0.08	0.52	-5.11	-2.24	N/A
C) Independent Replication Sample: SAD (n=14) vs. Controls (n=17) SVM model trained from Primary Sample, Above 2 features during Angry faces Sensitivity=0.71; specificity=0.71; AUC=0.71, p=0.01; (0.59,0.88) 90% CI	**SAD Mean R**	**Controls Mean R**	**T-value**	**SVM weight***	**Fsets**
Left_Temporal_Pole_PC1 - Left_Hippocampus_PC1	0.13	0.36	-1.65	-1.13	N/A
Right_Middle_Temporal_Gyrus_anterior_division_PC1 - Left_Frontal_Orbital_Cortex_PC1	0.24	0.27	-0.43	-1.10	N/A

Replication in an independent and longitudinal sample

Discriminating SAD vs. HCs in an independent replication sample: To see how well classification using the top 2 FC features identified above generalized to new data, these features (Left Hippocampus-Left Temporal Pole and Right Anterior Middle Temporal gyrus–Orbitofrontal Cortex) were tested in a second, independent sample of SAD (n=14) vs. HCs (n=17). This sample also performed implicit perception of emotional faces, but instead of color identification of fearful and neutral faces (primary sample), they identified the gender of angry, happy and neutral faces. For this an SVM model (line) was learned using the full primary dataset for the above two features (Figure 19A). To increase generalization ability of the model, features were corrected for the effects of age and gender and z-scored prior to SVM learning (under these preprocessing steps classification performance was only slightly reduced to AUC=0.86). This learned model was applied to the independent replication sample, and the highest AUC was achieved when using FC during angry faces (Angry: sensitivity =0.71, specificity=0.71, AUC=0.71, p=0.01 (0.59, 0.88) 90% CI, Figure 19B, Table 7C; Happy: AUC=0.47, p=0.77; Neutral: AUC=0.54, p=0.43; Full: AUC=0.57, p=0.31, data not shown).

Univariate group comparisons over each feature revealed that Left Hippocampus-Left Temporal Pole FC was significantly reduced in SAD vs. HCs, particularly during the Angry condition (mean difference = -0.27, p=0.017) and Neutral (mean difference= -0.25, p=0.056) conditions (Table 8, 1st row). There were no significant differences observed between SAD and HCs in the Right Anterior Middle Temporal gyrus– Orbitofrontal Cortex FC (all p>0.2, data not shown).

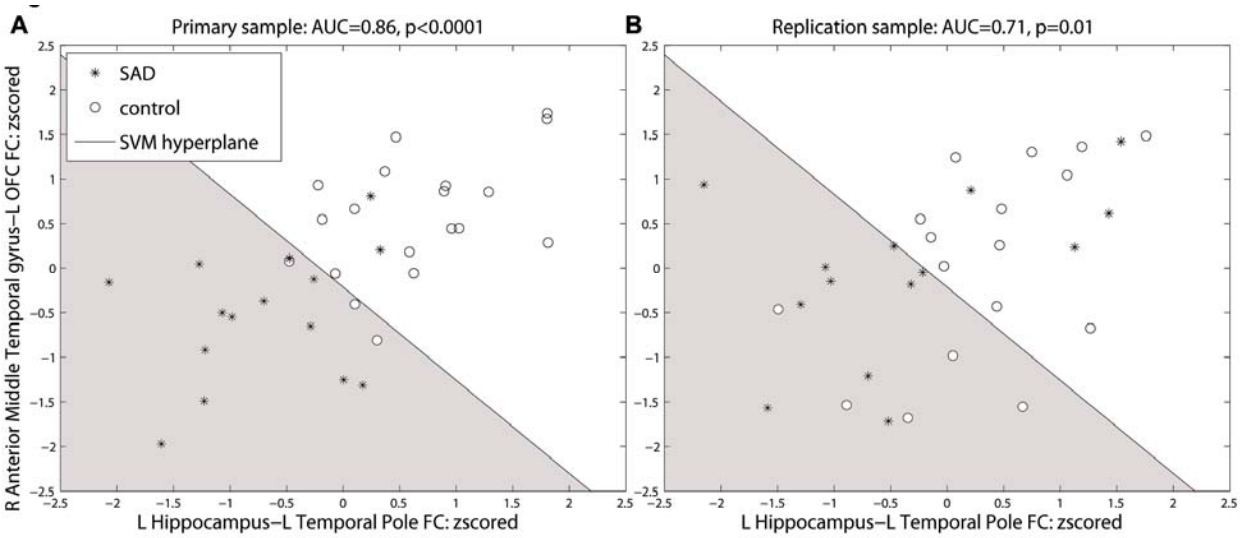

Figure 19. Chapter 7: Left-Hippocampus-Left Temporal and Left Anterior Middle Temporal gyrus-Left Orbitofrontal Cortex FC predict SAD in the replication sample. **(A)** Linear kernel SVM line when learning SAD (N=16) vs. Control (N=19) based on the full primary dataset using Left-Hippocampus-Left Temporal and Left Anterior Middle Temporal gyrus-Left Orbitofrontal Cortex FC during implicit neutral faces condition as features. Effects of age and gender were removed, and features were normalized (z-scored) prior to learning, so classification performance was slightly lower (AUC=0.86, p<0.0001) than the main text and Figure 1. Shaded grey (white) indicates area in which all points were predicted as SAD (control). **(B)** The same model learned above was used to classify SAD (N=14) vs. control (N=17) in the independent replication sample, using Left-Hippocampus-Left Temporal and Left Anterior Middle Temporal gyrus-Left Orbitofrontal Cortex FC during implicit angry faces (AUC=0.71, p=0.01, see main text for results from other conditions).

Table 8. Chapter 7: Univariate statistical tests of features identified in the primary sample tested in a second, independent replication sample.

Left Hippocampus-Left Temporal Pole	Angry		Happy		Neutral		Full	
	effect size	pval	effect size	pval	effect size	pval	effect size	pval
SAD (n=14) > Control (n=17)	-0.245	0.027	-0.176	0.197	-0.208	0.092	-0.190	0.042
SAD pre > post (n=12)	-0.414	0.007	-0.343	0.039	-0.245	0.098	-0.343	0.036
LSAS post-pre vs. FC pre-post (n=19)	0.546	0.008	0.583	0.004	0.335	0.081	0.371	0.059

Changes in Left Hippocampus-Left Temporal Pole functional connectivity following SSRI treatment, and correlation with decreases in symptom severity: We examined whether Left Hippocampus-Left Temporal Pole FC could be considered a possible biomarker for (SSRI)

treatment effects. At the group level, social anxiety symptom severity (as assessed through the Liebowitz Social Anxiety Scale, or LSAS) was significantly reduced following 8-weeks SSRI (paroxetine) treatment (cases (pre-post) > controls (pre-post) $t(17)=3.4$, $p=0.003$, Table 6, last row). Pre minus post comparisons in the SAD subjects (n=12) revealed the Left Hippocampus-Left Temporal Pole FC, particularly during Angry faces, increased following treatment (Angry pre>post, mean change in $R = -0.41$, $t(11) =-2.9$, $p=0.007$ paired t-test, Table 8, 2nd row).

To further examine whether Left Hippocampus-Left Temporal Pole FC tracks social anxiety symptom severity, we tested the extent to which changes in LSAS were associated with changes in this FC. A subset of the replication sample completed an additional scan following 8 weeks of paroxetine treatment (SAD n=12) or following 8 weeks without treatment (HCs n=7). This analysis included controls, because we were primarily interested in longitudinal symptom change that is not necessarily specific to treatment. Given that SAD subjects exhibited decreased FC relative to HCs at baseline, we hypothesized that, across both HCs and SAD subjects, increases in Left Hippocampus-Left Temporal Pole FC should be associated with decreases in symptom severity. This relationship was indeed observed for Left Hippocampus-Left Temporal Pole FC computed across all examined conditions (pre-post ΔLSAS vs. post-pre ΔFC: angry $R=0.55$, $p=0.008$, happy $R=0.58$, $p=0.004$, neutral $R=0.33$ $p=0.08$, and full run $R=0.37$ $p=0.06$) (Table 8, 3rd row, Figure 19). These results held, particularly for FC during angry, happy and neutral faces, after removal of the top 1 and top 2 outliers (indicated as boxed 1s and 2s in Figure 2) from each plot, (pre-post ΔLSAS vs. post-pre ΔFC top 1 removed: angry $R=0.59$, $p=0.01$, happy $R=0.63$, $p=0.005$, neutral $R=0.35$ $p=0.15$, full run $R=0.39$ $p=0.10$; top 2 removed: angry $R=0.57$, $p=0.017$, happy $R=0.62$, $p=0.007$, neutral $R=0.51$ $p=0.018$, and full run $R=0.36$ $p=0.16$).

When pre-post ΔLSAS vs. post-pre ΔFC was correlated among only cases (n=12), a positive, yet non-significant, correlation was observed (R=0.32, p=0.31). Left Hippocampus-Left Temporal Pole FC at baseline was not associated with ΔLSAS symptom improvement (R=0.21, p=0.5, data not shown). Change in right anterior middle temporal gyrus-left OFC FC did not correlate with change in symptom severity (angry: R=-0.10, p=0.34, happy: R=-0.20, p=0.2, neutral: R=0.04, p=0.44). Additional analyses suggest decreases in activation in left hippocampus and left temporal pole in response to angry and neutral faces following treatment, although effects were sub-threshold (see (Pantazatos et al., 2013) Supplementary Results).

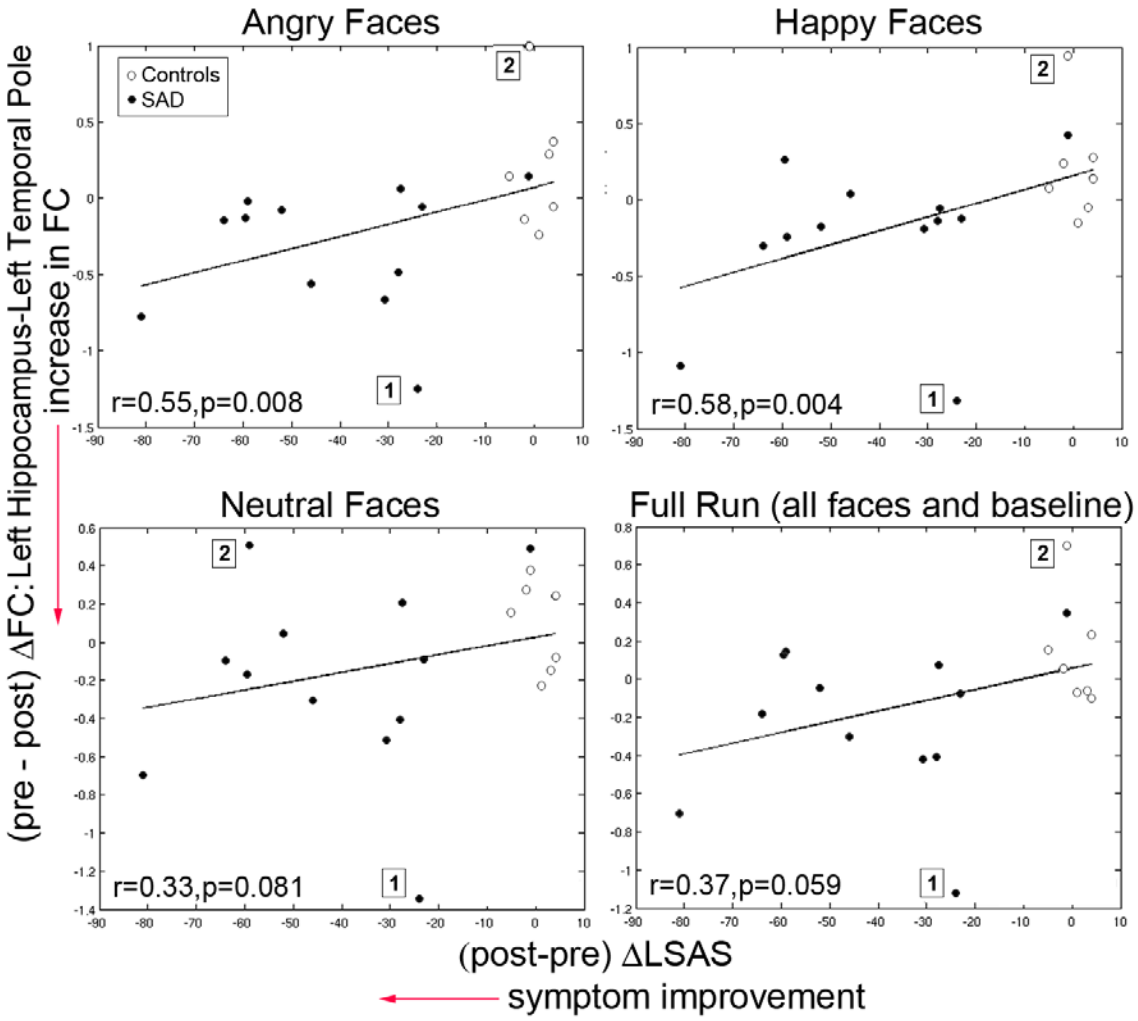

Figure 20. Chapter 7: Increases in Left Hippocampus-Left Temporal Pole connectivity correlate with greater decreases (ΔLSAS post-pre) in social anxiety symptom severity following 8 weeks paroxetine treatment (or non-treatment for control subjects) in a second, independent replication sample. Linear plots of change in correlations values (pre > post) during implicit angry, happy and neutral face viewing, as well as over the full run, vs. change (post > pre) in Liebowitz Social Anxiety Scale (LSAS) scores. Pre- and post-scans were obtained approximately 8 weeks apart. Cases (n=12) received 8-weeks paroxetine treatment, and seven healthy control subjects (n=7) were scanned following 8-weeks non-treatment. Correlation values were assessed using Spearman's rank correlation coefficient, and p-values are one-sided testing against the null hypothesis of correlation equal to or less than zero.

Discussion

In the current work a novel and exploratory approach based on multivariate pattern analysis of large-scale, condition-dependent FC (Pantazatos et al., 2012a) was used to identify FC that discriminated individual subjects with SAD. FC features that discriminated SAD from HCs in the primary sample also discriminated SAD from HCs and from subjects with the closely related diagnosis of PD with significant sensitivity and specificity. Additionally, following 8 weeks of treatment of SAD with paroxetine, the most discriminative FC feature normalized, with greater changes in FC correlating with greater decreases in symptom severity. Results suggest promise for FC-based biomarkers for psychiatric diagnosis and treatment effects.

Related diagnostic classification studies have applied pattern analysis to condition dependent activation to a particular probe or stimulus relevant to the disorder (i.e. responses to a sad or mother's face to predict depression (Fu et al., 2008)). While pattern analysis of activation maps takes into account multivariate interactions among regions, activation maps are usually beta maps (summary statistics of activation) or signal that has been averaged across multiple successive scans. Thus interactions are at a grosser temporal scale. In contrast, the current approach explicitly takes into account scan-to-scan covariation between regions. Here, pattern analysis of FC was more sensitive and specific in discriminating SAD than was multivariate pattern analysis of activation (when using the canonical HRF to model activity), likely due to the fact that it captures information inherent in the interactions among brain regions. Previous large-scale FC approaches capture this information, but only during resting state (i.e. resting-state fMRI BOLD to predict schizophrenia (Yu et al., 2013) and age (Dosenbach et al., 2010b). The current approach measures condition-dependent FC (i.e. large-scale FC during emotional face viewing), combining the sensitivity of multivariate machine-learning analysis with the advantages of both task-based and resting-state FC approaches.

A meta-analysis of both PET and fMRI studies of SAD prior to 2007 showed increased activation in amygdala and insula during negative emotional processing (Etkin and Wager, 2007), while many recent fMRI studies of SAD have applied activation analyses focused on the amygdala, and insula (Klumpp et al., 2010; Schmidt et al., 2010; Yoon and Zinbarg, 2007a) to show increased activation in these areas to intense vs. low or negative vs. neutral emotional stimuli. In addition, univariate analyses showed decreased activation of the amgydala and increased activation in the vmPFC in response to social threat stimuli following 12-weeks of SSRI treatment (Phan et al., 2013). However, although these univariate approaches can identify areas that respond more or less to a particular stimulus, they ignore interactions, or FC, between regions, which is thought to measure information transfer underlying complex cognitive-emotional processing such as during threat or facial affect perception and appraisal (Friston, 2002).

Although previous studies have demonstrated differences in activation and FC (Ding et al., 2011; Hahn et al., 2011; Klumpp et al., 2012; Liao et al., 2011; Prater et al., 2012) between SAD and HCs, the current work is among the first to use FC (and activation) to discriminate SAD vs. HC diagnostic membership. The current approach of combining machine learning with large-scale, condition dependent FC is more exploratory and data-driven in identifying FC differences than previously used techniques such as Psychophysiological Interactions (PPI) Analysis, which only assess FC with a single, a priori specified, "seed" region at a time. The additional discrimination of SAD from PD is particularly notable given that these disorders have a significant overlap of both symptoms and neurobiology, such as amygdala hyperactivation and decreased frontal regulation (Damsa et al., 2009; Rauch et al., 2003).

The most discriminative feature was significantly reduced Left Hippocampus-Left Temporal Pole FC in SAD, and greater increases in this FC predicted greater improvement in symptom severity following 8 weeks of SSRI treatment. Our finding of Left Hippocampus-Left Temporal Pole functional connectivity during face perception in healthy subjects is consistent with the observation of intrinsic FC between anterior hippocampus and anterior temporal pole in humans and non-human primates (Kahn et al., 2008), and with increased FC between hippocampus and left temporal pole during successful retrieval of memory for face-name associations (Tsukiura et al., 2010). Interestingly, we observed that this FC is reduced in subjects with SAD, particularly during neutral (primary sample) and angry face (replication sample) processing (see below for further discussion regarding differences between these samples). Previous findings indicate that the temporal pole has a role in both social and emotional processes including face recognition and theory of mind, (Wong and Gallate, 2012) and memory for face-name pairs (Damasio et al., 1996), and it has been proposed that the temporal pole binds complex, highly processed perceptual inputs to visceral emotional responses (Olson et al., 2007). It is also thought to be involved in access to social knowledge during mentalizing, the implicit attribution of intentions and other mental states (Frith and Frith, 2003). The left hippocampus is a key region for memory (i.e. autobiographical memory retrieval) (Spreng and Mar, 2010), and functional connectivity between this region and the temporal pole may reflect an integration of stored memory with social knowledge during face perception and mentalizing in healthy subjects. This neural process is presumably disrupted or under-utilized in SAD, which is characterized by excessive self-focused attention and fears of negative evaluation in interpersonal situations.

It may seem counterintuitive that the most predictive FC was during neutral faces in primary sample. However this is consistent with evidence suggesting that SAD is characterized by negative interpretation bias, particularly when presented with ambiguous social cues (i.e. neutral faces) (Winton et al., 1995; Yoon and Zinbarg, 2007b). Other studies demonstrate abnormal reactivity to emotional, and in particular harsh (i.e. angry, disgust), faces (Klumpp et al., 2010). In the current study, case vs. control and pre-post treatment differences in Left Hippocampus-Left Temporal Pole FC during neutral faces in the replication sample was observed on a trend level (Table 8, Neutral column: SAD>Control, p=0.09, SAD pre>post p=0.10). However the strongest effects in this sample were observed for this FC during angry faces (Table 8, Angry column: SAD > Control, p=0.027, pre>post p=0.007). One possible interpretation is that angry faces (relative to neutral) are more salient in SAD, and larger differences in Left Hippocampus-Left Temporal Pole FC might have observed in the primary sample if angry faces had been used. Alternatively, neutral (relative to angry) faces could be a more salient in SAD, but the signal was not apparent in the replication sample due to a minor technical issue that caused slightly fewer blocks of neutral face conditions relative to angry (see Methods: Replication Sample, last paragraph). Future studies using a balanced block design with both angry and neutral faces can facilitate a direct comparison that should help resolve this ambiguity.

Interestingly, we observed increased FC between Left Hippocampus-Left Temporal Pole concomitant with symptom improvement following 8-weeks SSRI treatment, yet there was a trend-level decrease in activity in each of these structures in response to angry and neutral faces following treatment (see Supplementary Results). Previous PET and SPECT studies have also shown reduced perfusion and cerebral blood flow (rCBF) in these regions following 8-weeks

SSRI treatment. PET imaging during a public speaking paradigm in SAD subjects demonstrated that regardless of treatment approach (SSRI citalopram or behavioral therapy), improvement was accompanied by a decreased rCBF-response to public speaking bilaterally in the amygdala, hippocampus, and the periamygdaloid, rhinal, and parahippocampal cortices (Furmark et al., 2002), while a related SPECT study demonstrated reduced cerebral perfusion in left hippocampus following 8 or 12 weeks of citalopram in a combined group of SAD, obsessive compulsive disorder and post-traumatic stress disorder patients (Carey et al., 2004). A related SPECT study observed reduced perfusion in anterior and lateral temporal cortex in SAD subjects following 8-weeks citalopram treatment (Van der Linden et al., 2000), while in a recent fMRI BOLD study, temporal pole activity during successful understanding of others' mental states correlated with neuroticism (Jimura et al., 2010). Taken together, these results suggest that while increased *activation* of hippocampus and temporal pole may be associated with increased social anxiety symptom severity, increased *functional connectivity* between these two structures is associated with decreased symptom severity.

In the absence of a placebo or comparison therapy group, we cannot infer to what extent changes in Left Hippocampus-Left Temporal Pole FC were specific to SSRI treatment or to clinical improvement. In a recent PET study in which SAD subjects responded to either placebo or SSRI treatment, reduction in (amygdala) brain activity was similar in both groups (Faria et al., 2012). Hence we cannot rule out that Left Hippocampus-Left Temporal Pole FC would increase in response to any effective treatment. From the current longitudinal analysis based on only two time points, we also cannot infer whether the changes in Left Hippocampus-Left Temporal Pole FC preceded, or instead followed, changes in symptom severity. A future study could be

designed to employ mediation analysis to more explicitly test whether changes in Left Hippocampus-Left Temporal Pole FC mediate changes in symptom severity, or vice versa.

Although baseline (pre-treatment), Left Hippocampus-Left Temporal Pole FC did not predict outcome in response to 8 weeks SSRI treatment, power to detect predictors of outcome was limited by limited heterogeneity in outcome, as most of the SAD patients improved during treatment. FC (as well as brain activity features identified in related studies (Ding et al., 2011; Doehrmann et al., 2012), may be a useful pre-biomarker to refine the diagnostic classification of psychiatric disorders and advance the development of personalized treatment approaches. For example, it is possible that Left Hippocampus-Left Temporal Pole FC could be modulated by particular conditions (e.g. social threat stimuli under various cognitive reappraisal strategies) within a single scan session, and the extent of this modulation may then be predictive of treatment outcome. Alternatively FC features might be used to identify targets for direct modification by techniques such as transcranial magnetic stimulation. If the FCs identified in this study are further validated by independent replications, future studies could examine the clinical features of individuals, regardless of diagnosis, that exhibit these features, who might thus also benefit from treatments designed to modulate this circuitry.

Limitations of this study include that the primary data set was not gender matched, and there were differences in ascertainment, diagnostic assessments and paradigm (i.e. color vs. gender identification) with the replication sample. However, the fact that replication was significant despite these differences suggests robustness of our approach, and encourage further refinement of the approach and replication in larger samples. An important future refinement would include node definitions based on functional parcellation of the brain (as opposed to atlas-based parcelation, which introduces arbitrary boundaries between regions). Future studies might

also utilize a variety of imaging paradigms that activate different regions, such as speech anticipation, eye gaze (Schneier et al., 2009), as well as other structural imaging modalities (Liao et al., 2011; Talati et al., 2013), as the best discrimination may ultimately result from combining several paradigms and imaging modalities that tap into various neural facets of the disorder.

CHAPTER 8

GREY MATTER ABNORMALITIES IN SOCIAL ANXIETY DISORDER: PRIMARY, REPLICATION, AND SPECIFICITY STUDIES[7]

Summary

BACKGROUND: Despite increasing evidence that structural brain abnormalities underlie pathological anxiety, social anxiety disorder (SAD), although among the most common of anxiety disorders, has received little attention. Using Magnetic Resonance Imaging, we (1) examined whole-brain grey matter (GM) volume differences between a group of subjects with generalized SAD and healthy controls; (2) retested the findings in an independent clinical sample; and (3) tested for specificity by contrasting the SAD group to a separate group of panic disorder (PD) subjects. METHODS: The primary group with SAD (N=16) was required to meet DSM-IV criteria for generalized SAD with onset by age 30. Controls (N=20) were required to have no lifetime history of any anxiety disorder. The replication sample included 17 generalized SAD and 17 control subjects. The PD comparison group (N = 16) was required to not have lifetime SAD. Images were acquired on a 1.5 Tesla GE Signa MRI scanner using a 3D T1-weighted spoiled gradient recalled (SPGR) pulse sequence with isomorphic voxels (1×1×1 mm) in a 24cm field of view (256×256 matrix, ~186 slices, TR 34ms, TE 3ms). Morphological differences were determined using optimized voxel based morphometry, implemented in the SPM8 software package. RESULTS: After adjusting for age, gender, and total intracranial volume, SAD (compared to control) subjects had larger GM volumes in the left parahippocampal and middle occipital, and bilateral supramarginal and angular cortices, and left cerebellum; they had decreased GM in bilateral temporal poles and left lateral orbitofrontal cortex. Cerebellar,

[7] Talati, Ardesheer, Spiro P Pantazatos*, Franklin R Schneier, Myrna M Weissman, and Joy Hirsch. 2013. Gray matter abnormalities in social anxiety disorder: primary, replication, and specificity studies. *Biol. Psychiatry.*

parahippocampal, and temporal pole differences were (1) observed in both samples individually as well as in a combined dataset analysis, (2) survived whole brain correction for multiple comparisons, and (3) were not observed in the PD group, suggesting specificity to SAD. CONCLUSIONS: These findings parallel the functional literature implicating a network of cortical and sub-cortical regions in SAD, and they suggest structural abnormalities that may underlie the functional disturbances. The specificity of the above regions in mediating constructs of social anxiety will require further investigation.

Introduction

Anxiety disorders, as defined by the current Diagnostic and Statistical Manual (DSM-IV) (Psychiatric Association, 1994), are among the most common psychiatric disorders. They share prominent anxiety as a clinical feature, as well as some abnormalities in brain circuitry associated with fear processing (Delgado et al., 2006). Anxiety is also clinically heterogeneous (3-4), however, and identifying abnormalities in brain structure and function that pertain to the different diagnoses may help our understanding of the bases of this heterogeneity. Social anxiety disorder (SAD; also referred to as social phobia), although among the most common anxiety disorders (Jefferys, 1997), has however received relatively little attention in this context.

SAD is characterized by significant and persistent fear of social situations wherein the individual might be exposed to unfamiliar persons or situations, or to scrutiny by others (Psychiatric Association, 1994). Lifetime prevalence is approximately 5-12%, with higher rates among females than males, and with mean onset in late childhood and early adolescence (Kessler et al., 2005). Persons suffering from SAD typically either avoid the feared situations, or endure them with intense anxiety or distress, leading to significant impairment in multiple domains of functioning. Generalized SAD— the subtype involving experience of fear and avoidance in most

social situations (and the focus of the investigation here)— is associated with greater severity, comorbidity, and impairment, and may also have greater genetic heritability (Schneier et al., 2009).

A substantial body of functional MRI studies has reported hyperactivity within limbic regions in SAD patients, particularly the amygdala, hippocampal region, and insula, when viewing emotionally charged faces (Freitas-Ferrari et al., 2010; Pietrini et al., 2010). These paradigms have particular face-validity for SAD, where fear of scrutiny and negative evaluation, and avoidance of eye contact are core symptoms (Safren et al., 1999). Disturbances in frontal, and particularly anterior cingulate, cortex have been reported as well, although specificity and directionality of findings have been inconsistent (Freitas-Ferrari et al., 2010). Other functional imaging paradigms targeting anticipation of public speaking (Lorberbaum et al., 2004), gaze or eye contact (Schneier et al., 2011), and judgment of self- versus non-self relevant information (Whitfield-Gabrieli et al., 2011) have yielded generally similar patterns.

Data from functional paradigms, however, are dependent on the type of task performed, as well as the subject's current state. This is of particular concern in studies of SAD, as the scanning environment may exacerbate performance anxiety— a common feature of the disorder— and impair task performance. Measures of brain structure, in contrast, are largely state- independent, and can complement functional studies by identifying morphological vulnerabilities that are robust to task parameters. Structural studies of SAD, however, have been extremely limited. A 2008 review of structural imaging studies of anxiety (Ferrari et al., 2008) identified only one report for SAD (Potts et al., 1994). That example failed to detect any differences between SAD cases and controls, but was restricted to examination of the thalamus, putamen, and an overall index of grey matter (GM). A subsequent meta-analysis of anxiety

disorders failed to find any studies of SAD that qualified for inclusion (Radua et al., 2010). Some studies have included SAD subjects within anxiety groups but without differentiating them from other fear-based disorders (van Tol et al., 2010). Finally, a recent treatment study reported volume decreases in the cerebellum and superior temporal cortex in SAD patients following 12 weeks of treatment with the selective serotonin reuptake inhibitor (SSRI) escitalopram (Cassimjee et al., 2010). SSRI treatment, however, is broadly efficacious for multiple anxiety and mood disorders, so the extent to which the changes reflect processes specific to social anxiety is unknown. These questions, coupled with the overall paucity of studies, invite additional investigation using complementary approaches and populations.

In the present study, we used magnetic resonance imaging (MRI) and optimized voxel based morphometry (VBM) to identify brain abnormalities associated with SAD. Given the absence of well-established structural abnormalities in SAD based on the current literature, we used a whole-brain approach. The investigation involved three stages. First, we compared a primary group of persons with DSM-IV generalized SAD to a group of healthy control participants, to identify differences in GM differences between the two groups. We then re-examined the same measures in an independent clinical sample of generalized SAD patients and healthy controls, to replicate and evaluate the generalizability of our findings. And finally, we asked whether the GM abnormalities identified above were specific to SAD, by contrasting the primary SAD group to a group of subjects with a different anxiety disorder: panic disorder (PD). PD is a complex anxiety disorder characterized by recurrent episodes of unexpected and uncontrollable fear, accompanied by cardio-respiratory, gastrointestinal, neurological, or other autonomic responses. Like SAD, it is more frequent among women and moderately heritable, although with later onset (Roy-Byrne et al., 2006; Weissman, 1993)}}. Although the two

disorders share some clinical symptoms as well as abnormal fear circuitry, (Kendler et al., 1995; Schneier et al., 1992), they also have distinguishing clinical and treatment profiles. Comparison to the PD group thus afforded us one mechanism to evaluate whether the aforementioned regional abnormalities specifically indexed social anxiety.

The goals of the study can thus be summarized as follows: (1) to identify structural abnormalities in the brain associated with SAD; (2) to retest the findings in an independent clinical population; and (3) to test specificity of these findings to SAD, as compared to other anxiety disorders.

Methods

Primary Sample ("Sample 1"): All subjects were 18-50 years of age. SAD cases were required to have a DSM-IV(1) diagnosis of generalized social anxiety disorder (Goldstein et al., 1997). To further minimize heterogeneity, we required cases to have demonstrated onset by age 30, and have a first-degree relative with an anxiety disorder. Controls were required to have no lifetime history of any psychiatric disorder, with exceptions for past minor depressive disorder, adjustment disorders, or brief periods of substance abuse (but not dependence) in adolescence or college. Additionally, controls could not have a history of an anxiety disorder in any first-degree relative, and were required to be at least 25 years old at the time of assessment, to minimize the possibility of including subjects who, although asymptomatic, might still be at risk for the disorder. For both SAD and control groups, subjects with a personal or family history of schizophrenia or bipolar disorder were excluded a priori.

Subjects were recruited through web advertisements (except for 7 SAD cases recruited from an ongoing genetic program project of fear and anxiety (Talati et al., 2008)). Subject selection involved two stages. First, persons responding to the advertisement were screened by a

research assistant using the screening sections of the SADS-LA-IV diagnostic modules for anxiety disorders. Subjects who screened positive for social anxiety, and were not contraindicated for an MRI scan, were invited to participate in a full DSM-IV interview (detailed below). Similar procedures were used to recruit the comparison sample of PD subjects. Subjects in the PD group, however, could not have a diagnosis of SAD, and vice versa. All procedures were approved by the Columbia University/ New York State Psychiatric Institute Institutional Review Boards, and all subjects gave written consent to participate.

Diagnostic assessments were administered by clinically trained doctoral- and masters-level mental health professionals using the Schedule for Affective Disorders and Schizophrenia-Lifetime Version modified for the study of anxiety disorders and updated for DSM-IV (SADS-LA-IV). Psychiatric history on first-degree relatives was obtained during the interview using the Family History Screen (FHS) (Weissman et al., 2000). Final psychiatric diagnoses were made by an experienced clinician based on all available diagnostic information using the Best Estimate Procedure (Leckman et al., 1982). Trait and state anxiety prior to the scan were assessed using the Spielberger State-Trait Anxiety Inventory (STAI) (Spielberger et al., 1983).

Replication Sample ("Sample 2"): Structural MRI data was obtained for 17 persons with SAD and 17 healthy controls (age 20-52) participating in an unrelated fMRI study (Schneier, P.I.) that used the same MRI scanner. The sample has been detailed elsewhere (Schneier et al., 2011). Briefly, subjects were recruited through media advertisements and clinical referrals, and interviewed using the Structured Clinical Interview for DSM-IV Axis I disorders (SCID IV) (First et al., 1997). Social anxiety severity was also rated by a clinician using the Liebowitz Social Anxiety Scale (LSAS) (Liebowitz, 1987). [Higher LSAS scores indicate greater severity].

The SAD group was required to have a current diagnosis of generalized SAD, but no other current Axis I disorder (except secondary diagnoses of generalized anxiety, dysthymia, or specific phobia). Controls, as with the primary sample, were required to have no lifetime history of any Axis I disorder. Because this was a treatment study, only images acquired at baseline (at which time all subjects had been medication-free for ≥ 4 weeks), were used.

Imaging and Data Analysis: Structural data were acquired on a 1.5 Tesla GE Signa MRI scanner using a 3D T1-weighted spoiled gradient recalled (SPGR) pulse sequence with isomorphic voxels (1 × 1 × 1 mm) in a 24 cm field of view (256 × 256 matrix, ~186 slices, TR 34 ms, TE 3 ms). Anatomical data were processed using whole-brain voxel based morphometry (VBM) (Ashburner and Friston, 2000), as implemented in the SPM8 software package (http://www.fil.ion.ucl.ac.uk/spm) using Matlab v7.13.The 3D T1-weighted images were segmented into the three main tissue classes (gray matter, GM; white matter, WM; and cerebrospinal fluid, CSF) using the SPM unified segmentation algorithm with default settings (Ashburner and Friston, 2005). Next the GM and WM images were spatially normalized to a group specific template (composed of all patients and controls) and then to MNI space using a diffeomorphic image registration toolkit (DARTEL) in 1.5 mm cubic resolution (Ashburner, 2007). The images were modulated with the individual Jacobian determinants to preserve the local amount of GM and WM. Modulation was achieved by multiplying voxel values in the segmented images by the Jacobian determinants derived from the spatial normalization step. In effect, the analysis of modulated data tests for regional differences in the absolute amount (volume) of grey matter. Finally, images were smoothed with an 8 mm full-width at half-maximum (FWHM) isotropic Gaussian kernel. This is the default used in SPM software, and has

been found empirically to be optimal for group inference (Mikl et al., 2008). Furthermore, because many VBM studies of other anxiety and mood disorders have used this kernel (Yoo et al., 2005; van Tol et al., 2010), this consistency should aid future qualitative and quantitative comparisons of our data with other studies.

Prior to statistical analysis, an inclusion mask was created by absolute thresholding which excluded all voxels with GM values less than 0.2. Statistical analysis on processed GM images was carried out by means of whole brain multiple regression, using binary variables to code for SAD cases vs. controls. Analyses were carried out in each independent dataset alone, and with the datasets combined. Sex, age, and total intracranial volume (TIV, which was the sum of GM, WM and CSF, for each subject normalized by 10,000) were entered as covariates in all analyses, as these are independently associated with GM differences in adults, and failure to adjust for these variables can result in false positives (Henley et al., 2010). For the combined dataset analysis, an additional variable coding for dataset was included in order to control for any possible systematic differences between samples.

For whole-brain analyses, tables and maps were thresholded at $p=0.001$ and cluster-size of 10. Additionally, significant clusters were identified by means non-stationary cluster extent correction using random fields (Hayasaka et al., 2004) as implemented using the NS toolbox (http://fmri.wfubmc.edu/cms/software#NS) for SPM5. This correction method confers increased sensitivity to spatially extended signals while remaining valid when cluster-size distribution varies depending on local smoothness as is the case in VBM data (Hayasaka et al., 2004). ROI analyses were conducted using the Marsbar Toolbox (http://marsbar.sourceforge.net/) within SPM8. Clusters in one sample that survived whole-brain cluster-extent correction (see above paragraph) at $p < 0.05$ or 0.1 were used to define ROIs for independent testing in the other

sample. Briefly, contrasts values of SAD > control or control > SAD contrasts from the 2nd level model of one sample were first averaged over all voxels within the above ROIs, and submitted to an independent 2nd level analysis (using the same group level design as for whole-brain analyses above).

An additional analysis was performed to formally quantify the significance in overlap of the case versus control contrast maps from each of the two independent datasets (dataset 1: 16 cases, 20 controls, dataset 2: 17 cases, 17 controls). For this we used the cluster_overlap_npm.m script available from the laboratory of Tor Wager, Ph.D. (http://wagerlab.colorado.edu) in which 2 T-maps (one from each sample for the cases > controls comparison) were thresholded at $p < 0.05$ uncorrected, cluster size > 10 and binarized to include only positive T-values (the analysis was repeated for negative T-values, or controls > cases). The number of overlapping voxels between the two maps was then calculated.. The probability of this overlap occurring by chance was calculated by comparing its observed value to a null distribution, which was derived by randomizing the locations of the centers of the clusters of each map 2,000 times.

Results

Sample 1

Demographic and Clinical Features: Sample characteristics are detailed in Table 9a. As compared to the healthy controls, the SAD group had a higher proportion of female subjects, and reported higher state and trait anxiety. The most frequently co-morbid lifetime diagnoses were major depressive disorder and specific phobia. Three subjects reported taking medication for anxiety in the past, but no subject was on any psychoactive medication in the 10 weeks preceding the scan.

Table 9. Chapter 7: Sample demographics and clinical features.

	Diagnostic Groups			Statistical Comparisons		
(a) SAMPLE 1	SAD	CON	PD	SAD vs CON	PD vs CON	SAD vs PD
	N = 16	N = 20	N = 16			
Gender [N(%), Female]	13 (81)	9 (45)	13 (76)	$x^2 = 4.9$*	$x^2 = 3.8^+$	$x^2 = 0.11$
Age [mean years, std]	34.1 (6.7)	31.4 (7.8)	31.8 (10)	t = 1.1	t = .41	t = .75
Age at onset [mean, std]	11.0 (5.9)	n/a	18.4 (3.4)			t = 4.4****
Trait Anxiety [mean, std]	35.7 (12.5)	27 (6.1)	39.4 (7.9)	t = 2.3*	t= 4.9****	t = .99
State Anxiety [mean, std]	39 (11.9)	26 (4.1)	35.5 (10)	t = 4.0****	t = 3.5***	t = .88
Lifetime Comorbid Diagnoses [N,%]						
MDD	5 (31)	0	3 (17)			$x^2 = .83$
GAD	2 (12)	0	2 (12)			$x^2 = .004$
SP	4 (25)	0	5 (29)			$x^2 = 0.08$
OCD	1 (6)	0	2 (12)			$x^2 = 0.1$
DUD	1 (6)	0	4 (23)			$x^2 = 1.9$
AUD	0	0	4 (34)			$x^2 = .3$
Lifetime Psych. Medication Use [N,%]	3 (20)	0	9 (52)			$x^2 = 3.7^+$
(b) SAMPLE 2	SAD	CON	PD	SAD vs CON		
	N = 17	N = 17	n/a			
Gender [N(%), Female]	11 (64)	10 (59)		$x^2 = 0.1$		
Age [mean years, std]	29.1 (8.9)	31.3 (10.7)		t = .66		
State Anxiety [mean, std]	44.7 (9.6)	24.4 (7.1)		t = 6.9****		
Liebowitz Social Anxiety Scale [mean, std]	81.4 [15.6]	8.1 [5.4]		t = 17.7****		
Lifetime Comorbid Diagnoses [N,%]						
MDD	6 (35)	0				
GAD	3 (18)	0				
AUD	2 (12)	0				
Lifetime Psych. Medication Use [N,%]	6 (35)	2 (12)				
(C): COMBINED SAMPLE	SAD	CON	PD	Sample	Group	Sample x Group
	N = 33	N = 37	n/a	(1 vs 2)	(SAD vs CON)	
Gender [N(%), Female]	24 (73)	19 (51)		$x^2 = 0.03$	$x^2 = 3.4$+	$x^2 = 1.8$
Age [mean years, std]	31.5 (8.2)	31.4 (9.1)		t = 1.3	t = .01	F = 1.5
State Anxiety [mean, std]	42.0 (11.0)	25.6 (5.7)		t = 1.5	t = 64.9****	F = 2.8

+ $p \leq .1$; * $p \leq .05$; **$p \leq .01$; ***$p \leq .005$; **** $p \leq .001$

Abbreviations:

AUD: Alcohol Use Disorder (abuse or dependence); DUD: Drug Use Disorder (abuse or dependence); GAD: Generalized Anxiety Disorder; MDD = Major Depressive Disorder; OCD: Obsessive Compulsive Disorder; SP: Specific phobia.

Medication frequencies only include those prescribed for a psychiatric condition.

\

Grey Matter Differences associated with SAD: We first examined grey matter (GM) differences between the SAD and healthy control groups on a voxel-by-voxel basis across the entire brain. Significant group differences (defined as clusters of 10 or more voxels at $p \leq .001$) are identified in Table 10a. All analyses were adjusted for age, gender, and total intracranial volume (TIV). There were no overall differences in total grey or white matter between the SAD and control groups.

The largest GM increases associated with SAD (i.e, the SAD > control contrast) were observed in a left hemisphere cluster encompassing the cerebellum and fusiform/parahippocampal cortex [Brodmann's Areas (BA) 37, 36]. Additional differences were detected in right and left lingual, middle occipital, and middle frontal gyri. The converse contrast (control > SAD) identified a cluster spanning right hemisphere primary motor and sensory cortices, multiple clusters in both hemispheres of the dorsal anterior cingulate, and a cluster in the temporopolar region of the left superior temporal cortex.

Table 10. Chapter 8: Grey Matter Abnormalities Associated with Social Anxiety Disorder

(a) Sample 1

	BA	Size	x	y	z	*t*
SAD > Control						
1 L Cerebellum, Parahippocampal, Fusiform	37, 36	451+	-24	-39	-21	4.40
2 R Middle Frontal	46, 10	224	45	51	9	4.95
3 R Lingual	19	41	24	-53	-5	3.67
4 R Cerebellum	-	35	15	-62	-44	3.95
5 L Middle Occipital	19	11	-39	-74	8	3.98
6 L Lingual	17	12	-8	-92	-15	3.49
Control > SAD						
1 R Precentral, Postcentral	6,4	678*	42	-18	38	-4.84
2 R Middle Cingulate	24	199	14	-21	48	-4.64
3 L Middle Cingulate	32	32	-11	21	38	-3.89
4 L Superior Temporal	22	29	-59	8	3	-4.13
5 R Temporal Pole, Superior Temporal	38	28	30	17	-29	-3.36
6 R Medial Frontal, Middle Cingulate	6,24	16	11	-6	51	-4.47
7 L Middle Cingulate	24	11	-14	-20	44	-3.59

(b) Sample 2

SAD > Control						
1 L,R Cerebellum	-	701	2	-41	-12	4.92
2 L Inferior Parietal, Supramarginal	40	214	-38	-42	53	3.92
3 R Paracentral Lobule, Supp.Motor Area	6	186	5	-17	48	4.24
4 L Inferior Temporal	20, 21	153	-57	-44	-14	4.97
5 R Post Central Gyrus	3,1,2	29	39	-24	48	3.95
Control > SAD						
1 R Temporal Pole, Superior Temporal	38	603*	38	17	-29	-4.91
2 R Middle Frontal, Orbitofrontal	11,47	366^{+}	33	47	-9	-5.66
3 L Temporal Pole, Superior Temporal	38	31	-42	20	-27	-3.71
4 L Inferior Frontal, Orbitofrontal	11	22	-36	33	-9	-4.14

(c) Combined Sample

SAD > Control						
1 L Cerebellum, Parahippocampal, Fusiform	37	1840*	0	-51	-12	4.12
2 R Supramarginal, Angular	40	192	53	-50	36	3.81
3 L Supramarginal, Angular	40	22	-42	-62	47	3.44
4 L Middle Occipital	19	28	-39	-71	8	3.73
Control > SAD						
1 R Temporal Pole, Superior Temporal	38	851*	32	17	-30	-5.22
2 L Temporal Pole, Superior Temporal	38	97	-42	15	-30	-3.56
3 L Inferior Frontal, Orbitofrontal	47	18	-38	35	-9	-3.69
4 R Superior Occipital		10	24	-74	29	-3.55

$P < .001$; $k = 10$
Sample 1: N = 36 (16 SAD, 20 Control);
Sample 2: N = 34 (17 SAD, 17 Control);
Combined Sample: N =70 (33 SAD, 37Control)

Clusters surviving whole brain correction are indicated as follows: *$p < .05$; $^{+}p < .1$

Clusters are listed in order of descending size; coordinates refer to the voxel with the peak t value in the cluster.

Sample 2

Demographic and Clinical Features: We next repeated the above analyses in an independently recruited and imaged clinical sample of SAD cases and healthy controls (hereon, "sample 2"). The SAD and control groups of sample 2 did not significantly differ on measures of age or gender, either from each other (Table 9b), or from the respective SAD and control groups in the first sample (Table 9c).

Grey Matter Differences associated with SAD: GM differences between the SAD and control groups in sample 2 are listed in Table 10b, adjusted for age, gender, and TIV. Significantly greater GM among the SAD group was detected in the bilateral cerebellum, left supramarginal, right paracentral lobule and supplementary motor area, left inferior temporal and right post-central regions. The control > SAD contrast identified clusters in both left and right temporal pole, and the regions of the middle and inferior frontal gyri encompassing orbitofrontal cortex.

We also performed a corollary analysis using a continuous clinician-rated measure of social anxiety, the Liebowitz Social Anxiety Scale (LSAS) total score [this measure was not collected in the first sample]. We first examined the association between symptom severity and GM across all subjects, regardless of their diagnostic status. The results, listed in Table 3a, show that cerebellar, inferior parietal and precentral GM volumes were positively correlated with social anxiety severity; conversely, temporal pole, as well as superior, middle and inferior frontal cortices, was negatively correlated with severity. We also explored whether severity could further predict GM variation within the SAD group. As listed in Table 3b, GM within left medial

frontal and right middle occipital gyri, as well as right thalamus and hippocampus, was associated with greater severity among subjects with SAD; conversely, three GM clusters in the (predominantly right hemispheric) dorsal anterior cingulate were inversely correlated with SAD severity

Table 11. Chapter 8: Relationship between Social Anxiety Severity and Grey Matter volume

	BA	Size	x	y	z	*t*
(a) GM-SAD Severity Correlation, Full Sample						
Positively Associated with LSAS						
1 L,R Cerebellum (Vermis)	-	294	0	-39	-14	4.11
2 Inferior Parietal Lobule	40	145	-38	-44	53	3.82
3 L Middle Temporal, L Inferior Temporal	20,21	92	-59	-44	-15	4.73
4 L Precentral	6	69	-26	-12	63	4.57
5 R Precentral	6	26	30	-11	56	3.58
6 R Cerebellum (Posterior)	-	25	14	-57	-18	3.57
7 R Precentral	6	22	39	-8	56	3.79
Negatively Associated with LSAS						
1 R Superior Temporal, Temporal Pole	38	480	35	15	-30	-4.37
2 R Middle Frontal	11	341	33	47	-11	-5.85
3 L Superior Frontal	11	69	-17	44	-15	-3.97
4 L Inferior Frontal	11	33	-26	29	-15	-3.67
5 L Inferior Frontal	47	23	-35	32	-8	-3.80
6 L Superior Temporal, Temporal Pole	38	19	-42	20	-27	-3.67
7 L Inferior Frontal	10	14	35	35	-8	-4.10
(b) GM-SAD Severity Correlation, within SAD Group						
Positively Associated with LSAS						
1 L Superior / Medial Frontal	6	103	-9	26	57	5.36
2 Thalamus (Pulvinar Nuclei)	-	73	8	-33	2	6.19
3 R Middle Occipital	19	13	33	-80	8	6.83
4 R Hippocampus	-	11	32	-24	-8	4.52
Negatively Associated with LSAS						
1 R Middle Cingulate	23,31	52	11	-36	33	-5.31
2 L Cerebellum (Tonsil)	-	36	-3	-50	-45	-4.49
3 R Middle Cingulate	24	26	9	2	35	-4.70
4 L Middle Temporal	22	20	-51	-45	0	-4.55
5 L Cingulate	24	16	-6	-5	36	-4.74

$P < .001$; $k = 10$
Analysis includes Sample 2 only as the LSAS measure was not collected in sample 1.
Table a: N = 34 (17 SAD, 17 Control)
Table b: N = 17 SAD only
LSAS: Liebowitz Social Anxiety Scale. Higher scores indicate greater anxiety.
All correlations between LSAS severity and GM volume were > .4 with the peak voxel of each cluster.

Combined Sample

Testing for Overall Replicability between samples: Prior to combining the two samples, we first tested the extent to which individual findings from one sample were replicated in the other. We used non-stationary cluster extent correction to identify clusters significant at $p < 0.05$ or 0.1, corrected, in either sample alone (indicated by a * or + in Table 10). This analysis identified three clusters: (1) Sample 1 SAD > Control: left cerebellum/parahippocampal gyrus [peak coordinate: -24 -39 -21], (2) Sample 1 Control > SAD: right precentral/postcentral gyrus [peak 42 -18 38] and 3) Sample 2; Control > Case: right temporal pole [peak 38 17 -29]. Independent ROI analyses (a single test of the same contrast in the other sample) for Clusters 1, 2, and 3, yielded $t29 = 1.92$, $p=0.032$/ $t29 = -1.2$, $p=0.88$/ $t31 = 1.62$, $p=0.058$ respectively. Thus, findings for left cerebellum/parahippocampal gyrus and right temporal pole were replicated across samples, whereas findings for right precentral/postcentral gyrus did not.

Second, we tested for consistency between the two samples in terms of the overlap in the overall spatial patterns of SAD > control and control > SAD differences at a loosened threshold (see methods). We observed a significant overlap of voxels for the SAD > control contrast across both samples (observed: 3096, expected under null: 910, $p=0.007$), but not for the control > case contrast (observed: 188, expected: 533 under null, $p=0.89$). Thus, the spatial overlap in regions with greater GM volume among the SAD groups (which included cerebellum, parahippocampal gyrus, fusiform and inferior parietal lobe, figure not shown) was relatively extensive and significantly greater than that expected by chance, whereas the spatial overlap across regions with greater GM in the control groups (right temporal pole, see ROI analyses above) was not extensive and was less than the overlap expected by chance.

Grey Matter Differences associated with SAD in combined sample: Finally, we combined the two samples into a single dataset and examined overall differences between SAD and control groups, adjusting for the previously noted variables, as well as for sample of origin. The final results, detailed in Table 10c, preserve a number of the regions observed in the individual samples. Specifically, the SAD > control contrast revealed large increases in the cerebellum, left parahippocampal and fusiform gyri, bilateral supramarginal and angular gyri, and left middle occipital gyrus. The control > SAD contrast identified lower temporal pole (both hemispheres, but predominantly right) and left inferior prefrontal / orbitofrontal GM in the SAD group. Cerebellum, parahippocampal and temporal pole differences were robust to multiple comparison correction at the whole-brain level (asterisked clusters in Table 10). The main findings are illustrated in Figure 21, with clusters shown in red illustrating regions with greater GM volume among the SAD group than the controls, and clusters in blue, the converse. The numbering of regions in the figures corresponds to the clusters in Table 10.

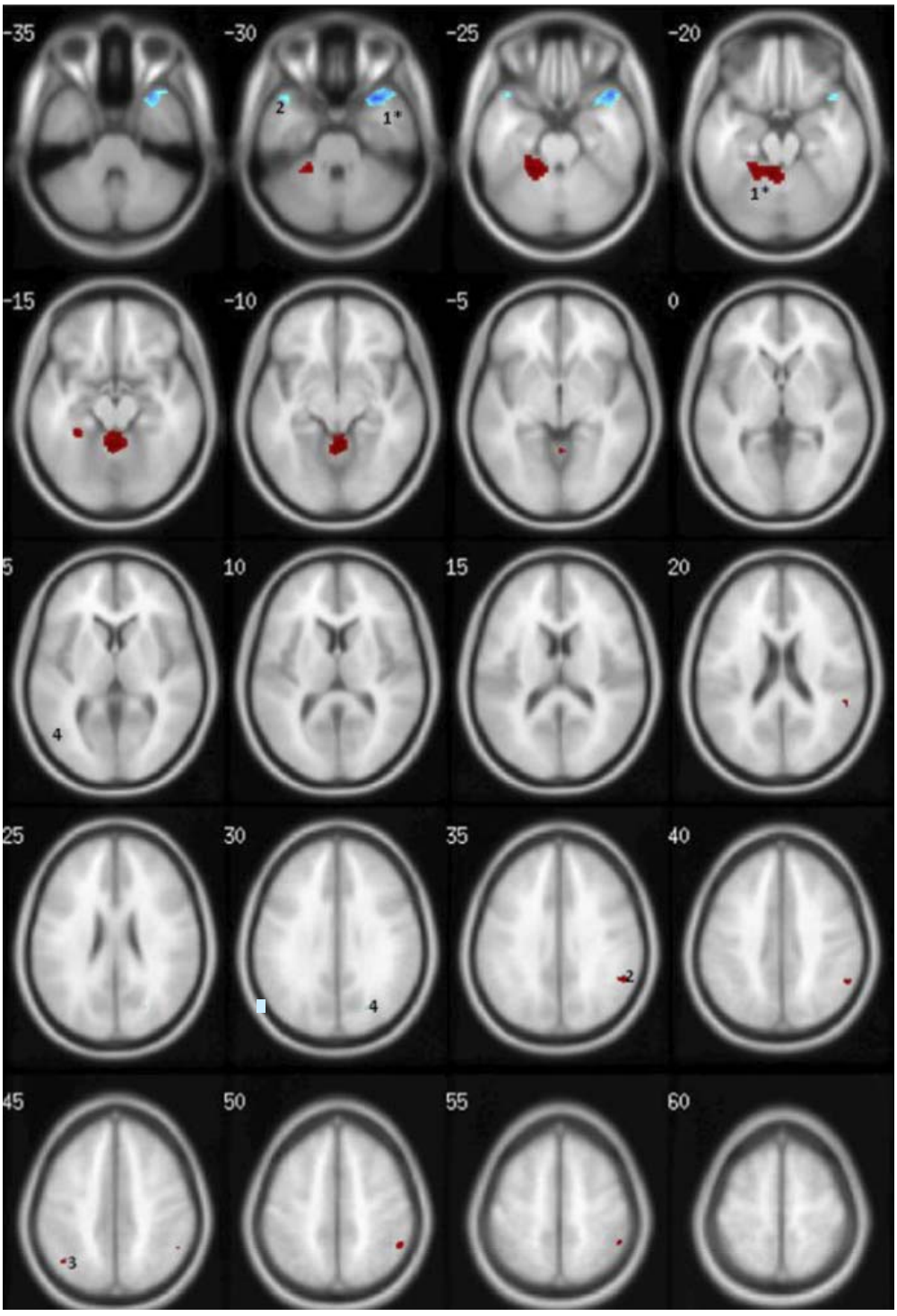

Figure 21. Chapter 8: Gray matter differences associated with social anxiety disorder (SAD); $p < 0.001$; k= 10; n=70 (33 SAD, 37 Control). T1-weighted axial images; image left is brain left. Images Group differences are adjusted for differences in age, gender, intracranial volume, and sample source. *Regions surviving multiple comparison correction at the whole brain level. Clusters are numbered corresponding to their listing in Table 10 (Combined

Sample). SAD > Control (red): 1: left (L) cerebellum, parahippocampal, fusiform; 2: right (R) supramarginal,angular; 3: L supramarginal, angular; 4: L middle occipital. Control > SAD (blue): 1: R superior temporal, anterior temporal pole; 2: L superior temporal, anterior temporal pole; 3; L inferior frontal (orbitofrontal); 4: L middle occipital.

We also conducted an additional exploratory analysis in the combined sample within three ROIs which have been implicated in the functional neurobiology of social anxiety (see introduction), but were not detected in our whole-brain analysis: (1) bilateral amygdala; (2) bilateral insula; and (3) anterior cingulate cortex (ACC). For these analyses we employed a looser statistical threshold than that used for the preceding analyses ($p < 0.05$, $k = 10$,) and also applied small-volume, non-stationary cluster extent correction. We found no voxels that survived the above uncorrected threshold for the SAD > control contrast within any ROI. However, GM in the left ACC [87 voxels, peak: $t = 2.92$, $p = 0.009$ (uncorrected); $x = -3$, $y = 36$, $z = 22$], bilateral insula [LEFT: 108 voxels, peak: $t=2.78$, $p = 0.004$; -46,12, -8; RIGHT:100 voxels, peak: $t = 2.4$, $p = 0.008$; 42, -13, -6], and the right amygdala [87 voxels, $t = 2.92$, $p = 0.002$; 36,3, -26] were lower in subjects with SAD. None of these regional differences survived whole-brain cluster extent correction, and only the amygdala observations survived small-volume and cluster extent correction ($p = 0.03$, corrected); these coordinates should thus be viewed provisionally and probed further in subsequent studies.

Testing for Specificity to SAD: Comparison with Panic Disorder (PD): To further investigate whether the GM differences identified above were specific to SAD, we compared the SAD group from sample 1 (who had documented no lifetime history of PD) to a group of separate subjects who had been recruited in sample 1 with PD (who were selected to be free of SAD). Demographic and clinical features of the PD group are included in Table 9a. As with the SAD

group, subjects with PD were more likely than controls to be female. Mean age of onset was later in adolescence for PD than for SAD (18.4 vs. 11.0 yrs), consistent with the epidemiology of the two disorders. Importantly, the two anxiety groups did not differ from each other on age, gender, or state or trait anxiety.

We first examined brain-wide differences between the PD and the control groups. As shown in Table 12a, and illustrated in Figure22a, subjects with PD, as compared to controls, had large areas of parieto-occipital GM increases— specifically, in bilateral cuneate and precuneate, lingual, and superior occipital cortices— as well as larger insular cortex. Conversely, a number of frontal cortical (right pre- and post-central gyri, left and right middle cingulate, supplementary motor area) as well as sub-cortical (thalamus, caudate) regions showed reduced GM among the PD cases.

Table 12. Chapter 8: Grey Matter Differences between Panic Disorder and Social Anxiety Disorder

(a) PD Vs. CONTROL	**BA**	**Size**	**x**	**y**	**z**	**t**
PD > Control						
1 L,R Cuneus, Lingual	17,18	1620*	0	-98	6	5.03
2 L Insula	-	379	-30	9	5	4.44
3 L, R, Cuneus, Precuneus	7	355	0	-71	24	4.30
4 R Cuneus, Superior Occipital	7	23	21	-75	30	3.56
Control > PD						
1 R Precentral, Postcentral	6,1-4	884*	44	-14	42	-5.29
2 R Middle Cingulate	32	504*	5	20	41	-4.69
3 L Inferior Parietal	40	104	-50	-45	42	-4.36
4 R Middle Cingulate, R Supp. Motor Area	24	29	11	-6	50	-4.32
5 L Caudate	-	98	-14	12	18	-4.14
6 L Precentral	6	40	-56	-5	36	-3.64
7 R Middle Cingulate	24	13	15	-18	44	-3.57
8 R Thalamus	-	23	8	-20	15	-3.46
(b) PD vs SAD						
PD > SAD						
1 L Cuneus	7	149	-6	-77	36	4.43
2 L Middle Frontal	9	35	-53	20	30	4.19
3 L, R Lingual	18	25	2	-87	-8	3.56
4 R Superior Occipital	18,31	12	23	-74	29	3.74
SAD > PD						
1 R Parahippocampal, Fusiform, Cerebellum	37,36,19	534*	30	-48	-11	-4.52
2 L Parahippocampal,Fusiform	37,36	402	-30	-41	-17	-4.42
3 R Middle Frontal, Inferior Frontal	10	106	42	45	5	-3.94
4 R Anterior Cingulate	32	10	15	47	2	-3.55
5 L Middle Frontal	8	12	-21	21	44	-3.34

$p < .001$; $k = 10$
Table 4a: N = 16 PD, 20 Control; Table 4b: N = 16 SAD, 16 PD
Clusters surviving whole brain correction ($p < .05$) are asterisked.
Clusters are listed in order of descending size; coordinates refer to the voxel with the peak t value in the cluster.

A: PD vs Control

B: PD vs SAD

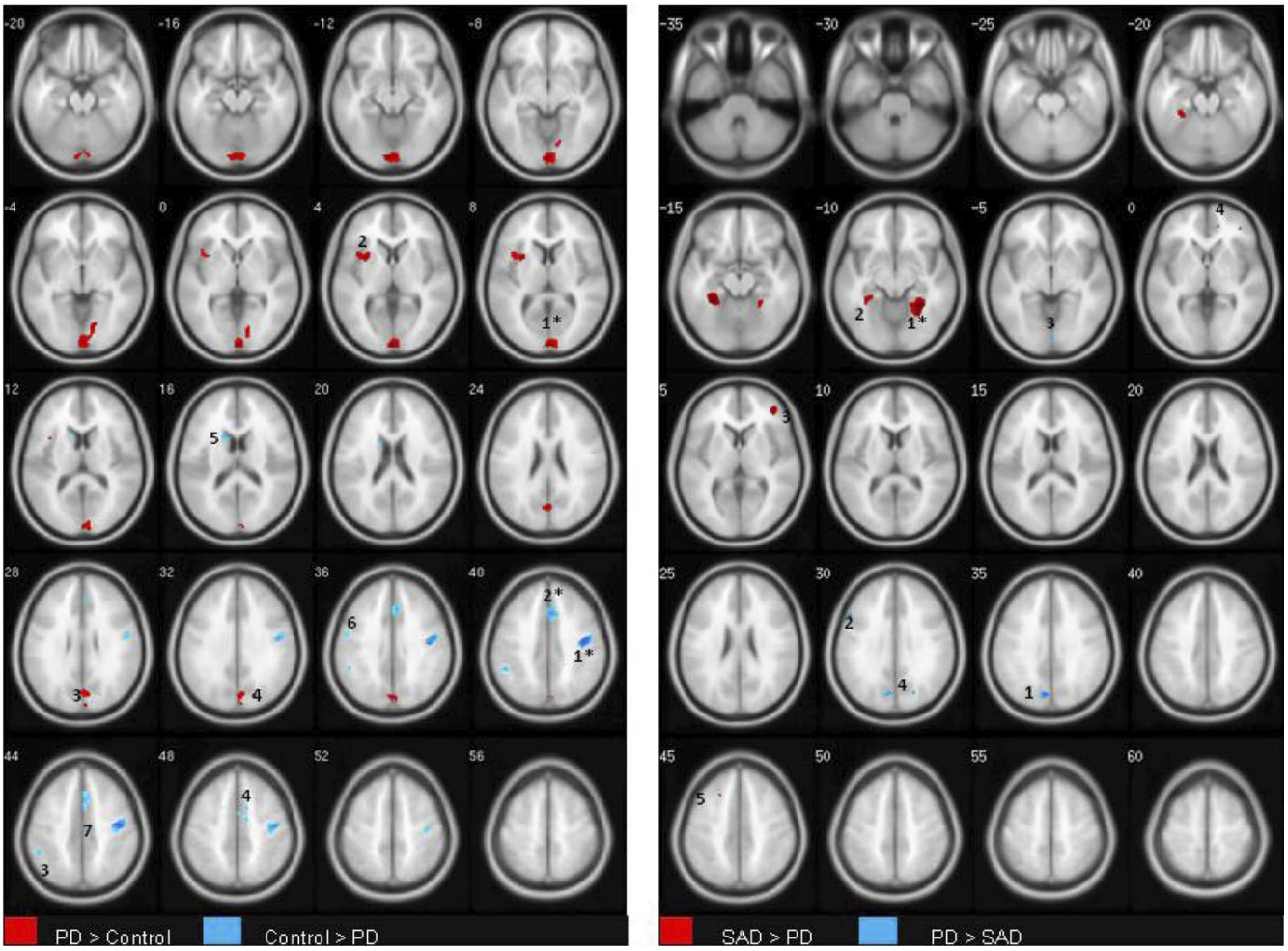

Figure 22. Chapter 8: Gray matter differences between social anxiety disorder (SAD) and panic disorder (PD); $p < 0.001$; k=10. (A) n=16 PD, n= 20 Control; (B) n=16 SAD, n=16 PD. T1-weighted axial images; image left is brain left. Images Group differences are adjusted for differences in age, gender, and intracranial volume. Clusters surviving whole brain correction are indicated as follows: *$p < 0.05$; $^{+}p < 1$. Clusters are numbered corresponding to their listings in Table 11, PD vs. Control and PD. vs. Sad, respectively. (A) PD > Control (red): 1: bilateral cuneate, lingual; 2: L insula; 3: bilateral cuneus, precuneus; 4: R cuneus, superior occipital. Control > PD (blue) 1: R precentral, postcentral; 2: R middle cingulate; 3: L inferior parietal; 4: R middle cingulate, supplementary motor area; 5: L caudate; 6: precentral; 7: R middle cingulate. (B) SAD > PD (red): 1: R parahippocampal, fusiform; 2: L parahippocampal, fusiform; 3: R middle frontal, inferior frontal; 4: R anterior cingulate; 5: L middle frontal. PD > SAD (blue) 1: L cuneus; 2: L middle frontal; 3; L and R lingual; 4: R superior occipital.

We then formally contrasted the PD and SAD groups. As shown in Table 12b and Figure 21b, subjects with PD showed larger mean occipital GM volume, particularly in the cuneate cortex, calcarine sulcus, and lingual gyrus. Conversely, both hemispheres of the parahippocampal and fusiform gyri were significantly larger in the SAD group. Finally, right inferior frontal (orbitofrontal), and anterior cingulate were larger among the SAD groups, though it should be noted that both anxiety groups had reduced GM vis a vis healthy controls.

Discussion

Summary of Findings: We report here on morphological abnormalities associated with generalized social anxiety disorder (SAD). We found that subjects with SAD, as compared to healthy controls, had higher GM volume in the cerebellum and the left parahippocampal cortex, and lower GM in the temporal pole of the superior temporal lobe. Several observations together strengthen our confidence in these findings. First, these differences were observed in both individual samples as well as the combined dataset Analysis. Second, the clusters remained significant after correction for multiple comparisons at the whole-brain level. Third, similar clusters were identified when using a clinician-rated measure of social anxiety severity instead of diagnosis (tested in sample 2 only). And finally, a separate group of subjects with panic disorder (PD) did not show these patterns, pointing to the relative specificity of these findings to SAD. We thus weight the ensuing discussion primarily toward the above regions. Other GM differences that were not observed in both samples, or did not survive corrections for multiple comparisons, may play a role, but such findings should be considered provisional.

Grey Matter Increases Associated with SAD: The largest differences were within the cerebellum, where we detected significantly greater GM, particularly the vermis and posterior lobe, among subjects with SAD. These differences were observed in both samples, rendering them unlikely to be an artifact of sample ascertainment. Few studies have examined the role of the cerebellum in phobic disorders. Resting state perfusion studies have reported both hyper- and hypo-perfusion in the cerebellum among subjects with SAD (Warwick et al., 2008), and a Positron Emission Tomography (PET) study found anxiety induced in SAD patients to increase blood flow to the cerebellum (Kilts et al., 2006). The aforementioned treatment study (Cassimjee et al., 2010) reported decreases in cerebellar volumes among SAD patients following three months of SSRI treatment, but because there was no control group, it is unclear whether the patients had abnormalities prior to being treated. Although the mechanisms are unclear, cerebellar abnormalities may increase vulnerability to anxiety states via modulation of arousal. Many cerebellar subdivisions, and the vermis in particular, project to the midbrain regions of the pons and medulla, which mediate the autonomic responses that are exaggerated in persons with anxiety (Baldaçara et al., 2008).

Also having higher GM volume in the SAD group was the parahippocampal gyrus (PHG). The PHG consolidates memories and social communication cues, and hyperactivation has been reported in SAD patients during conditions of social threat (Goldin et al., 2009; Straube et al., 2004), as well as during non-threatening tasks involving human, as compared to non-human or computer-simulated, interaction (Polosan et al., 2011). Moreover, the adjacent fusiform gyrus—part of the parahippocampal cortex (and included in the detected clusters)— is cardinal in facial recognition (Fairhall and Ishai, 2007) and processing of facial expression (Gentili et al., 2008; Straube et al., 2004). A recent fMRI study reported that when asked to

passively view socially threatening stimuli, persons with SAD had higher BOLD signal increases in bilateral PHG than controls; however, if asked to try to actively regulate their negative responses to the same stimuli, the SAD group had decreased responses in fusiform (Goldin et al., 2009). These differences were not replicated if social threat was replaced with physical threat. In the present study, PHG and fusiform GM differences were observed only in the SAD group (Table 12a). GM volume in the PD group was not only significantly lower than in the SAD group, as shown in Table 12b, but lower than in the controls as well. Whilst no other study to our knowledge has directly contrasted these two anxiety disorders at the morphological level, a number of reports, including a pilot meta-analysis (Lai, 2011; Massana et al., 2003; Uchida et al., 2008), have reported reduced PHG volume among panic patients. Our anatomical data, coupled with the functional literature on SAD, suggest that increased PHG activity may serve as a marker for social-based anxiety constructs. Incidentally, lower caudate volume, the only other regional abnormality associated with PD in the aforementioned PD meta-analysis (Lai, 2011), was also replicated in our PD group (Table 12a, control > PD).

Grey Matter Decreases Associated with SAD: The temporal pole, that is, the anterior region of the superior temporal cortex corresponding to Brodmann's Area 38, had significantly lower GM volume in both samples of SAD subjects. The anterior temporal cortex has been implicated in the processing of abstract conceptual knowledge, but the BA 38 region— and particularly its right hemisphere— may more specifically index social concepts (Zahn et al., 2007; 2009). Functional MRI studies of healthy subjects have reported activation in this region during social competition and perception of others' mental states (Polosan et al., 2011). Conversely, lesions and degeneration of BA 38 have led to changes in social behavior as well as in the ability to

characterize social attributes of behavior (Liu et al., 2004; Zahn et al., 2007). Attachment anxiety is also associated with decreased GM matter in this region (Benetti et al., 2010), and among persons with SAD, public speaking (Tillfors et al., 2001) and anticipation thereof (Tillfors et al., 2002) have been associated with decreased blood flow to the temporal pole. Interestingly, in one study, left temporal pole was the only region showing significantly increased surface area, concomitant with significantly reduced cortical thickness, in in adults with Williams Syndrome (WS), a rare genetic disorder that in terms of its behavioral phenotype seems the opposite of SAD (e.g., hyper-sociability, lack of fear of interacting with strangers) (Meda et al., 2012). That, as well as one other report (Reiss et al., 2004) also showed decreased PHG volume in WS patients, again the opposite of what we find here with SAD. Though WS and SAD may be etiologically different disorders, the common regional focus of abnormalities suggests that the above regions may mediate common constructs of social cognition, with different neuroanatomical aberrations leading to different clinical syndromes.

The SAD group also had lower GM in the lateral orbitofrontal cortex (~BA 11, 47). OFC regulates expression of emotion, and assigns positive and negative stimulus response contingencies (Blackmon et al., 2011; Milad and Rauch, 2007). Concordantly, GM disturbances (particularly in the left hemisphere) have been linked to multiple anxiety and mood disorders (Whitfield-Gabrieli et al., 2011). The OFC also receives direct reciprocal input from the amygdala, a central mediator of the fear response, and in persons with SAD, the uncinate fasiculus— the white matter tract connecting OFC to temporal cortex— is compromised (Baur et al., 2011; 2013). Although our study does not address temporal sequence, these disturbances are likely to begin early in life, as infants with high-reactive and inhibited temperament— which are risk factors for later onset of SAD (Biederman et al., 2001; Schwartz et al., 1999) — show

reduced cortical thickness in similar left OFC regions when imaged in adulthood, even if they did not go on to develop the full disorder (Schwartz et al., 2010).

Finally, two other interesting but inconsistently observed regional differences deserve comment. First, significantly lower GM among SAD cases was identified in the primary motor and sensory cortex in sample 1 only. Although the right hemispheric precentral gyrus is thought to control motor function, it also has been associated with self-face recognition (Kilts et al., 2006) and imitations of facial expressions (Baldaçara et al., 2008) that could hold implications for social anxiety. In fMRI studies, this region is hypoactive in SAD patients during emotional regulation tasks (Goldin et al., 2009). Second, multiple clusters were observed for the control > SAD contrast in the middle cingulate in sample 1 (Table 10a). Although this lower cingulate GM volume in SAD was not mirrored in sample 2 (Table 10b), within the SAD cases of that sample, increased severity of social anxiety was associated with lower cingulate GM volume (Table 11b). The inconsistency of these findings across sample suggests that they may not reflect robust population differences. Furthermore, it is unlikely that these patterns are specific to social anxiety, as they were also observed in the PD group, and similar abnormalities have been reported for other anxiety and mood disorders (Radua et al., 2010). Nevertheless, the overall inverse relationships with GM-SAD diagnosis (sample 1) and GM-severity (sample 2) are broadly consistent with functional models positing anxiety as a failure of the frontal cortex to down-regulate limbic activation (Etkin and Wager, 2007).

Limitations: The reported findings should be interpreted within the context of the following limitations. First, the study is cross-sectional and does not therefore speak to the causal relationship between brain structure and diseased state, as the identified GM differences could

either predispose to, or be a result of the disorder. Disentangling causal from compensatory pathways would require more complex epidemiological approaches (Weissman et al., 2011) — e.g., selecting subjects who are at high-risk (by virtue of family history, presence of a prodrome, etc) but asymptomatic at recruitment, and then tracking brain changes longitudinally as a subset go on to develop the syndrome. Related, the GM differences reported here should also not be used to make diagnostic inferences, as they are based on overall group differences and do not account for important individual brain, behavioral, and environmental variations that shape whether a given subjects will have a diagnosis (Davatzikos, 2004). Second, standard methodological limitations to VBM, particularly its vulnerability to normalization and smoothing errors (Crum et al., 2003) apply here as well. Third, in order to obtain a more population-representative sample, we did not exclude lifetime occurrence of other anxiety or mood disorders. Although we required that SAD symptoms occur first and not be explainable by other psychiatric or medical conditions, and the individual frequencies of comorbid conditions were low, we cannot rule out that other lifetime anxiety, or behavioral traits that are related to, but do not directly index SAD, contributed to the group differences. And fourth, the analysis only compared SAD with one other anxiety disorder: PD. Different patterns might well have been observed had we instead use a different comparison group. For example, a comparison with specific phobia, another disorder of aberrant fear processing, might have yielded largely overlapping regions; on the other hand, a more complex emotion dysregulation syndrome like PTSD may diverge significantly from SAD, particularly within frontal regions sub-serving executive control (Etkin and Wager, 2007). Related, it should be noted that to facilitate interpretation, we only included SAD subjects without a history of PD, and vice versa. This could have biased selection toward milder or less generalizable cases of either disorder.

Alternative approaches would have been to include a third group with both SAD and PD, or to permit all comorbidity and then model the variance statistically. Both approaches, however, would have necessitated a substantially larger study sample.

Conclusions: This report contributes to the currently limited literature on the neurobiology of social anxiety by identifying grey matter deficits that may predispose to abnormalities in neural circuitry. The rigorous ascertainment criteria, retest in an independent sample, and comparison with another anxiety disorder strengthen both the reliability and the interpretability of our findings. The confirmation in a second sample is particularly valuable for MRI studies, given the high type I error rates and preponderance of failures to replicate original reports, and should be considered in future study designs when possible (Ioannidis, 2011). Finally, because the results include regions (e.g., cerebellum, temporal pole) that are not primary nodes of functional fear-processing circuits, the validity of these regions, as well as specific roles in mediating constructs of social anxiety, will require further investigation.

REFERENCES

Adolphs R, Tranel D, Damasio AR. Dissociable neural systems for recognizing emotions. Brain and cognition 2003; 52: 61-69.

Adolphs R. The neurobiology of social cognition. Current opinion in neurobiology 2001; 11: 231-239.

Allen R, Hill E, Heaton P. 'Hath charms to soothe . . .': an exploratory study of how high-functioning adults with ASD experience music. Autism 2009; 13: 21-41.

Amedi A, Malach R, Hendler T, Peled S, Zohary E. Visuo-haptic object-related activation in the ventral visual pathway. Nature neuroscience 2001; 4: 324-330.

Amedi A, Malach R, Pascual-Leone A. Negative BOLD differentiates visual imagery and perception. Neuron 2005; 48: 859-72.

Anderson JS, Ferguson MA, Lopez-Larson M, Yurgelun-Todd D. Connectivity gradients between the default mode and attention control networks. Brain Connect 2011; 1: 147-57.

Andrews-Hanna JR. The brain's default network and its adaptive role in internal mentation. Neuroscientist 2012; 18: 251-70.

Ashburner J, Friston KJ. Voxel-based morphometry--the methods. Neuroimage 2000; 11: 805-21.

Ashburner J, Friston KJ. Unified segmentation. NeuroImage 2005; 26: 839-851.

Ashburner J. A fast diffeomorphic image registration algorithm. Neuroimage 2007; 38: 95-113.

Baldaçara L, Borgio JG, Lacerda AL, Jackowski AP. Cerebellum and psychiatric disorders. Rev Bras Psiquiatr 2008; 30: 281-9.

Banks SJ, Eddy KT, Angstadt M, Nathan PJ, Phan KL. Amygdala-frontal connectivity during emotion regulation. Social cognitive and affective neuroscience 2007; 2: 303-312.

Bar M. A cortical mechanism for triggering top-down facilitation in visual object recognition. Journal of cognitive neuroscience 2003; 15: 600-609.

Baur V, Brühl AB, Herwig U, Eberle T, Rufer M, Delsignore A, et al. Evidence of frontotemporal structural hypoconnectivity in social anxiety disorder: A quantitative fiber tractography study. Hum Brain Mapp 2013; 34: 437-46.

Baur V, Hänggi J, Rufer M, Delsignore A, Jäncke L, Herwig U, et al. White matter alterations in social anxiety disorder. J Psychiatr Res 2011; 45: 1366-72.

Behrens TE, Berg HJ, Jbabdi S, Rushworth MF, Woolrich MW. Probabilistic diffusion tractography with multiple fibre orientations: What can we gain?. NeuroImage 2007; 34: 144-155.

Behrens TE, Woolrich MW, Jenkinson M, Johansen-Berg H, Nunes RG, Clare S, et al. Characterization and propagation of uncertainty in diffusion-weighted MR imaging. Magnetic resonance in medicine 2003; 50: 1077-1088.

Belmonte MK, Allen G, Beckel-Mitchener A, Boulanger LM, Carper RA, Webb SJ. Autism and abnormal development of brain connectivity. J. Neurosci 2004; 24: 9228-31.

Benetti S, McCrory E, Arulanantham S, De Sanctis T, McGuire P, Mechelli A. Attachment style, affective loss and gray matter volume: a voxel-based morphometry study. Hum Brain Mapp 2010; 31: 1482-9.

Biederman J, Hirshfeld-Becker DR, Rosenbaum JF, Hérot C, Friedman D, Snidman N, et al. Further evidence of association between behavioral inhibition and social anxiety in children. Am J Psychiatry 2001; 158: 1673-9.

Bishop SJ, Duncan J, Lawrence AD. State anxiety modulation of the amygdala response to unattended threat-related stimuli. The Journal of neuroscience 2004; 24: 10364-10368.

Bishop SJ, Jenkins R, Lawrence AD. Neural processing of fearful faces: effects of anxiety are gated by perceptual capacity limitations. Cerebral cortex (New York, N.Y 2007; 17: 1595-1603.

Blackmon K, Barr WB, Carlson C, Devinsky O, Dubois J, Pogash D, et al. Structural evidence for involvement of a left amygdala-orbitofrontal network in subclinical anxiety. Psychiatry Res 2011; 194: 296-303.

Born RT, Bradley DC. Structure and function of visual area MT. Annu. Rev. Neurosci 2005; 28: 157-89.

Britz J, Landis T, Michel CM. Right parietal brain activity precedes perceptual alternation of bistable stimuli. Cereb. Cortex 2009; 19: 55-65.

Buckner RL, Andrews-Hanna JR, Schacter DL. The brain's default network: anatomy, function, and relevance to disease. Ann. N. Y. Acad. Sci 2008; 1124: 1-38.

Calhoun VD, Adali T, Pearlson GD, Pekar JJ. A method for making group inferences from functional MRI data using independent component analysis. Hum Brain Mapp 2001; 14: 140-51.

Carey PD, Warwick J, Niehaus DJ, van der Linden G, van Heerden BB, Harvey BH, et al. Single photon emission computed tomography (SPECT) of anxiety disorders before and after treatment with citalopram. BMC Psychiatry 2004; 4: 30.

Cassimjee N, Fouche JP, Burnett M, Lochner C, Warwick J, Dupont P, et al. Changes in regional brain volumes in social anxiety disorder following 12 weeks of treatment with escitalopram. Metab Brain Dis 2010; 25: 369-74.

Ceponiene R, Lepistö T, Shestakova A, Vanhala R, Alku P, Näätänen R, et al. Speech-sound-selective auditory impairment in children with autism: they can perceive but do not attend. Proc. Natl. Acad. Sci. U.S.A 2003; 100: 5567-72.

Chadick JZ, Gazzaley A. Differential coupling of visual cortex with default or frontal-parietal network based on goals. Nat. Neurosci 2011; 14: 830-2.

Clark DM, McManus F. Information processing in social phobia. Biological psychiatry 2002; 51: 92-100.

Coplan JD, Lydiard RB. Brain circuits in panic disorder. Biological psychiatry 1998; 44: 1264-1276.

Corbetta M, Shulman GL. Control of goal-directed and stimulus-driven attention in the brain. Nat. Rev. Neurosci 2002; 3: 201-15.

Courchesne E, Pierce K. Why the frontal cortex in autism might be talking only to itself: local over-connectivity but long-distance disconnection. Curr. Opin. Neurobiol 2005; 15: 225-30.

Cox DD, Savoy RL. Functional magnetic resonance imaging (fMRI) "brain reading": detecting and classifying distributed patterns of fMRI activity in human visual cortex. NeuroImage 2003; 19: 261-270.

Cox RW. AFNI: software for analysis and visualization of functional magnetic resonance neuroimages. Computers and biomedical research, an international journal 1996; 29: 162-173.

Craddock RC, Holtzheimer PE, Hu XP, Mayberg HS. Disease state prediction from resting state functional connectivity. Magn Reson Med 2009; 62: 1619-28.

Craddock RC, James GA, Holtzheimer PE, Hu XP, Mayberg HS. A whole brain fMRI atlas generated via spatially constrained spectral clustering. Hum Brain Mapp 2012; 33: 1914-28.

Crum WR, Griffin LD, Hill DL, Hawkes DJ. Zen and the art of medical image registration: correspondence, homology, and quality. Neuroimage 2003; 20: 1425-37.

Damasio H, Grabowski TJ, Tranel D, Hichwa RD, Damasio AR. A neural basis for lexical retrieval. Nature 1996; 380: 499-505.

Damsa C, Kosel M, Moussally J. Current status of brain imaging in anxiety disorders. Current opinion in psychiatry 2009; 22: 96-110.

Das P, Kemp AH, Liddell BJ, Brown KJ, Olivieri G, Peduto A, et al. Pathways for fear perception: modulation of amygdala activity by thalamo-cortical systems. NeuroImage 2005; 26: 141-148.

Davatzikos C. Why voxel-based morphometric analysis should be used with great caution when characterizing group differences. Neuroimage 2004; 23: 17-20.

Davis MH, Coleman MR, Absalom AR, Rodd JM, Johnsrude IS, Matta BF, et al. Dissociating speech perception and comprehension at reduced levels of awareness. Proc. Natl. Acad. Sci. U.S.A 2007; 104: 16032-7.

Delgado MR, Olsson A, Phelps EA. Extending animal models of fear conditioning to humans. Biological psychology 2006; 73: 39-48.

Di Martino A, Kelly C, Grzadzinski R, Zuo XN, Mennes M, Mairena MA, et al. Aberrant striatal functional connectivity in children with autism. Biol. Psychiatry 2011; 69: 847-56.

Di Martino A, Scheres A, Margulies DS, Kelly AM, Uddin LQ, Shehzad Z, et al. Functional Connectivity of Human Striatum: A Resting State fMRI Study. Cerebral cortex (New York, N.Y 2008

Ding J, Chen H, Qiu C, Liao W, Warwick JM, Duan X, et al. Disrupted functional connectivity in social anxiety disorder: a resting-state fMRI study. Magn Reson Imaging 2011; 29: 701-11.

Dodel S, Golestani N, Pallier C, Elkouby V, Le Bihan D, Poline JB. Condition-dependent functional connectivity: syntax networks in bilinguals. Philosophical transactions of the Royal Society of London.Series B, Biological sciences 2005; 360: 921-935.

Doehrmann O, Ghosh SS, Polli FE, Reynolds GO, Horn F, Keshavan A, et al. Predicting Treatment Response in Social Anxiety Disorder From Functional Magnetic Resonance Imaging. Arch. Gen. Psychiatry 2012: 1-11.

Dosenbach NU, Fair DA, Miezin FM, Cohen AL, Wenger KK, Dosenbach RA, et al. Distinct brain networks for adaptive and stable task control in humans. Proc. Natl. Acad. Sci. U.S.A 2007; 104: 11073-8.

Dosenbach NU, Nardos B, Cohen AL, Fair DA, Power JD, Church JA, et al. Prediction of individual brain maturity using fMRI. Science (New York, N.Y.) 2010a; 329: 1358-1361.

Dosenbach NU, Nardos B, Cohen AL, Fair DA, Power JD, Church JA, et al. Prediction of individual brain maturity using fMRI. Science (New York, N.Y.) 2010b; 329: 1358-1361.

Dyck M, Loughead J, Kellermann T, Boers F, Gur RC, Mathiak K. Cognitive versus automatic mechanisms of mood induction differentially activate left and right amygdala. NeuroImage 2011; 54: 2503-2513.

Ekman P, Friesen W. Pictures of Facial Affect. 1976.

Engell AD, Haxby JV. Facial expression and gaze-direction in human superior temporal sulcus. Neuropsychologia 2007; 45: 3234-3241.

Etkin A, Egner T, Peraza DM, Kandel ER, Hirsch J. Resolving emotional conflict: a role for the rostral anterior cingulate cortex in modulating activity in the amygdala. Neuron 2006; 51: 871-882.

Etkin A, Klemenhagen KC, Dudman JT, Rogan MT, Hen R, Kandel ER, et al. Individual differences in trait anxiety predict the response of the basolateral amygdala to unconsciously processed fearful faces. Neuron 2004; 44: 1043-1055.

Etkin A, Wager TD. Functional neuroimaging of anxiety: a meta-analysis of emotional processing in PTSD, social anxiety disorder, and specific phobia. The American Journal of Psychiatry 2007; 164: 1476-1488.

Ewbank MP, Lawrence AD, Passamonti L, Keane J, Peers PV, Calder AJ. Anxiety predicts a differential neural response to attended and unattended facial signals of anger and fear. NeuroImage 2009; 44: 1144-1151.

Fairhall SL, Ishai A. Effective connectivity within the distributed cortical network for face perception. Cerebral cortex (New York, N.Y 2007; 17: 2400-2406.

Faria V, Appel L, Åhs F, Linnman C, Pissiota A, Frans Ö, et al. Amygdala subregions tied to SSRI and placebo response in patients with social anxiety disorder. Neuropsychopharmacology 2012; 37: 2222-32.

Fenske MJ, Aminoff E, Gronau N, Bar M. Top-down facilitation of visual object recognition: object-based and context-based contributions. Progress in brain research 2006a; 155: 3-21.

Fenske MJ, Aminoff E, Gronau N, Bar M. Top-down facilitation of visual object recognition: object-based and context-based contributions. Progress in brain research 2006b; 155: 3-21.

Ferrari MC, Busatto GF, McGuire PK, Crippa JA. Structural magnetic resonance imaging in anxiety disorders: an update of research findings. Rev Bras Psiquiatr 2008; 30: 251-64.

First MB, Spitzer RL, Gibbon M, Williams JBW. Structured clinical interview for DSM-IV clinical version (SCID-I/CV). Washington, American Psychiatric 1997

Fletcher PT, Whitaker RT, Tao R, DuBray MB, Froehlich A, Ravichandran C, et al. Microstructural connectivity of the arcuate fasciculus in adolescents with high-functioning autism. Neuroimage 2010; 51: 1117-25.

Forman SD, Cohen JD, Fitzgerald M, Eddy WF, Mintun MA, Noll DC. Improved assessment of significant activation in functional magnetic resonance imaging (fMRI): use of a cluster-size threshold. Magnetic resonance in medicine 1995; 33: 636-647.

Fox MD, Snyder AZ, Vincent JL, Corbetta M, Van Essen DC, Raichle ME. The human brain is intrinsically organized into dynamic, anticorrelated functional networks. Proc. Natl. Acad. Sci. U.S.A 2005; 102: 9673-8.

Fransson P. How default is the default mode of brain function?: Further evidence from intrinsic BOLD signal fluctuations. Neuropsychologia 2006; 44: 2836-2845.

Freitas-Ferrari MC, Hallak JE, Trzesniak C, Filho AS, Machado-de-Sousa JP, Chagas MH, et al. Neuroimaging in social anxiety disorder: a systematic review of the literature. Prog. Neuropsychopharmacol. Biol. Psychiatry 2010; 34: 565-80.

Friston K. Functional integration and inference in the brain. Progress in neurobiology 2002; 68: 113-143.

Friston KJ, Buechel C, Fink GR, Morris J, Rolls E, Dolan RJ. Psychophysiological and modulatory interactions in neuroimaging. NeuroImage 1997; 6: 218-229.

Friston KJ, Harrison L, Penny W. Dynamic causal modelling. Neuroimage 2003; 19: 1273-302.

Friston KJ. Modalities, modes, and models in functional neuroimaging. Science 2009; 326: 399-403.

Frith U, Frith CD. Development and neurophysiology of mentalizing. Philos. Trans. R. Soc. Lond., B, Biol. Sci 2003; 358: 459-73.

Fu CH, Mourao-Miranda J, Costafreda SG, Khanna A, Marquand AF, Williams SC, et al. Pattern classification of sad facial processing: toward the development of neurobiological markers in depression. Biological psychiatry 2008; 63: 656-662.

Furmark T, Tillfors M, Marteinsdottir I, Fischer H, Pissiota A, Långström B, et al. Common changes in cerebral blood flow in patients with social phobia treated with citalopram or cognitive-behavioral therapy. Arch. Gen. Psychiatry 2002; 59: 425-33.

Fusar-Poli P, Bhattacharyya S, Allen P, Crippa JA, Borgwardt S, Martin-Santos R, et al. Effect of image analysis software on neurofunctional activation during processing of emotional human faces. Journal of clinical neuroscience 2010

Fusar-Poli P, Placentino A, Carletti F, Landi P, Allen P, Surguladze S, et al. Functional atlas of emotional faces processing: a voxel-based meta-analysis of 105 functional magnetic resonance imaging studies. Journal of psychiatry & neuroscience 2009; 34: 418-432.

Gazzaley A, Rissman J, Cooney J, Rutman A, Seibert T, Clapp W, et al. Functional interactions between prefrontal and visual association cortex contribute to top-down modulation of visual processing. Cerebral cortex (New York, N.Y 2007; 17 Suppl 1: i125-35.

Gentili C, Gobbini MI, Ricciardi E, Vanello N, Pietrini P, Haxby JV, et al. Differential modulation of neural activity throughout the distributed neural system for face perception in patients with Social Phobia and healthy subjects. Brain Res. Bull 2008; 77: 286-92.

Ginestet CE, Simmons A. Statistical parametric network analysis of functional connectivity dynamics during a working memory task. NeuroImage 2011; 55: 688-704.

Goense JB, Logothetis NK. Neurophysiology of the BOLD fMRI signal in awake monkeys. Curr. Biol 2008; 18: 631-40.

Goldin PR, Manber T, Hakimi S, Canli T, Gross JJ. Neural bases of social anxiety disorder: emotional reactivity and cognitive regulation during social and physical threat. Archives of General Psychiatry 2009; 66: 170-180.

Goldstein RB, Wickramaratne PJ, Horwath E, Weissman MM. Familial aggregation and phenomenology of 'early'-onset (at or before age 20 years) panic disorder. Arch. Gen. Psychiatry 1997; 54: 271-8.

Golland P, Fischl B. Permutation tests for classification: towards statistical significance in image-based studies. Inf Process Med Imaging 2003; 18: 330-41.

Gordon E, Koslow S. Integrative Neuroscience and Personalized Medicine. 2010.

Gorman JM, Kent JM, Sullivan GM, Coplan JD. Neuroanatomical hypothesis of panic disorder, revised. The American Journal of Psychiatry 2000; 157: 493-505.

Greicius MD, Krasnow B, Reiss AL, Menon V. Functional connectivity in the resting brain: a network analysis of the default mode hypothesis. Proc. Natl. Acad. Sci. U.S.A 2003; 100: 253-8.

Grill-Spector K, Kourtzi Z, Kanwisher N. The lateral occipital complex and its role in object recognition. Vision Res 2001; 41: 1409-22.

Groen WB, Zwiers MP, van der Gaag RJ, Buitelaar JK. The phenotype and neural correlates of language in autism: an integrative review. Neurosci Biobehav Rev 2008; 32: 1416-25.

Grossberg S. How does a brain build a cognitive code?. Psychological review 1980; 87: 1-51.

Gusnard DA, Raichle ME, Raichle ME. Searching for a baseline: functional imaging and the resting human brain. Nat. Rev. Neurosci 2001; 2: 685-94.

Haas BW, Constable RT, Canli T. Functional magnetic resonance imaging of temporally distinct responses to emotional facial expressions. Social neuroscience 2009; 4: 121-134.

Habeck C, Krakauer JW, Ghez C, Sackeim HA, Eidelberg D, Stern Y, et al. A new approach to spatial covariance modeling of functional brain imaging data: ordinal trend analysis. Neural computation 2005; 17: 1602-1645.

Hahn A, Stein P, Windischberger C, Weissenbacher A, Spindelegger C, Moser E, et al. Reduced resting-state functional connectivity between amygdala and orbitofrontal cortex in social anxiety disorder. Neuroimage 2011; 56: 881-9.

Hahn B, Ross TJ, Stein EA. Neuroanatomical dissociation between bottom-up and top-down processes of visuospatial selective attention. NeuroImage 2006; 32: 842-853.

Hanson SJ, Matsuka T, Haxby JV. Combinatorial codes in ventral temporal lobe for object recognition: Haxby (2001) revisited: is there a "face" area?. NeuroImage 2004; 23: 156-166.

Harms MB, Martin A, Wallace GL. Facial emotion recognition in autism spectrum disorders: a review of behavioral and neuroimaging studies. Neuropsychology review 2010; 20: 290-322.

Harris GJ, Chabris CF, Clark J, Urban T, Aharon I, Steele S, et al. Brain activation during semantic processing in autism spectrum disorders via functional magnetic resonance imaging. Brain Cogn 2006; 61: 54-68.

Haxby JV, Gobbini MI, Furey ML, Ishai A, Schouten JL, Pietrini P. Distributed and overlapping representations of faces and objects in ventral temporal cortex. Science (New York, N.Y.) 2001; 293: 2425-2430.

Haxby JV, Hoffman EA, Gobbini MI. The distributed human neural system for face perception. Trends in cognitive sciences 2000; 4: 223-233.

Haxby JV, Hoffman EA, Gobbini MI. Human neural systems for face recognition and social communication. Biological psychiatry 2002; 51: 59-67.

Hayasaka S, Phan KL, Liberzon I, Worsley KJ, Nichols TE. Nonstationary cluster-size inference with random field and permutation methods. Neuroimage 2004; 22: 676-87.

Haynes JD, Rees G. Predicting the orientation of invisible stimuli from activity in human primary visual cortex. Nature neuroscience 2005; 8: 686-691.

Henley SM, Ridgway GR, Scahill RI, Klöppel S, Tabrizi SJ, Fox NC, et al. Pitfalls in the use of voxel-based morphometry as a biomarker: examples from huntington disease. AJNR Am J Neuroradiol 2010; 31: 711-9.

Hirsch J, Ruge MI, Kim KH, Correa DD, Victor JD, Relkin NR, et al. An integrated functional magnetic resonance imaging procedure for preoperative mapping of cortical areas associated

with tactile, motor, language, and visual functions. Neurosurgery 2000; 47: 711-21; discussion 721-2.

Horwitz B, Tagamets MA, McIntosh AR. Neural modeling, functional brain imaging, and cognition. Trends Cogn. Sci. (Regul. Ed.) 1999; 3: 91-98.

Ioannidis JP. Excess significance bias in the literature on brain volume abnormalities. Arch. Gen. Psychiatry 2011; 68: 773-80.

Ishai A, Schmidt CF, Boesiger P. Face perception is mediated by a distributed cortical network. Brain research bulletin 2005; 67: 87-93.

Ishai A, Ungerleider LG, Martin A, Haxby JV. The representation of objects in the human occipital and temporal cortex. Journal of cognitive neuroscience 2000; 12 Suppl 2: 35-51.

Ishai A. Let's face it: it's a cortical network. NeuroImage 2008; 40: 415-419.

Jefferys D. Social phobia. The most common anxiety disorder. Australian Family Physician 1997; 26: 1061,-1064.

Jenkinson M, Smith S. A global optimisation method for robust affine registration of brain images. Medical image analysis 2001; 5: 143-156.

Jimura K, Konishi S, Asari T, Miyashita Y. Temporal pole activity during understanding other persons' mental states correlates with neuroticism trait. Brain Res 2010; 1328: 104-12.

Just MA, Cherkassky VL, Keller TA, Minshew NJ. Cortical activation and synchronization during sentence comprehension in high-functioning autism: evidence of underconnectivity. Brain 2004; 127: 1811-21.

Järvinen-Pasley A, Heaton P. Evidence for reduced domain-specificity in auditory processing in autism. Dev Sci 2007; 10: 786-93.

Kahn I, Andrews-Hanna JR, Vincent JL, Snyder AZ, Buckner RL. Distinct cortical anatomy linked to subregions of the medial temporal lobe revealed by intrinsic functional connectivity. J. Neurophysiol 2008; 100: 129-39.

Kamitani Y, Tong F. Decoding the visual and subjective contents of the human brain. Nature neuroscience 2005; 8: 679-685.

Kana RK, Keller TA, Cherkassky VL, Minshew NJ, Just MA. Sentence comprehension in autism: thinking in pictures with decreased functional connectivity. Brain 2006; 129: 2484-93.

Karama S, Armony J, Beauregard M. Film excerpts shown to specifically elicit various affects lead to overlapping activation foci in a large set of symmetrical brain regions in males. PloS one 2011; 6: e22343.

Karten A, Pantazatos S, Khalil D, Zhang X, Hirsch J. Dynamic Coupling between the Lateral Occipital Cortex, Default Mode and Frontoparietal Networks During Bistable Perception. Brain Connect 2013

Kastner S, Ungerleider LG. Mechanisms of visual attention in the human cortex. Annu. Rev. Neurosci 2000; 23: 315-41.

Kelly AM, Uddin LQ, Biswal BB, Castellanos FX, Milham MP. Competition between functional brain networks mediates behavioral variability. Neuroimage 2008; 39: 527-37.

Kendler KS, Walters EE, Neale MC, Kessler RC, Heath AC, Eaves LJ. The structure of the genetic and environmental risk factors for six major psychiatric disorders in women. Phobia, generalized anxiety disorder, panic disorder, bulimia, major depression, and alcoholism. Arch. Gen. Psychiatry 1995; 52: 374-83.

Kennedy DP, Courchesne E. The intrinsic functional organization of the brain is altered in autism. NeuroImage 2008; 39: 1877-1885.

Kent JM, Rauch SL. Neurocircuitry of anxiety disorders. Current psychiatry reports 2003; 5: 266-273.

Kessler RC, Berglund P, Demler O, Jin R, Merikangas KR, Walters EE. Lifetime prevalence and age-of-onset distributions of DSM-IV disorders in the National Comorbidity Survey Replication. Archives of General Psychiatry 2005; 62: 593-602.

Kessler RC, McGonagle KA, Zhao S, Nelson CB, Hughes M, Eshleman S, et al. Lifetime and 12-month prevalence of DSM-III-R psychiatric disorders in the United States. Results from the National Comorbidity Survey. Archives of General Psychiatry 1994; 51: 8-19.

Kilts CD, Kelsey JE, Knight B, Ely TD, Bowman FD, Gross RE, et al. The neural correlates of social anxiety disorder and response to pharmacotherapy. Neuropsychopharmacology 2006; 31: 2243-53.

Kim J, Horwitz B. Investigating the neural basis for fMRI-based functional connectivity in a blocked design: application to interregional correlations and psycho-physiological interactions. Magnetic resonance imaging 2008; 26: 583-593.

Kiss M, Eimer M. ERPs reveal subliminal processing of fearful faces. Psychophysiology 2008; 45: 318-326.

Kleinschmidt A, Büchel C, Zeki S, Frackowiak RS. Human brain activity during spontaneously reversing perception of ambiguous figures. Proc. Biol. Sci 1998; 265: 2427-33.

Klumpp H, Angstadt M, Nathan PJ, Phan KL. Amygdala reactivity to faces at varying intensities of threat in generalized social phobia: an event-related functional MRI study. Psychiatry Res 2010; 183: 167-9.

Klumpp H, Angstadt M, Phan KL. Insula reactivity and connectivity to anterior cingulate cortex when processing threat in generalized social anxiety disorder. Biol Psychol 2012; 89: 273-6.

Knapen T, Brascamp J, Pearson J, van Ee R, Blake R. The role of frontal and parietal brain areas in bistable perception. J. Neurosci 2011; 31: 10293-301.

Kober H, Barrett LF, Joseph J, Bliss-Moreau E, Lindquist K, Wager TD. Functional grouping and cortical-subcortical interactions in emotion: a meta-analysis of neuroimaging studies. NeuroImage 2008; 42: 998-1031.

Koelsch S, Gunter TC, v Cramon DY, Zysset S, Lohmann G, Friederici AD. Bach speaks: a cortical "language-network" serves the processing of music. Neuroimage 2002; 17: 956-66.

Kogan MD, Blumberg SJ, Schieve LA, Boyle CA, Perrin JM, Ghandour RM, et al. Prevalence of parent-reported diagnosis of autism spectrum disorder among children in the US, 2007. Pediatrics 2009; 124: 1395-403.

Kouider S, Eger E, Dolan R, Henson RN. Activity in face-responsive brain regions is modulated by invisible, attended faces: evidence from masked priming. Cerebral cortex (New York, N.Y 2009; 19: 13-23.

Kriegeskorte N, Goebel R, Bandettini P. Information-based functional brain mapping. Proc. Natl. Acad. Sci. U.S.A 2006; 103: 3863-8.

Krishnan A, Williams LJ, McIntosh AR, Abdi H. Partial Least Squares (PLS) methods for neuroimaging: a tutorial and review. Neuroimage 2011; 56: 455-75.

Lai CH. Gray matter deficits in panic disorder: a pilot study of meta-analysis. J Clin Psychopharmacol 2011; 31: 287-93.

Lai G, Pantazatos SP, Schneider H, Hirsch J. Neural systems for speech and song in autism. Brain 2012; 135: 961-75.

Lai G, Schneider HD, Schwarzenberger JC, Hirsch J. Speech stimulation during functional MR imaging as a potential indicator of autism. Radiology 2011; 260: 521-30.

Lampe L, Slade T, Issakidis C, Andrews G. Social phobia in the Australian National Survey of Mental Health and Well-Being (NSMHWB). Psychological medicine 2003; 33: 637-646.

Lawrence NS, Ross TJ, Hoffmann R, Garavan H, Stein EA. Multiple neuronal networks mediate sustained attention. Journal of cognitive neuroscience 2003; 15: 1028-1038.

Leckman JF, Sholomskas D, Thompson WD, Belanger A, Weissman MM. Best estimate of lifetime psychiatric diagnosis: a methodological study. Arch. Gen. Psychiatry 1982; 39: 879-83.

Lee TS, Mumford D. Hierarchical Bayesian inference in the visual cortex. Journal of the Optical Society of America.A, Optics, image science, and vision 2003; 20: 1434-1448.

Leopold DA, Logothetis NK. Multistable phenomena: changing views in perception. Trends Cogn. Sci. (Regul. Ed.) 1999; 3: 254-264.

Li K, Guo L, Nie J, Li G, Liu T. Review of methods for functional brain connectivity detection using fMRI. Computerized medical imaging and graphics 2009; 33: 131-139.

Li YO, Adali T, Calhoun VD. Estimating the number of independent components for functional magnetic resonance imaging data. Human brain mapping 2007; 28: 1251-1266.

Liao W, Xu Q, Mantini D, Ding J, Machado-de-Sousa JP, Hallak JE, et al. Altered gray matter morphometry and resting-state functional and structural connectivity in social anxiety disorder. Brain Res 2011; 1388: 167-77.

Liddell BJ, Brown KJ, Kemp AH, Barton MJ, Das P, Peduto A, et al. A direct brainstem-amygdala-cortical 'alarm' system for subliminal signals of fear. NeuroImage 2005; 24: 235-243.

Liebowitz MR. Social phobia. Modern problems of pharmacopsychiatry 1987

Limb CJ. Structural and functional neural correlates of music perception. Anat Rec A Discov Mol Cell Evol Biol 2006; 288: 435-46.

Liu W, Miller BL, Kramer JH, Rankin K, Wyss-Coray C, Gearhart R, et al. Behavioral disorders in the frontal and temporal variants of frontotemporal dementia. Neurology 2004; 62: 742-8.

Lochner C, Mogotsi M, du Toit PL, Kaminer D, Niehaus DJ, Stein DJ. Quality of life in anxiety disorders: a comparison of obsessive-compulsive disorder, social anxiety disorder, and panic disorder. Psychopathology 2003; 36: 255-262.

Lohmann G, Erfurth K, Müller K, Turner R. Critical comments on dynamic causal modelling. Neuroimage 2012; 59: 2322-9.

Lorberbaum JP, Kose S, Johnson MR, Arana GW, Sullivan LK, Hamner MB, et al. Neural correlates of speech anticipatory anxiety in generalized social phobia. Neuroreport 2004; 15: 2701-5.

Machado-de-Sousa JP, Arrais KC, Alves NT, Chagas MH, de Meneses-Gaya C, Crippa JA, et al. Facial affect processing in social anxiety: tasks and stimuli. Journal of neuroscience methods 2010; 193: 1-6.

Malach R, Reppas JB, Benson RR, Kwong KK, Jiang H, Kennedy WA, et al. Object-related activity revealed by functional magnetic resonance imaging in human occipital cortex. Proc. Natl. Acad. Sci. U.S.A 1995; 92: 8135-9.

Marreiros AC, Kiebel SJ, Friston KJ. Dynamic causal modelling for fMRI: a two-state model. NeuroImage 2008; 39: 269-278.

Massana G, Serra-Grabulosa JM, Salgado-Pineda P, Gastó C, Junqué C, Massana J, et al. Parahippocampal gray matter density in panic disorder: a voxel-based morphometric study. Am J Psychiatry 2003; 160: 566-8.

McKeown MJ, Sejnowski TJ. Independent component analysis of fMRI data: examining the assumptions. Human brain mapping 1998; 6: 368-372.

Mechelli A, Price CJ, Friston KJ, Ishai A. Where bottom-up meets top-down: neuronal interactions during perception and imagery. Cerebral cortex (New York, N.Y 2004; 14: 1256-1265.

Meda SA, Pryweller JR, Thornton-Wells TA. Regional brain differences in cortical thickness, surface area and subcortical volume in individuals with Williams syndrome. PLoS ONE 2012; 7: e31913.

Meng M, Tong F. Can attention selectively bias bistable perception? Differences between binocular rivalry and ambiguous figures. J Vis 2004; 4: 539-51.

Mikl M, Marecek R, Hlustík P, Pavlicová M, Drastich A, Chlebus P, et al. Effects of spatial smoothing on fMRI group inferences. Magn Reson Imaging 2008; 26: 490-503.

Milad MR, Rauch SL. The role of the orbitofrontal cortex in anxiety disorders. Ann. N. Y. Acad. Sci 2007; 1121: 546-61.

Minshew NJ, Williams DL. The new neurobiology of autism: cortex, connectivity, and neuronal organization. Arch. Neurol 2007; 64: 945-50.

Mohlman J, Carmin CN, Price RB. Jumping to interpretations: social anxiety disorder and the identification of emotional facial expressions. Behaviour research and therapy 2007; 45: 591-599.

Monk CS, Telzer EH, Mogg K, Bradley BP, Mai X, Louro HM, et al. Amygdala and ventrolateral prefrontal cortex activation to masked angry faces in children and adolescents with generalized anxiety disorder. Arch. Gen. Psychiatry 2008; 65: 568-76.

Monti MM. Statistical Analysis of fMRI Time-Series: A Critical Review of the GLM Approach. Front Hum Neurosci 2011; 5: 28.

Morris JS, Ohman A, Dolan RJ. A subcortical pathway to the right amygdala mediating "unseen" fear. Proceedings of the National Academy of Sciences of the United States of America 1999; 96: 1680-1685.

Mottron L, Peretz I, Ménard E. Local and global processing of music in high-functioning persons with autism: beyond central coherence?. J Child Psychol Psychiatry 2000; 41: 1057-65.

Mourao-Miranda J, Bokde AL, Born C, Hampel H, Stetter M. Classifying brain states and determining the discriminating activation patterns: Support Vector Machine on functional MRI data. NeuroImage 2005; 28: 980-995.

Mumford D. On the computational architecture of the neocortex. II. The role of cortico-cortical loops. Biological cybernetics 1992; 66: 241-251.

Newcombe RG. Two-sided confidence intervals for the single proportion: comparison of seven methods. Stat Med 1998; 17: 857-72.

Norman KA, Polyn SM, Detre GJ, Haxby JV. Beyond mind-reading: multi-voxel pattern analysis of fMRI data. Trends in cognitive sciences 2006; 10: 424-430.

O'Reilly JX, Woolrich MW, Behrens TE, Smith SM, Johansen-Berg H. Tools of the Trade: Psychophysiological Interactions and Functional Connectivity. Social cognitive and affective neuroscience 2012

O'Toole AJ, Jiang F, Abdi H, Haxby JV. Partially distributed representations of objects and faces in ventral temporal cortex. Journal of cognitive neuroscience 2005; 17: 580-590.

Ohrmann P, Pedersen A, Braun M, Bauer J, Kugel H, Kersting A, et al. Effect of gender on processing threat-related stimuli in patients with panic disorder: sex does matter. Depression and anxiety 2010; 27: 1034-1043.

Olson IR, Plotzker A, Ezzyat Y. The Enigmatic temporal pole: a review of findings on social and emotional processing. Brain 2007; 130: 1718-31.

Otto MW, Pollack MH, Maki KM, Gould RA, Worthington 3JJ,, Smoller JW, et al. Childhood history of anxiety disorders among adults with social phobia: rates, correlates, and comparisons with patients with panic disorder. Depression and anxiety 2001; 14: 209-213.

Pantazatos SP, Talati A, Pavlidis P, Hirsch J. Decoding unattended fearful faces with whole-brain correlations: an approach to identify condition-dependent large-scale functional connectivity. PLoS Comput. Biol 2012a; 8: e1002441.

Pantazatos SP, Talati A, Pavlidis P, Hirsch J. Cortical functional connectivity decodes subconscious, task-irrelevant threat-related emotion processing. NeuroImage 2012b; 61: 1355-1363.

Pantazatos SP, Talati A, Schneier FR, Hirsch J. Reduced Anterior Temporal and Hippocampal Functional Connectivity During Face Processing Discriminates Individuals with Social Anxiety Disorder from Healthy Controls and Panic Disorder, and Increases Following Treatment. Neuropsychopharmacology 2013

Pantazatos SP, Yanagihara TK, Zhang X, Meitzler T, Hirsch J. Frontal-occipital connectivity during visual search. Brain Connect 2012; 2: 164-75.

Patel AD. Why would Musical Training Benefit the Neural Encoding of Speech? The OPERA Hypothesis. Front Psychol 2011; 2: 142.

Peelen MV, Atkinson AP, Vuilleumier P. Supramodal representations of perceived emotions in the human brain. The Journal of neuroscience 2010; 30: 10127-10134.

Peelen MV, Kastner S. A neural basis for real-world visual search in human occipitotemporal cortex. Proc. Natl. Acad. Sci. U.S.A 2011; 108: 12125-30.

Pegna AJ, Darque A, Berrut C, Khateb A. Early ERP Modulation for Task-Irrelevant Subliminal Faces. Frontiers in psychology 2011; 2: 88.

Penny WD, Stephan KE, Mechelli A, Friston KJ. Modelling functional integration: a comparison of structural equation and dynamic causal models. Neuroimage 2004; 23 Suppl 1: S264-74.

Pessoa L, Adolphs R. Emotion processing and the amygdala: from a 'low road' to 'many roads' of evaluating biological significance. Nature reviews.Neuroscience 2010; 11: 773-783.

Pessoa L, Adolphs R. Emotion and the brain: multiple roads are better than one. Nature reviews.Neuroscience 2011; 12: 425-c2.

Pessoa L, Kastner S, Ungerleider LG. Attentional control of the processing of neural and emotional stimuli. Brain research.Cognitive brain research 2002; 15: 31-45.

Pessoa L, Padmala S. Decoding near-threshold perception of fear from distributed single-trial brain activation. Cerebral cortex (New York, N.Y 2007; 17: 691-701.

Pessoa L. To what extent are emotional visual stimuli processed without attention and awareness?. Current opinion in neurobiology 2005; 15: 188-196.

Pezawas L, Meyer-Lindenberg A, Drabant EM, Verchinski BA, Munoz KE, Kolachana BS, et al. 5-HTTLPR polymorphism impacts human cingulate-amygdala interactions: a genetic susceptibility mechanism for depression. Nature neuroscience 2005; 8: 828-834.

Phan KL, Coccaro EF, Angstadt M, Kreger KJ, Mayberg HS, Liberzon I, et al. Corticolimbic brain reactivity to social signals of threat before and after sertraline treatment in generalized social phobia. Biol. Psychiatry 2013; 73: 329-36.

Pietrini F, Godini L, Lazzeretti L, Benni L, Pracucci C, Talamba GA, et al. [Neuroimaging and neurobiology of social anxiety]. Riv Psichiatr 2010; 45: 349-60.

Ploran EJ, Nelson SM, Velanova K, Donaldson DI, Petersen SE, Wheeler ME. Evidence accumulation and the moment of recognition: dissociating perceptual recognition processes using fMRI. The Journal of neuroscience 2007; 27: 11912-11924.

Polosan M, Baciu M, Cousin E, Perrone M, Pichat C, Bougerol T. An fMRI study of the social competition in healthy subjects. Brain Cogn 2011; 77: 401-11.

Potts NL, Davidson JR, Krishnan KR, Doraiswamy PM. Magnetic resonance imaging in social phobia. Psychiatry Res 1994; 52: 35-42.

Prater KE, Hosanagar A, Klumpp H, Angstadt M, Phan KL. ABERRANT AMYGDALA-FRONTAL CORTEX CONNECTIVITY DURING PERCEPTION OF FEARFUL FACES AND AT REST IN GENERALIZED SOCIAL ANXIETY DISORDER. Depress Anxiety 2012

Psychiatric Association American. Diagnostic and statistical manual of psychiatric disorders. Washington, DC 1994

Qi R, Zhang LJ, Zhong J, Zhang Z, Ni L, Zheng G, et al. Disrupted thalamic resting-state functional connectivity in patients with minimal hepatic encephalopathy. European journal of radiology 2013

Radua J, van den Heuvel OA, Surguladze S, Mataix-Cols D. Meta-analytical comparison of voxel-based morphometry studies in obsessive-compulsive disorder vs other anxiety disorders. Arch. Gen. Psychiatry 2010; 67: 701-11.

Raichle ME, MacLeod AM, Snyder AZ, Powers WJ, Gusnard DA, Shulman GL. A default mode of brain function. Proc. Natl. Acad. Sci. U.S.A 2001; 98: 676-82.

Randall CL, Thomas S, Thevos AK. Concurrent alcoholism and social anxiety disorder: a first step toward developing effective treatments. Alcoholism, Clinical and Experimental Research 2001; 25: 210-220.

Rapee RM, Heimberg RG. A cognitive-behavioral model of anxiety in social phobia. Behaviour research and therapy 1997; 35: 741-756.

Rauch SL, Shin LM, Wright CI. Neuroimaging studies of amygdala function in anxiety disorders. Ann. N. Y. Acad. Sci 2003; 985: 389-410.

Reiss AL, Eckert MA, Rose FE, Karchemskiy A, Kesler S, Chang M, et al. An experiment of nature: brain anatomy parallels cognition and behavior in Williams syndrome. J. Neurosci 2004; 24: 5009-15.

Richiardi J, Eryilmaz H, Schwartz S, Vuilleumier P, Van De Ville D. Decoding brain states from fMRI connectivity graphs. NeuroImage 2011; 56: 616-626.

Roebroeck A, Formisano E, Goebel R. Mapping directed influence over the brain using Granger causality and fMRI. Neuroimage 2005; 25: 230-42.

Rosen AC, Rao SM, Caffarra P, Scaglioni A, Bobholz JA, Woodley SJ, et al. Neural basis of endogenous and exogenous spatial orienting. A functional MRI study. Journal of cognitive neuroscience 1999; 11: 135-152.

Ross TD. Accurate confidence intervals for binomial proportion and Poisson rate estimation. Comput. Biol. Med 2003; 33: 509-31.

Roy-Byrne PP, Craske MG, Stein MB. Panic disorder. Lancet 2006; 368: 1023-32.

Sabatinelli D, Bradley MM, Fitzsimmons JR, Lang PJ. Parallel amygdala and inferotemporal activation reflect emotional intensity and fear relevance. NeuroImage 2005; 24: 1265-1270.

Sabatinelli D, Fortune EE, Li Q, Siddiqui A, Krafft C, Oliver WT, et al. Emotional perception: meta-analyses of face and natural scene processing. NeuroImage 2011; 54: 2524-2533.

Safren SA, Heimberg RG, Horner KJ, Juster HR, Schneier FR, Liebowitz MR. Factor structure of social fears: The Liebowitz Social Anxiety Scale. J Anxiety Disord 1999; 13: 253-70.

Sahyoun CP, Belliveau JW, Soulières I, Schwartz S, Mody M. Neuroimaging of the functional and structural networks underlying visuospatial vs. linguistic reasoning in high-functioning autism. Neuropsychologia 2010; 48: 86-95.

Said CP, Moore CD, Engell AD, Todorov A, Haxby JV. Distributed representations of dynamic facial expressions in the superior temporal sulcus. Journal of vision 2010; 10: 11.

Schmidt S, Mohr A, Miltner WH, Straube T. Task-dependent neural correlates of the processing of verbal threat-related stimuli in social phobia. Biol Psychol 2010; 84: 304-12.

Schneier FR, Heckelman LR, Garfinkel R, Campeas R, Fallon BA, Gitow A, et al. Functional impairment in social phobia. The Journal of clinical psychiatry 1994; 55: 322-331.

Schneier FR, Johnson J, Hornig CD, Liebowitz MR, Weissman MM. Social phobia. Comorbidity and morbidity in an epidemiologic sample. Arch. Gen. Psychiatry 1992; 49: 282-8.

Schneier FR, Kent JM, Star A, Hirsch J. Neural circuitry of submissive behavior in social anxiety disorder: A preliminary study of response to direct eye gaze. Psychiatry Res 2009; 173: 248-50.

Schneier FR, Pomplun M, Sy M, Hirsch J. Neural response to eye contact and paroxetine treatment in generalized social anxiety disorder. Psychiatry Res 2011; 194: 271-8.

Schwartz CE, Kunwar PS, Greve DN, Moran LR, Viner JC, Covino JM, et al. Structural differences in adult orbital and ventromedial prefrontal cortex predicted by infant temperament at 4 months of age. Arch. Gen. Psychiatry 2010; 67: 78-84.

Schwartz CE, Snidman N, Kagan J. Adolescent social anxiety as an outcome of inhibited temperament in childhood. J Am Acad Child Adolesc Psychiatry 1999; 38: 1008-15.

Schön D, Gordon R, Campagne A, Magne C, Astésano C, Anton JL, et al. Similar cerebral networks in language, music and song perception. Neuroimage 2010; 51: 450-61.

Seeley WW, Menon V, Schatzberg AF, Keller J, Glover GH, Kenna H, et al. Dissociable intrinsic connectivity networks for salience processing and executive control. The Journal of neuroscience 2007; 27: 2349-2356.

Shirer WR, Ryali S, Rykhlevskaia E, Menon V, Greicius MD. Decoding Subject-Driven Cognitive States with Whole-Brain Connectivity Patterns. Cerebral cortex (New York, N.Y 2011

Shmuel A, Yacoub E, Pfeuffer J, Van de Moortele PF, Adriany G, Hu X, et al. Sustained negative BOLD, blood flow and oxygen consumption response and its coupling to the positive response in the human brain. Neuron 2002; 36: 1195-210.

Slotnick SD, Yantis S. Common neural substrates for the control and effects of visual attention and perceptual bistability. Brain Res Cogn Brain Res 2005; 24: 97-108.

Smith SM, Jenkinson M, Woolrich MW, Beckmann CF, Behrens TE, Johansen-Berg H, et al. Advances in functional and structural MR image analysis and implementation as FSL. NeuroImage 2004; 23 Suppl 1: S208-19.

Smith SM, Miller KL, Salimi-Khorshidi G, Webster M, Beckmann CF, Nichols TE, et al. Network modelling methods for FMRI. NeuroImage 2011; 54: 875-891.

Souweidane MM, Kim KH, McDowall R, Ruge MI, Lis E, Krol G, et al. Brain mapping in sedated infants and young children with passive-functional magnetic resonance imaging. Pediatr Neurosurg 1999; 30: 86-92.

Spielberger CD, Gorsuch RL, Lushene R, Vagg PR. Consulting Psychologists Press, Inc. 2». Palo Alto (CA 1983

Spiridon M, Fischl B, Kanwisher N. Location and spatial profile of category-specific regions in human extrastriate cortex. Human brain mapping 2006; 27: 77-89.

Spreng RN, Mar RA. I remember you: A role for memory in social cognition and the functional neuroanatomy of their interaction. Brain research 2010

Spreng RN, Stevens WD, Chamberlain JP, Gilmore AW, Schacter DL. Default network activity, coupled with the frontoparietal control network, supports goal-directed cognition. Neuroimage 2010; 53: 303-17.

Spreng RN. The fallacy of a "task-negative" network. Front Psychol 2012; 3: 145.

Stein JL, Wiedholz LM, Bassett DS, Weinberger DR, Zink CF, Mattay VS, et al. A validated network of effective amygdala connectivity. NeuroImage 2007; 36: 736-745.

Stein T, Moritz C, Quigley M, Cordes D, Haughton V, Meyerand E. Functional connectivity in the thalamus and hippocampus studied with functional MR imaging. AJNR.American journal of neuroradiology 2000; 21: 1397-1401.

Stephan KE, Penny WD, Moran RJ, den Ouden HE, Daunizeau J, Friston KJ. Ten simple rules for dynamic causal modeling. NeuroImage 2010; 49: 3099-3109.

Sterzer P, Kleinschmidt A, Rees G. The neural bases of multistable perception. Trends Cogn. Sci. (Regul. Ed.) 2009; 13: 310-8.

Stoodley CJ, Schmahmann JD. Evidence for topographic organization in the cerebellum of motor control versus cognitive and affective processing. Cortex; a journal devoted to the study of the nervous system and behavior 2010; 46: 831-844.

Straube T, Kolassa IT, Glauer M, Mentzel HJ, Miltner WH. Effect of task conditions on brain responses to threatening faces in social phobics: an event-related functional magnetic resonance imaging study. Biol. Psychiatry 2004; 56: 921-30.

Summerfield C, Egner T, Greene M, Koechlin E, Mangels J, Hirsch J. Predictive codes for forthcoming perception in the frontal cortex. Science (New York, N.Y.) 2006; 314: 1311-1314.

Talati A, Pantazatos SP, Schneier FR, Weissman MM, Hirsch J. Gray matter abnormalities in social anxiety disorder: primary, replication, and specificity studies. Biol. Psychiatry 2013; 73: 75-84.

Talati A, Ponniah K, Strug LJ, Hodge SE, Fyer AJ, Weissman MM. Panic disorder, social anxiety disorder, and a possible medical syndrome previously linked to chromosome 13. Biol. Psychiatry 2008; 63: 594-601.

Tamietto M, de Gelder B. Neural bases of the non-conscious perception of emotional signals. Nature reviews.Neuroscience 2010; 11: 697-709.

Tillfors M, Furmark T, Marteinsdottir I, Fischer H, Pissiota A, Långström B, et al. Cerebral blood flow in subjects with social phobia during stressful speaking tasks: a PET study. Am J Psychiatry 2001; 158: 1220-6.

Tillfors M, Furmark T, Marteinsdottir I, Fredrikson M. Cerebral blood flow during anticipation of public speaking in social phobia: a PET study. Biol. Psychiatry 2002; 52: 1113-9.

Toppino TC, Long GM. Selective adaptation with reversible figures: don't change that channel. Percept Psychophys 1987; 42: 37-48.

Tsuchiya N, Kawasaki H, Oya H, Howard 3MA,, Adolphs R. Decoding face information in time, frequency and space from direct intracranial recordings of the human brain. PloS one 2008; 3: e3892.

Tsukiura T, Mano Y, Sekiguchi A, Yomogida Y, Hoshi K, Kambara T, et al. Dissociable roles of the anterior temporal regions in successful encoding of memory for person identity information. J Cogn Neurosci 2010; 22: 2226-37.

Turk-Browne NB. Functional interactions as big data in the human brain. Science 2013; 342: 580-4.

Turner R, Howseman A, Rees GE, Josephs O, Friston K. Functional magnetic resonance imaging of the human brain: data acquisition and analysis. Exp Brain Res 1998; 123: 5-12.

Uchida RR, Del-Ben CM, Busatto GF, Duran FL, Guimarães FS, Crippa JA, et al. Regional gray matter abnormalities in panic disorder: a voxel-based morphometry study. Psychiatry Res 2008; 163: 21-9.

Uddin LQ, Kelly AM, Biswal BB, Castellanos FX, Milham MP. Functional connectivity of default mode network components: correlation, anticorrelation, and causality. Hum Brain Mapp 2009; 30: 625-37.

Ugurbil K, Xu J, Auerbach EJ, Moeller S, Vu AT, Duarte-Carvajalino JM, et al. Pushing spatial and temporal resolution for functional and diffusion MRI in the Human Connectome Project. Neuroimage 2013

Umarova RM, Saur D, Schnell S, Kaller CP, Vry MS, Glauche V, et al. Structural connectivity for visuospatial attention: significance of ventral pathways. Cereb. Cortex 2010; 20: 121-9.

Van der Linden G, van Heerden B, Warwick J, Wessels C, van Kradenburg J, Zungu-Dirwayi N, et al. Functional brain imaging and pharmacotherapy in social phobia: single photon emission computed tomography before and after treatment with the selective serotonin reuptake inhibitor citalopram. Prog. Neuropsychopharmacol. Biol. Psychiatry 2000; 24: 419-38.

Vapnik VN. An overview of statistical learning theory. IEEE transactions on neural networks / a publication of the IEEE Neural Networks Council 1999; 10: 988-999.

Veit R, Flor H, Erb M, Hermann C, Lotze M, Grodd W, et al. Brain circuits involved in emotional learning in antisocial behavior and social phobia in humans. Neurosci. Lett 2002; 328: 233-6.

Vuilleumier P, Armony JL, Clarke K, Husain M, Driver J, Dolan RJ. Neural response to emotional faces with and without awareness: event-related fMRI in a parietal patient with visual extinction and spatial neglect. Neuropsychologia 2002; 40: 2156-2166.

Vuilleumier P, Pourtois G. Distributed and interactive brain mechanisms during emotion face perception: evidence from functional neuroimaging. Neuropsychologia 2007; 45: 174-194.

Vuilleumier P, Richardson MP, Armony JL, Driver J, Dolan RJ. Distant influences of amygdala lesion on visual cortical activation during emotional face processing. Nature neuroscience 2004; 7: 1271-1278.

Wade AR. The negative BOLD signal unmasked. Neuron 2002; 36: 993-5.

Warwick JM, Carey P, Jordaan GP, Dupont P, Stein DJ. Resting brain perfusion in social anxiety disorder: a voxel-wise whole brain comparison with healthy control subjects. Prog. Neuropsychopharmacol. Biol. Psychiatry 2008; 32: 1251-6.

Weissman MM, Brown AS, Talati A. Translational epidemiology in psychiatry: linking population to clinical and basic sciences. Arch. Gen. Psychiatry 2011; 68: 600-8.

Weissman MM, Wickramaratne P, Adams P, Wolk S, Verdeli H, Olfson M. Brief screening for family psychiatric history: the family history screen. Arch. Gen. Psychiatry 2000; 57: 675-82.

Weissman MM. Family genetic studies of panic disorder. J Psychiatr Res 1993; 27 Suppl 1: 69-78.

Whitfield-Gabrieli S, Moran JM, Nieto-Castañón A, Triantafyllou C, Saxe R, Gabrieli JD. Associations and dissociations between default and self-reference networks in the human brain. Neuroimage 2011; 55: 225-32.

Williams LM, Liddell BJ, Kemp AH, Bryant RA, Meares RA, Peduto AS, et al. Amygdala-prefrontal dissociation of subliminal and supraliminal fear. Human brain mapping 2006; 27: 652-661.

Winton EC, Clark DM, Edelmann RJ. Social anxiety, fear of negative evaluation and the detection of negative emotion in others. Behav Res Ther 1995; 33: 193-6.

Wong C, Gallate J. The function of the anterior temporal lobe: a review of the empirical evidence. Brain Res 2012; 1449: 94-116.

Yeterian EH, Pandya DN. Corticothalamic connections of the superior temporal sulcus in rhesus monkeys. Experimental brain research.Experimentelle Hirnforschung.Experimentation cerebrale 1991; 83: 268-284.

Yoo HK, Kim MJ, Kim SJ, Sung YH, Sim ME, Lee YS, et al. Putaminal gray matter volume decrease in panic disorder: an optimized voxel-based morphometry study. Eur. J. Neurosci 2005; 22: 2089-94.

Yoon KL, Zinbarg RE. Threat is in the eye of the beholder: social anxiety and the interpretation of ambiguous facial expressions. Behaviour research and therapy 2007a; 45: 839-847.

Yoon KL, Zinbarg RE. Threat is in the eye of the beholder: social anxiety and the interpretation of ambiguous facial expressions. Behaviour research and therapy 2007b; 45: 839-847.

Yu Y, Shen H, Zhang H, Zeng LL, Xue Z, Hu D. Functional connectivity-based signatures of schizophrenia revealed by multiclass pattern analysis of resting-state fMRI from schizophrenic patients and their healthy siblings. Biomed Eng Online 2013; 12: 10.

Zahn R, Moll J, Krueger F, Huey ED, Garrido G, Grafman J. Social concepts are represented in the superior anterior temporal cortex. Proc. Natl. Acad. Sci. U.S.A 2007; 104: 6430-5.

Zahn R, Moll J, Paiva M, Garrido G, Krueger F, Huey ED, et al. The neural basis of human social values: evidence from functional MRI. Cereb. Cortex 2009; 19: 276-83.

Zalesky A, Fornito A, Bullmore ET. Network-based statistic: identifying differences in brain networks. NeuroImage 2010; 53: 1197-1207.

de Gelder B, van Honk J, Tamietto M. Emotion in the brain: of low roads, high roads and roads less travelled. Nature reviews.Neuroscience 2011; 12: 425-c1.

van Tol MJ, van der Wee NJ, van den Heuvel OA, Nielen MM, Demenescu LR, Aleman A, et al. Regional brain volume in depression and anxiety disorders. Arch. Gen. Psychiatry 2010; 67: 1002-11.

APPENDIX A
SCHEMATIC REPRESENTATION OF FUNCTIONAL CONNECTIVITY APPROACHES ALONG TWO DIMENSIONS: ABILITY TO ASSESS CONDITION-DEPENDENCY VS. EXPLORATORY ABILITY

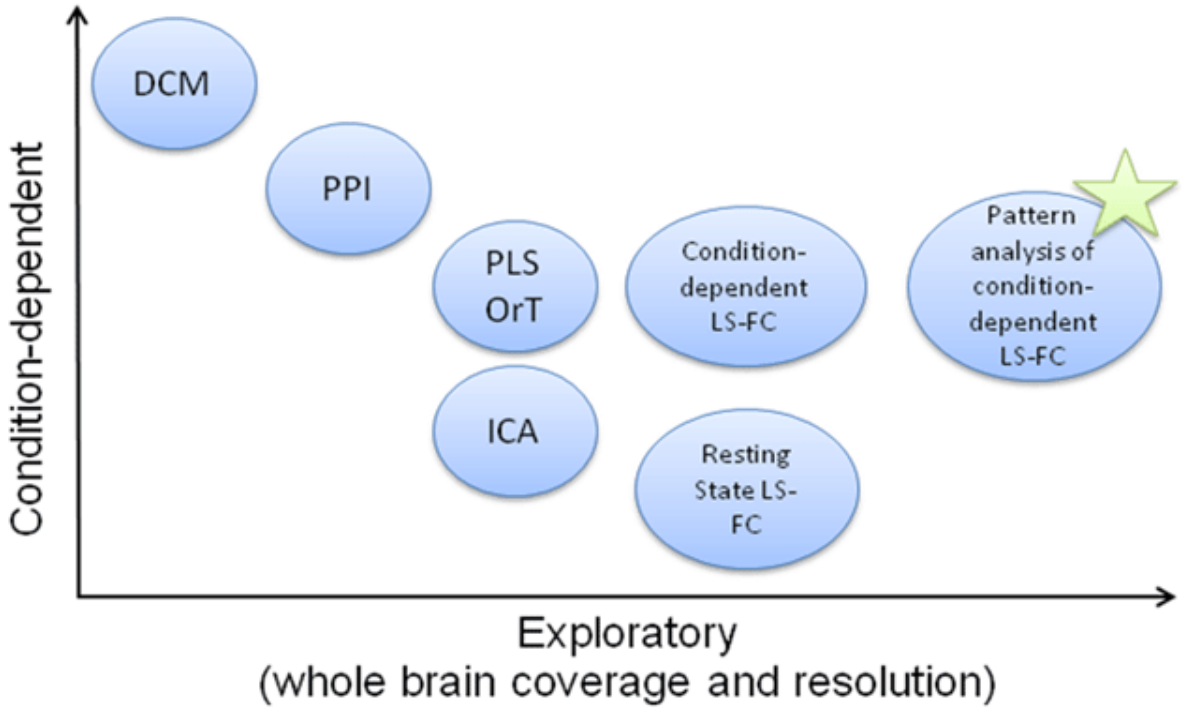

Figure 23. APPENDIX A: Current functional connectivity approaches along two dimensions. Dimension 1 (x-axis) refers to both the extent to which the approach can assess functional connectivity across the whole-brain as well as the ability to identify functional connectivity between discrete pairs of regions at high-spatial resolution. Dimension 2 (y-axis) refers to the ability of the approach to model and assess functional connectivity during specific cognitive contexts and conditions. DCM=Dynamic Causal Modeling, PPI=Psychophysiological Internaction Anslysis, PLS=Partial Least Squares, OrT=Ordinal Trends Analysis, ICA=Independent Components Analysis, LS-FC=Large-scale functional connectivity.